SYNTHESIS OF BENZENEDICARBOXYLIC ACID BASED METAL ORGANIC FRAMEWORK AND ITS APPLICATION IN CARBON DIOXIDE ADSORPTION

GOWSALYA R

20PCH004

Dissertation work submitted to

Avinashilingam Institute for Home Science and Higher Education for Women, Coimbatore – 641043,

Tamil Nadu, India.

In Partial fulfilment of the Requirement for the Degree of

MASTER OF SCIENCE IN CHEMISTRY

May 2022

SYNTHESIS OF BENZENEDICARBOXYLIC ACID BASED METAL ORGANIC FRAMEWORK AND ITS APPLICATION IN CARBON DIOXIDE ADSORPTION

GOWSALYA R

20PCH004

Dissertation work submitted to

Avinashilingam Institute for Home Science and Higher Education for Women, Coimbatore – 641043,

Tamil Nadu, India.

In Partial fulfilment of the Requirement for the Degree of

MASTER OF SCIENCE IN CHEMISTRY

May 2022

M. Jmuthaselvi

Signature of the Supervisor

25/5/2022

Signature of the Head of the Department

ACKNOWLEDGEMENT

I owe my gratitude towards Lord Almighty for his blessings rendered with great support, good health and clear mind throughout my work.

I am grateful to **Dr. S.P. Thyagarajan, Chancellor**, Avinashilingam Institute For Home Science and Higher Education for Women, Coimbatore, for providing alearning opportunity being in this university.

I owe my sincere thanks to **Dr. Bharathi Harishankar, Vice Chancellor**, Avinashilingam Institute for Home Science and Higher Education for Women, Coimbatore, for providing a learning opportunity at this university.

I am thankful to **Dr. S. Kowsalya**, **Registrar**, Avinashilingam Institute for Home Science and Higher Education for Women, Coimbatore, for extending adequate facilities for the progress of the work.

I am highly thankful to **Dr. G. Padmavathi, Dean of School of Physical Sciences and Computational Sciences,** Avinashilingam Institute for Home Science and Higher Education for Women, Coimbatore, for making all necessary arrangements during the course of the work.

With great pleasure and respect, I would like to extend my gratitude to **Dr. R. Saratha, Professor and Head,** Department of Chemistry, Avinashilingam Institute for Home Science and Higher Education for Women, Coimbatore, for being a great support and for extending all the facilities during the entire course of work.

With deep sense of gratitude and respect, I humbly extend my heartfelt thanks to my guide, **Dr. M. Amutha Selvi** Assistant professor, Department of Chemistry, Avinashilingam Institute for Home Science and Higher Education for Women, Coimbatore, for her care, innovative ideas, highly motivating guidance, encouragement and constant support during the entire course of the work.

I also thank all other staff members in the Department of Chemistry for extending their support and encouragement.

I wish to express my gratitude to all my senior research scholars and my friends of the Chemistry Department for their help, moral support and encouragement.

I also wish to extend a word appreciation for the Non-teaching staff, Department Of Chemistry, Avinashilingam Institute for Home Science and Higher Education for Women, Coimbatore, for their cooperation and timely help.

I owe my gratitude to all those who rendered their help for the completion of my work in the form of physical help and mental strength.

At length, with deep respect and honour my gratitude highlights on my parents, my siblings and all my family members without whom there is no glossary to my glory.

Gowsalya R

CONTENTS

LIST OF TABLES

LIST OF FIGURES

LIST OF ABBREVIATIONS

CO_2	Carbondioxide
CSS	Carbon capture and sequestration
MOFs	Metal Organic Frameworks
SBUs	Secondary Building Units
BDC	Benzenedicarboxylic acid
DMF	Dimethylformamide
Cr	Chromium
Mn	Manganese
Fe	Iron
Co	Cobalt
Mg	Magnesium
Sr	Strontium
FT-IR	Fourier transform infrared Spectroscopy
PXRD	Powder X-ray Diffraction
TGA	Thermogravimetric analysis
FESEM	Field Emission Scanning Electron Microscopy

1. INTRODUCTION

Energy consumption has increased significantly in tandem with the rapid rise of the global population **(Taravat Ghanbari et al., 2019).** One of the most important sources of energy in the world is fossil fuel, which has received a lot of attention and demand as an energy source all over the world **(Ali Sadat Shojaei et al., 2020).** The combustion of fossil fuels provides 81 percent of the world's commercial energy while emitting 30×10^{12} kg of CO_2 per year **(Samira Salehi et al., 2017).** The accumulation of carbon dioxide (CO_2) pollutants in the atmosphere begets global warming, forcing us to face tangible catastrophes worldwide **(Alemayehu Kidanemariam et al., 2019).** The steadily increasing CO_2 concentration in the earth's atmosphere has resulted in a slew of climate and environmental problems, necessitating the removal of this major greenhouse gas from the atmosphere **(Changwei Chen et al., 2018).** Carbon capture and sequestration (CCS) is considered as one of the most viable options to reduce the emissions of CO_2 into the atmosphere from anthropogenic sources. It is a three-step process including separation of CO_2 emissions before entering the atmosphere, CO_2 transportation, and its permanent storage. Among them, the CO_2 capture is the most challenging key step **(Elliot A. Roth et al., 2013).**

1.1 CO_2 capture systems

1.1.1 Post Combustion Capture

Post-combustion capture is the process of capturing CO_2 from flue gases produced by the combustion of fossil fuels and biomass in the atmosphere. Flue gas is passed through equipment that separates the majority of the CO_2 before being released into the atmosphere. The CO_2 is stored in a reservoir, and the flue gas is released into the atmosphere **(Kelly (Kailai) Thambimuthu et al., 2018)**

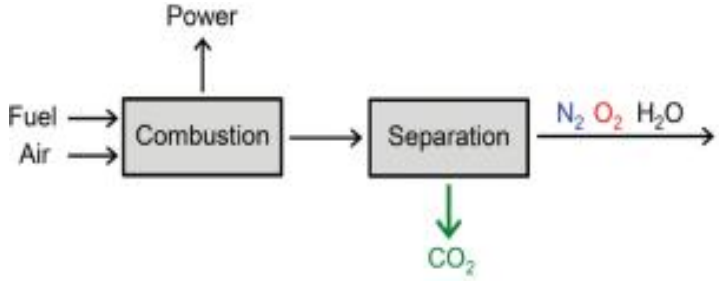

Fig: 1.1 Post Combustion Capture(Kenji Sumida et al., 2012)

1.1.2 Pre-combustion Capture

Pre-combustion capture entails combining a fuel with oxygen, air, and/or steam to produce a synthesis gas (syngas) or "fuel gas" primarily made up of carbon monoxide and hydrogen. In a catalytic reactor known as a shift converter, carbon monoxide is reacted with steam to produce CO_2 and more hydrogen, CO_2 is then separated, usually through a physical or chemical absorption process, yielding a hydrogen-rich fuel suitable for use in boilers, furnaces, gas turbines, engines, and fuel cells **(Kelly (Kailai) Thambimuthu et al., 2018)**

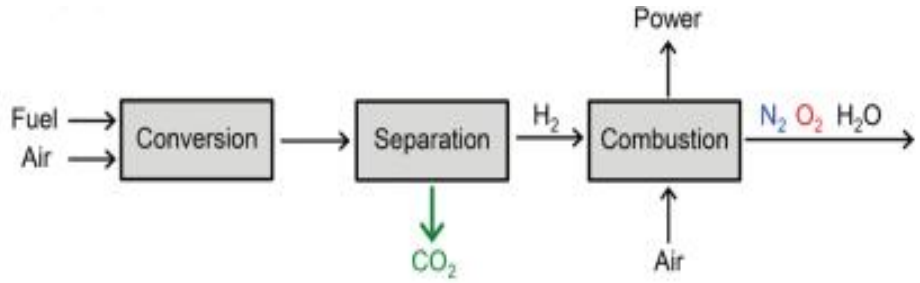

Fig: 1.2 Pre-Combustion Capture(Kenji Sumida et al., 2012)

1.1.3 Oxy-fuel combustion capture

Oxy-fuel combustion is a CO_2 reduction technology in which coal or other carbon-based fuel is burned in a pure O_2 environment. After removing H_2O and impurities, the fuel produced by oxy-combustion is almost entirely CO_2, making the CO_2 capture step easier, **(Claudio Pettinari et.al., 2020)**. Oxy-fuel combustion is similar to post combustion but with a modified combustion process that results in a higher carbon dioxide concentration in the flue gas.

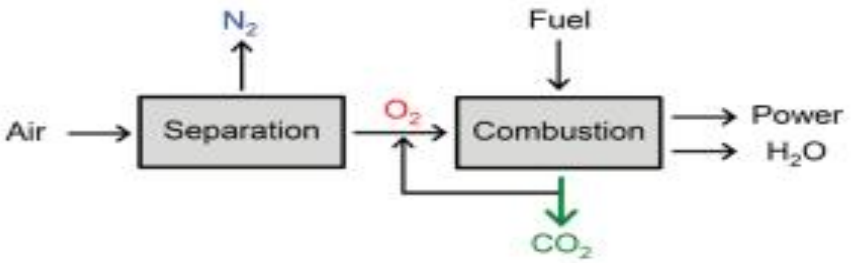

Fig: 1.3 Oxy- fuel Combustion Capture(Kenji Sumida et al., 2012)

1.2 CO_2 CAPTURE ROUTES

Various methods have been developed to capture CO_2 gas. Among them **Amine based techniques** which come under absorption process**, the use of Zeolites, activated carbons, MOFs** based on adsorption process **and Membrane separation** are most commonly and currently existing technologies to effectively remove CO_2 gas. Among them absorption and adsorption plays a major role.

1.2.1 AMINE SCRUBBING

Amine scrubbing is one of the most important techniques that has been used commercially all over the world. The liquid phase amine-based absorption process, in which alkanolamines such as Monoethanolamine (MEA) in aqueous solution act as absorbent, captures CO_2. During the absorption process, water amine molecules selectively react with CO_2 to form water soluble chemical compounds. Amine solutions have a high CO_2 capture capacity and selectivity, and the CO_2 capture capacity is unaffected by the partial pressure of CO_2. As a result, amine-based systems can efficiently remove CO_2 from the flue gas of pulverized coal-fired power plants **(Chao Chen et al., 2016).**

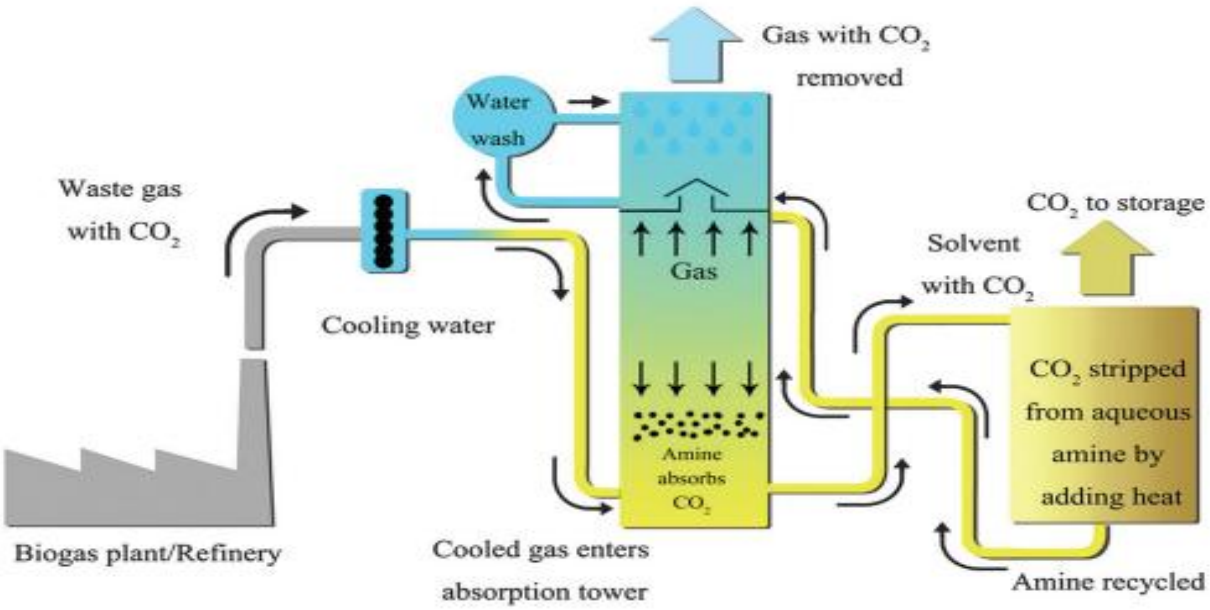

Fig: 1.4 Carbon dioxide capture plant by liquid amines (Somboon Chaemchuen et al., 2013)

Limitations

Yangyang Liu, et.al (2012), in their article mentioned that this method of removing CO_2 from power plants suffer from number of drawbacks such as,

- During adsorbent regeneration, large amounts of heat are required to release absorbed CO_2
- When subjected to heat, the amine scrubbing solutions become corrosive and chemically unstable
- They are also difficult to contain due to their liquid form, and their handling is significantly more challenging

On the other hand, Physisorption between solid adsorbents and CO_2 molecules is a reversible process that requires much less energy for desorption. Traditional CO_2 adsorbents such as zeolites and activated carbons have been extensively researched.

1.2.2 ZEOLITES

It is a type of sorbent with a large surface area and pore volume. They are alumina silicate porous materials with a uniform pore structure and a minimum channel diameter of 0.3 to 1.0 nm. The molecular sized pores remove CO_2 both through mechanical sieving and surface adsorption **(Vaidya B. P et al., 2016)**

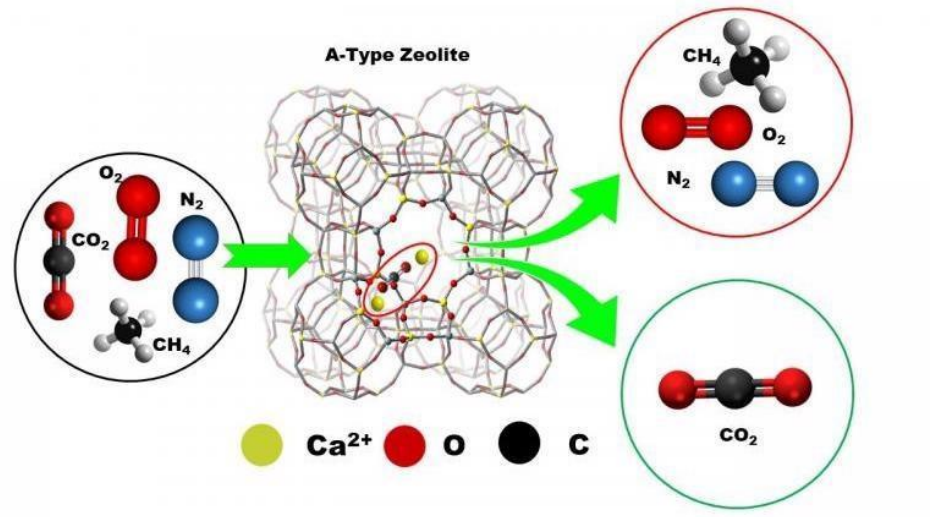

Fig: 1.5 Zeolites for CO_2 capture

Image credit: [2021 OKAYAMA UNIVERSITY-INORGCHEM]

Limitations

- Temperature, pressure, and the presence of water vapor all have a strong influence on them. The capacity of zeolites for CO_2 adsorption decreases with increasing temperature and increases with increasing CO_2 gas-phase partial pressure. Furthermore, because zeolites are highly sensitive to the amount of water in the flue gas, extensive drying of the flue gas is required prior to CO_2 capture **(Rana Sabouni et.al., 2013)**

1.2.3 ACTIVATED CARBONS

Because of their large specific surface area and its adsorption ability, ACs have been widely reported as efficient adsorbents in the removal of CO_2. Any carbonaceous material with a high carbon content and low ash content, as well as inexpensive sources and low volatile matter, can aid in the formation of activated carbon pores **(Ammar Ali Abd et al., 2020).** Thus, they have a significant advantage over other adsorbents in terms of raw material cost, and the wide range of sources results in variations in pore size distribution, pore structure, and active surface area of the activated carbons

Limitations

- Activated carbons have higher CO_2 adsorption at high pressure, but they have low CO_2/N_2 selectivity(i.e., poor adsorption at low pressure). There is very little CO_2 adsorption in post combustion carbon capture, which operates at low pressure **(Yangyang Liu et.al., 2012).**

1.2.4 METAL ORGANIC FRAMEWORKS

Metal-organic frameworks (MOFs) are a relatively new class of porous, crystalline materials **(Avery E. Baumann et al., 2019)** formed by self-assembly of central metal ions or clusters and bridging organic ligand via coordination bonds **(Luning Chenv et al., 2020),** in which bivalent or trivalent aromatic carboxylic acids or N-containing aromatics are frequently used to form frameworks with zinc, copper, chromium, aluminum, zirconium, and other elements **(Yu-Ri Lee et al., 2013)**. A large number of different metal ions and organic linkers can be used to make MOFs, resulting in an enormous number of different structures of varying pore dimensions, geometry and functionality **(Pablo Cubillas et al., 2014)**. The study of MOF began in the late 1990s, and the term "MOF" was first coined in 1995. Prof. Omar Yaghi at UC Berkeley was the first to pioneer MOF, and it has since become a rapidly growing area in the research field **(Isobel Tibbetts et al., 2020).**

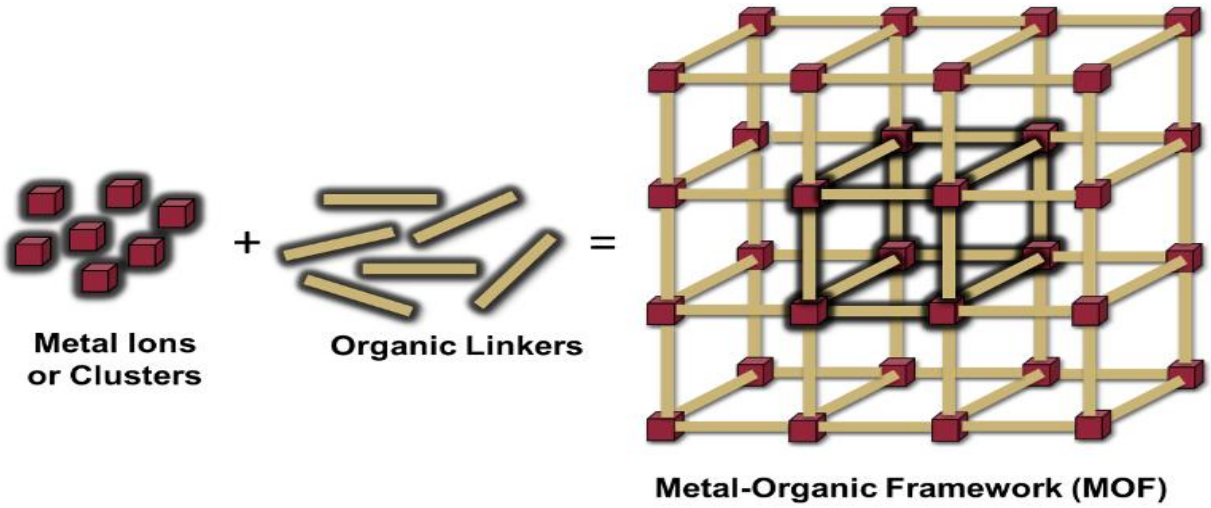

Fig: 1.6 Schematic of the metal-organic framework (MOF) Structure
Image Credit: Google Image

The synthesis and understanding of Metal Organic Frameworks can be described based on the assembly and structural diversity role of multi-metallic Secondary Building Units(SBUs). Coordination networks built by assembling single metal ions with neutral donor ligands gets irreversibly collapsed due to structural fragility, which was attributed to the resultant coordination geometries based on single metal **(Junsu Ha et al., 2020).** The polynuclear nature of SBUs, in contrast to the single-metal nodes found in coordination networks, allows the structures to serve as rigid, directional, and stable building units in the design of robust crystalline materials with predetermined structures and properties.

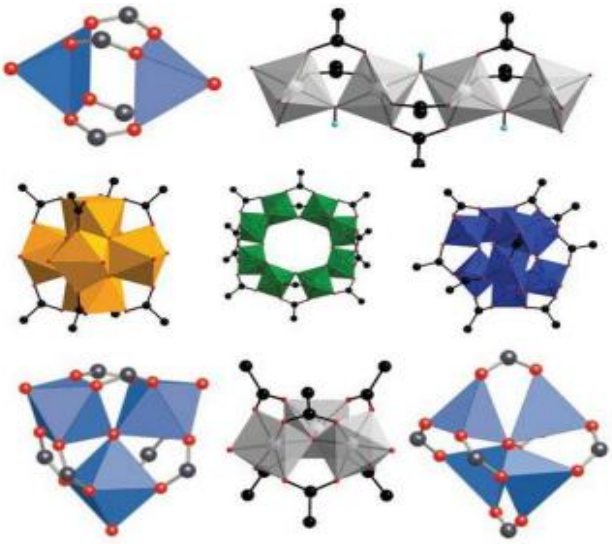

Fig : 1.7 Secondary Building Units Of MOFs (Sanju Soni et al., 2020)

MOFs with ultrahigh porosity and structural complexity have also been developed using this concept. Thus, the secondary building unit (SBU) approach was a turning point in the discovery of permanently porous metal organic frameworks (MOFs) **(Markus J. Kalmutzk et al., 2018).**

Featured with extremely high surface area (typically ranging from 1000 to 10,000 m2/g), large porosity, tunable pore size, and flexible functionality, MOFs have gained extensive explorations as a highly versatile platform for functional applications in many research fields **(Long Jiao et al., 2018)**, such as catalysis, gas storage, drug delivery, gas vapor separation, luminescence, lithium-ion batteries, water treatment, and carbon dioxide capture, as well as photo- and bio-sensors **(Yoshie Sakamaki et al., 2020).**

In history of MOF, a benchmark was reported by the synthesizing MOF-5 ($ZnO_4(bdc)_3$, bdc = terephthalate), comprising of Secondary Building Unit of ZnO_4 tetrahedra is regarded as rigid and stable framework, following this work HKUST-1($Cu_3(btc)_2$, btc = 1,3,5-benzenetricarboxylate) was synthesized and characterized which showed high porosity that indicated by its crystal structure and low pressure gas sorption studies **(Eram Sharmin et al., 2016).**

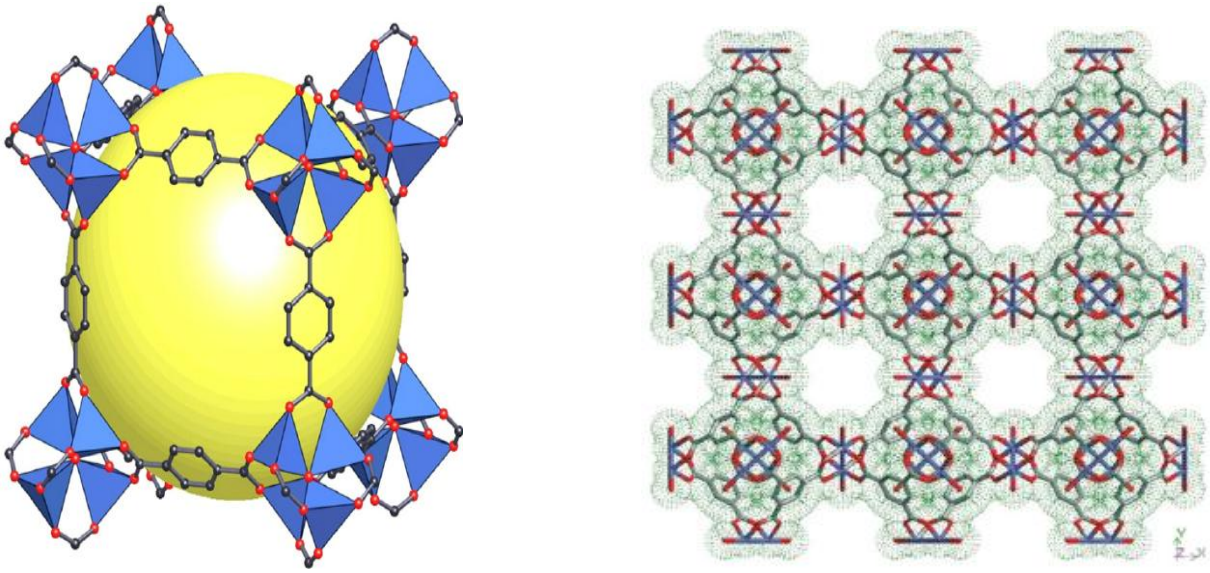

(a) **(b)**

Fig: 1.8 (a) The structure of MOF-5 shown as Zn_4O tetrahedra (blue polyhedra) joined by benzene dicarboxylate linkers (O: red and C: black) to give an extended 3D cubic Framework (b) The structure of HKUST-1 Copper atoms, carbon atoms and oxygen atoms are shown in blue, grey and red (Yujia Sun et al., 2015)

1.2.4.1 Properties of MOF

With respect to CO_2 capture and conversion, MOFs serve as promising adsorbents and catalysts because of their unique advantages such as,

- Structures that are predictable and functionalizable; the structures of many MOFs can be predicted, and the structural designability and chemical tunability of the materials allow for the incorporation of various types of accessible capture and catalytically active sites

- MOFs are highly compatible with other materials and can be used as precursors and/or templates to create MOF composites or MOF derivatives with extraordinary physical and chemical properties

- MOFs have unique catalytic properties, combining the benefits of homogeneous and heterogeneous catalysts, such as high catalytic efficiency, easy separation and reusability, and stability

- MOFs well-defined and tailorable structures make it much easier to understand structure property relationships in MOF-based catalysts. As a result of these characteristics, MOFs are well suited for CO2 capture and conversion **(Meili Ding et al., 2019)**

1.2.4.2 MOF as CO_2 adsorbent

In order for an MOF adsorbent to be an efficient adsorbent material for carbon capture, important benchmark points must be considered.

- The amount of adsorbate taken up by the adsorbent per unit mass (gravimetric CO_2 uptake mg/g, w/w) or volume (volumetric CO_2 uptake -v/v) of the adsorbent is required to have a high adsorption capacity **(Claudio Pettinari, et.al 2020). Yangyang Liu, et. al (2012)** reported that MOF adsorbents with extremely high surface area and pore volume tend to capture more CO_2

- MOF-177, for example, has a volumetric CO_2 adsorption capacity of 320 cm^3 (STP)/cm^3 at 35 bar, which is approximately 9 times higher than the quantity stored at this pressure in a container without the metal organic framework and higher than conventional materials used in this application, such as zeolite 13X **(Kenji Sumida, et. al., 2012)**

- Another important parameter is adsorption heat, which indicates the strength of the interaction between the pore surface and CO_2 required to regenerate the sorbent. It's usually expressed as Qst, or isostatic adsorption heat, which is calculated from adsorption isotherms at various temperatures and pressures **(Claudio Pettinari et.al., 2020)**

- MOFs must exhibit fast adsorption and desorption. While high affinity of the MOF adsorbent toward CO_2 generally would enable high capacity and selectivity, they could also result in difficult desorption if the interaction between adsorbents and CO_2 is too strong

- Continuous adsorption and desorption requires high strength. Because MOF life and replacement frequency are determined by stability, the number of cycles must be increased

- MOF must have good mechanical stability and be able to withstand humidity. When exposed to water-containing flue gas for an extended period of time, many MOFs will collapse and lose their adsorption power

- The adsorbent should be simple to make in large quantities at a low cost. The ligand synthesis process should begin with low-cost materials and be completed in as few steps as possible**(Ayesha Rehman et al., 2019)**

- In CO_2 capture applications, high CO_2 selectivity over other components is critical. Depending on the separation mechanism, such as kinetic or thermodynamic separation, selective adsorption can be defined in a variety of ways. The size/shape exclusion (molecular sieving) principle is used in kinetic separation, where the size of pores in the framework allows molecular diffusion for specific kinetic diameters. Adsorbate physical properties such as polarizability and quadrupole moment can be attributed to adsorptive selectivity in thermodynamic separation **(Claudio Pettinari et.al., 2020)**

1.2.5 STRATEGIES TO ENHANCE CO_2 ADSORPTION IN MOF

1.2.5.1 Generation of Open Metal Sites

The metal sites in the structure of some MOFs are partially coordinated by solvent molecules present in the synthesis mixture, such as water, DMF, and others. Treating such

MOF under heat or vaccum remove such solvents results in open metal sites which enhance MOFs' performance in CO_2 capture process **(Meili Ding et al., 2019).**

1.2.5.2 Functionalization of MOF- Lewis Basic Sites(LBSs)

Alternative approaches to increasing CO_2 capture capacity include MOF with functional groups that can donate electrons. The electronegative atom nitrogen is commonly used to build active sites for CO_2 capture. The N atom in an amine group can have a basic property if it has one pair of electrons in its outer orbital. MOFs can be functionalized either directly during synthesis with a functionalized ligand or indirectly with various post-synthesis grafting techniques. This approach was first used by **Yaghi and co-workers** where they used a functionalized organic linker to produce functionalized MOF.

1.2.5.3 Pore Space Partition

Maximizing host-guest interactions by encasing gas molecules in snug pockets of pore space can be a fruitful approach for efficient capture of small gas molecules at ambient conditions. **Xiang Zhao et al. (2014)** proposed the pore space partition concept to put this concept into practice. The basic idea behind these strategies is to anchor a metal ion or cluster at the cage or channel centers and then run hooks (functional groups) from the framework to these metal species, dividing the pore space into multiple domains.

1.2.5.4 Flexible Framework

Yet another property of MOF in enhancing CO_2 capture capacity is structural flexibility. Certain MOF undergo structural changes in response to external stimuli such as pressure and/or temperature, resulting in "gated" CO_2 adsorption. The CO_2 adsorption capacities of these MOF suddenly and dramatically increase at a specific relative pressure known as the gate pressure in such cases **(Meili Ding et al., 2019)**

So, by considering MOFs exceptional structural, physical and chemical properties and its adsorption capacities over other conventional CO_2 capture techniques, this work will focus on employing Metal-Organic Frameworks (MOFs) to adsorb CO_2 gas that helps to establish environmental carbon balance for long-term development.

SCOPE OF THE WORK

Metal–organic frameworks (MOFs) are attractive material to meet the needs of next-generation carbon dioxide adsorption. MOFs are a class of porous materials composed of metal nodes and organic linkers. Their modular nature allows for great synthetic tunability, affording both fine chemical and structural control. With creative synthetic design, properties such as porosity, stability, particle morphology, and conductivity can be tailored for specific applications.

Due to structural flexibility, large surface area and tailorable pore size, MOFs have wide applications in field of gas adsorption and storage. The development of novel materials with high carbon dioxide adsorption capacity and selectivity is becoming increasingly appealing for use in clean energy and pollution control applications.

The significance of having a sorbent with high carbon dioxide adsorption capacity at a low cost is mostly attributed to the entire carbon capture and storage strategy. Practices such as amine-based absorption and adsorption materials such as zeolites and activated carbons have been proven to have a variety of drawbacks, driving a quest for alternative CO_2 capture and separation technologies.

With this above scope we synthesized MOF using an affordable and commercially available acid based linker, for the CO_2 gas adsorption.

2. REVIEW OF LITERATURE

Omid T et al., 2021, reported on a hydrogen bonded water stable robust microporous material, synthesized by combining commercially available inexpensive linker 5-aminoisophthalic acid [Haip] and Cobalt(II) salt in methanol solvent that produced pink plate like crystals with 92% yield in just 2 hours. Single Crystal X-ray diffraction unraveled that pore dimensions of the respective MOF material well matched to the CO_2 molecule, so that it can be enveloped to multiple non-covalent contacts which favors the strong interaction between CO_2, amine and non-coordinated carboxyl functionalities. By heating the framework to 130 °C in vacuo, guest free MUF-16 can be generated which posses good thermal stability. Based on single gas isotherm measurements, it was determined that MUF-16 absorbs a large amount of CO_2 at ambient conditions (47.8 and 61.1 cm^3/g of CO_2 at 1 and 20 bar) and rejects H_2 and N_2 molecules. The isosteric heat of adsorption(Qst) of CO_2 for MUF-16 is moderately high which is useful for effective separation of CO_2 from other gasses. As a result, the application of MUF-16 to the separation of gas mixtures composition of 15/85 and 1/99 or CO_2/N_2 at 293k, 1.1 and 9 bar showed the CO_2 capture efficiency of 1.08 and 0.12mmol and finally the occluded CO_2 can be removed by placing the bed under vacuum or purging with flow of dry air at 293k. This work showed that MUF-16 could serve as promising CO_2 adsorbent from a mixture of gasses.

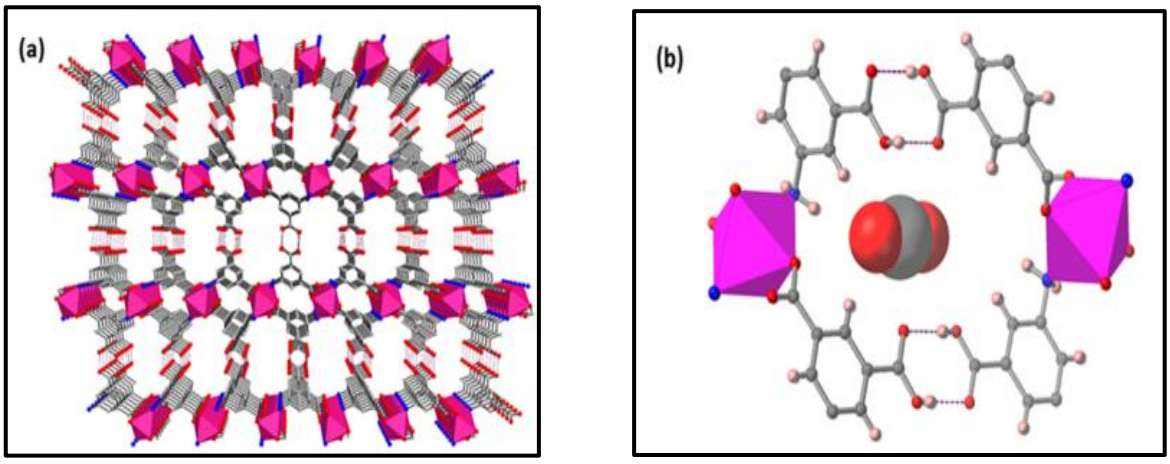

Fig: 2.1 (a) MUF-16 Secondary Building Unit(SBUs); (b) Adsorption sites of CO_2 molecules in the pores of MUF-16

To prepare Cu-BTC, with high CO_2 adsorption efficiency, **Mei Mei Peng et al., 2012** used three different synthetic methods - Solvothermal 1, 2 & Microwave method. According to the XRD result of the synthesized MOF, the crystal structure of three samples generated using three different procedures is all the same. SEM images revealed that the size of the sample synthesized by the solvothermal methods is nearly identical, whereas the microwave method produced a smaller sample, owing to the homogeneous effect, in which more seeds were generated in a short period of time, resulting in a low possibility of seed grouping. The nitrogen adsorption - desorption isotherms of Cu-BTC samples generated using various procedures showed a Type I isotherm, which is a trademark of microporous materials. It is concluded from this work that the CO_2 adsorption capacity of three samples reduced as the temperature raised, indicating that physical adsorption was the primary mode of CO_2 adsorption in Cu-BTC. At 25 °C Cu-BTC-MW had a high CO_2 uptake of about 23.3wt%, while Cu-BTC-ST 1 & 2 had 16.7 & 22.3wt%. Thus as a result, Cu-BTC-MW outperformed the competition due to its high adsorption at room temperature and atmospheric pressure.

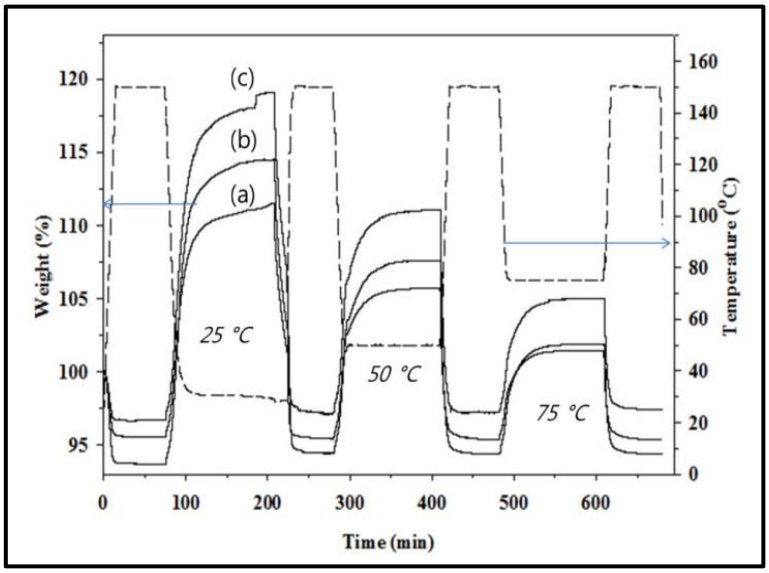

Fig:2.2 CO_2 adsorption-desorption curves of Cu-BTC MOF prepared with different methods (a) Cu-BTC-ST1, (b) Cu-BTC-ST2 (c) Cu-BTC-MW

Li et al., 2013 investigated the influence of the long chain on the CO_2 adsorption capability of Co adenine series MOFs (Bio-MOF-11 to 14). According to the findings, increasing the length of the aliphatic chain (acetate, propionate, butyrate, and valerate, respectively) decreased CO_2 capacity at 1 bar and 273 and 298 K. The tangling of the long chain was

responsible for this reduction. At both temperatures and 1 pressure, Bio-MOF-11 had the maximum adsorption capacity (105 cm^3 g^{-1}). The tiny diameter of the pores (compatible with CO_2), as well as Lewis basic pyrimidine and amino groups of the adenine in the framework, are credited with these promising CO_2 absorption capabilities.

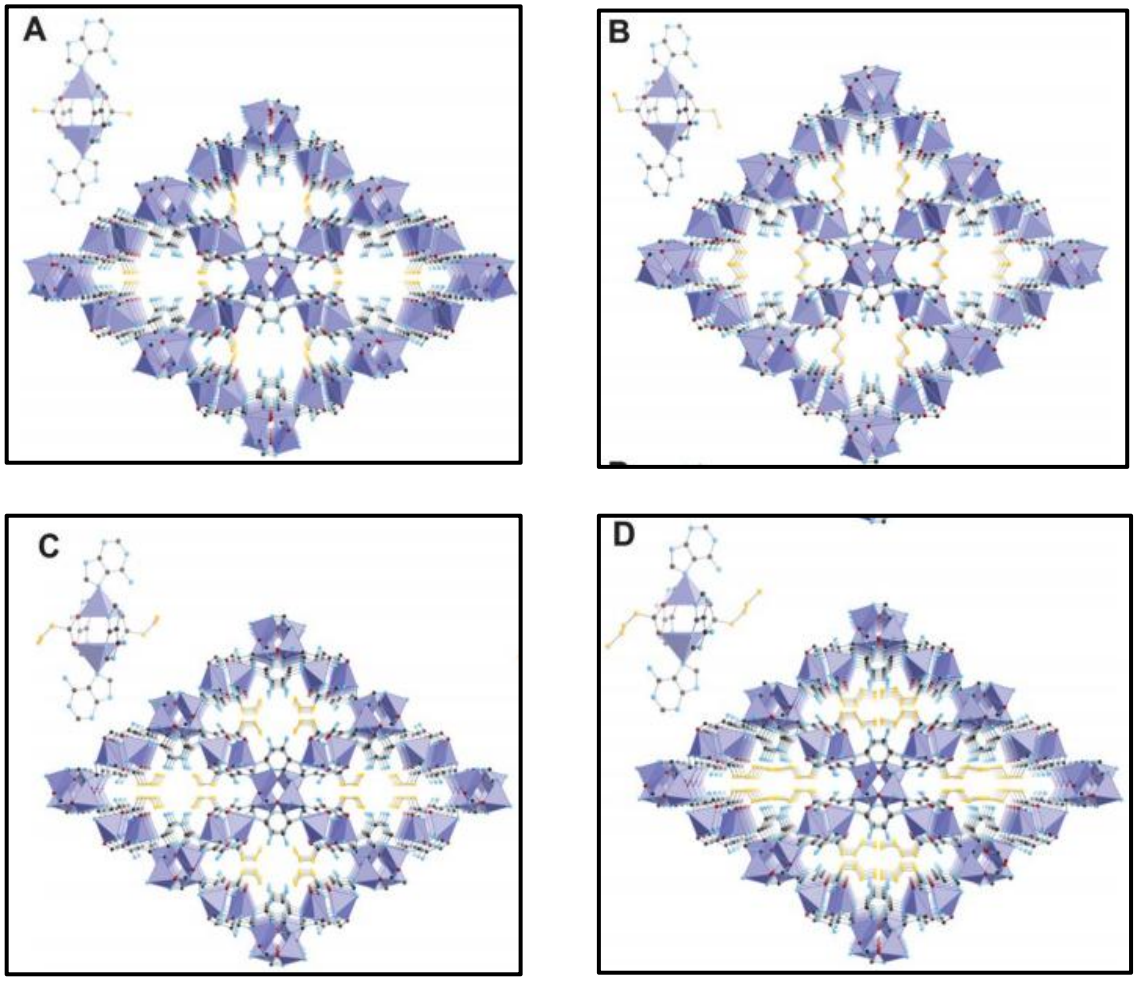

Fig: 2.3 Secondary building units (SBUs) and crystal structures of bio-MOF-11, 12, 13, and 14 (A, B, C, and D, respectively)

A comparative research was conducted by **Chen et al., 2015** on Zinc based MOF-$[Zn_4(bpydb)_3(datz)_2(H_2O)(DMF)_4(EtOH)_5(H_2O)8n$ (1) and Zn(bpydb)(bpy)n (2) as a mixed ligand functionalization. The pore walls of activated MOF (1) were decorated with pyridine and amino groups, resulting in a greater CO_2 absorption capacity (80.9 cm^3 g^{-1} at 273 K and 1 bar) and excellent selectivity over CH_4 and N_2 than MOF 2 (40 cm^3g^{-1} under the same conditions). MOF 1's CO_2 adsorption characteristics were improved by combining free pyridine-N atoms with amino functional groups. The heat of adsorption value, which showed an increasing trend (30.33 kJ/mol)

at zero coverage, was the turning point in this study, demonstrating a strong interaction between CO_2 molecules and the framework.

Using a linear organic linker H_2bcpp (5,15-bis(4- carboxyphenyl)porphyrin) and a tetra nuclear zinc cluster, **Gao et al., 2017,** presented a 4-folded interpenetrated framework MMPF-18(metalloporphyrin framework). At ambient conditions, they studied the CO_2 adsorption capabilities of this interpenetrated MOF. The CO_2 adsorption capacity was moderate (11.8 wt%), and the heat of CO_2 adsorption was roughly 23 KJ mol^{-1}, according to their findings. The framework showed good CO_2 / CH_4 selectivity despite a low CO_2 uptake. This characteristic is due not only to the interpenetrated network's tiny pores, but also to the presence of the ligand's epoxy groups, which allow for the size-selective chemical transformation of CO_2 and the creation of cyclic carbonates.

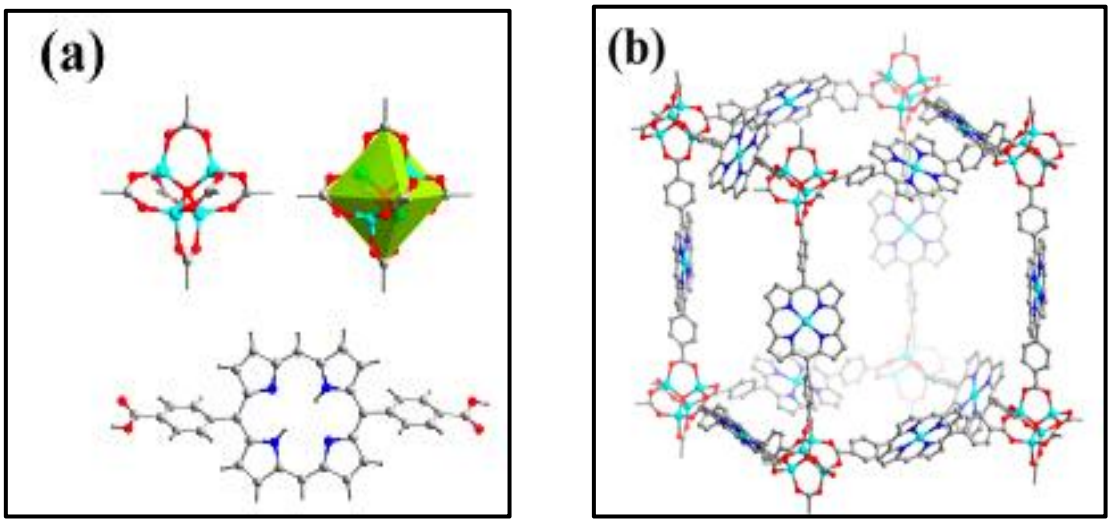

Fig: 2.4 SBU of $Zn_4(\mu_4\text{-}O)(-COO)_6$ and the linear porphyrin linker of H_2bcpp used in the construction of MMPF-18. (b) Topology of MMPF-18 structure containing the in situ metalated Zn-based porphyrin.

Safarifard et al., 2017 created a unique three-fold interpenetrated MOFs (TMU-22, -23, and -24) that were functionalized with various amide groups. The selectivity of CO_2 over N_2 in TMU-24 was substantially higher than in TMU-22 and -23, according to kinetics and breakthrough experiments. TMU-24 also had the largest quantity of Qst for CO_2 at various temperatures (24 & 26 kJ mol-1). The TMU-24's amide functional groups are more accessible, resulting in strong CO_2 selective adsorption in this MOF. This indicates that the amide groups in this framework were guided more into the pores than those in other isoreticular frameworks

(TMU-22, -23).

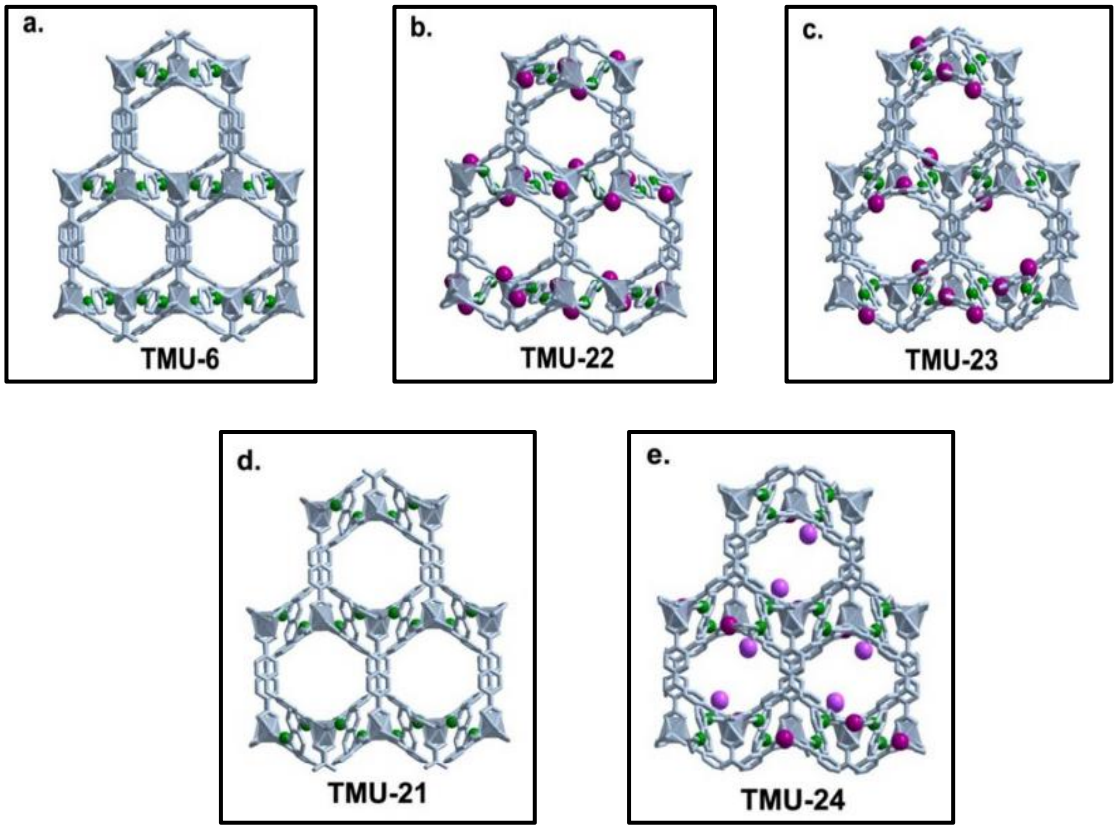

Fig: 2.5 View of the pore channels of a) TMU-6, b) TMU-22, c) TMU-23, d) TMU-21 and e) TMU-24; N (green), O (purple), the more accessible O atoms in TMU-24 (lavender)

Benoit et al., 2017 created a titanium-based MOF (MIL-91(Ti)) with tiny pores. Due to the presence of the phosphonate group in the ligand site, this hydrophilic MOF showed high water stability after numerous cyclic water adsorption/desorption cycles. It also had the highest CO_2 uptake of the small pore MOFs (3 mmol g^{-1} at 303 K and 1 bar), which was the highest among the other small pore MOFs. This metal bisphosphonate framework also has strong selectivity of CO_2 over other gasses, quick kinetics, and a high Qst(-47 kJ mol^{-1} at zero coverage).

Pal et al., 2016 used fluorine and amine ligand functionalization as well as transmetalation to increase the water stability of the carboxylate MOF (Zn to Cu). They used a solvothermal approach to synthesize $[Zn_2(L)(H_2O)_2](5DMF)(2H_2O)n$ (Zn(II)-MOF), which was then followed by a metal interchange reaction to make Cu(II)-MOF without affecting the crystallinity of the framework. Water stability, CO_2 uptake, and CO_2 selectivity over N_2 were all improved with the new MOF. The lining effect of the fluorine molecule, which turned the surface of the pores

hydrophobic, was attributed to an increase in water stability. Additionally, the higher stability of Cu (II) than Zn (II) strengthened the metal-ligand interaction, which boosted the framework strength in humid conditions.

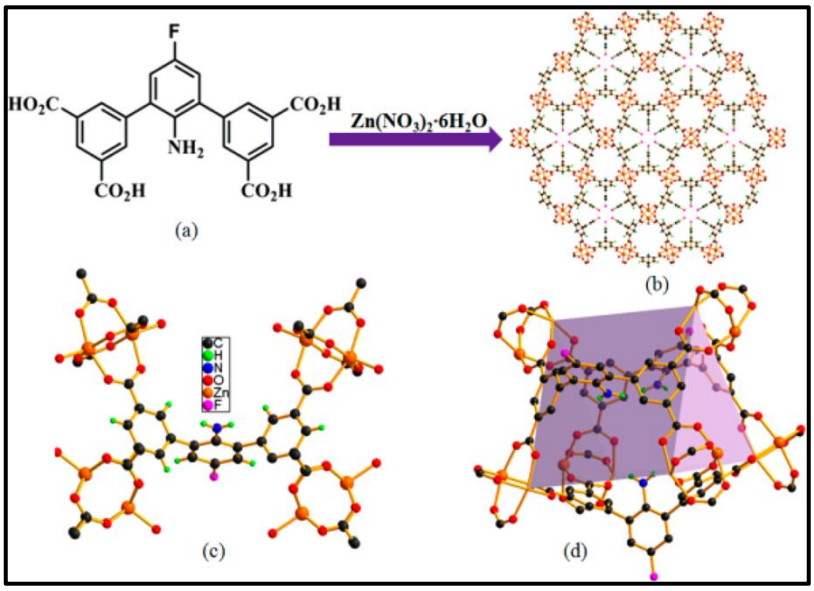

Fig: 2.6 (a) Tetracarboxylic acid ligand H_4L (b) a perspective view of the 3D packing of (Zn(II)-MOF) along the crystallographic c axis, (c) a view of the SBU and (d) supermolecular building blocks (SBBs)

Chen et al., 2018 used a hydrothermal (solvothermal) method to produce a GO@MOF-505 composite from graphite oxide and copper-based MOF. CO_2 selectivity over CH_4 and N_2 has been demonstrated in this combination. When compared to MOF-505, the composite's CO_2 adsorption capability has increased by 37.3 percent (parent). This extraordinary increase in CO_2 adsorption can be attributed to the presence of unsaturated metal sites, which create new micropores and strengthen dispersive forces on the composite framework's surface. Furthermore, GO@MOF-505 has demonstrated exceptional moisture stability at a RH of 80%. The strong coordination interaction between Cu ions and carboxylate groups in GO is responsible for this stability.

Linfeng Liang et al., 2017 reported the design and synthesis of Cu(II) metal organic framework (FJI-H14) with a high density of active sites that displayed outstanding acid and basic stability as well as thermal stability up to 230 °C, as evidenced by TGA studies. At 77k and 1atm, FJI-H14 showed a 279cm^3g^{-1} CO_2 uptake and a low 170cm^3g^{-1} N_2 uptake. The reduced N_2 adsorption could be attributed to the relatively small pores in FJI-H14 being easily occluded by the relatively large N_2 molecule, hindering further N_2 diffusion into the FJI-H14 framework. At

298k, the selectivity of CO_2/N_2(15/85) at 1 atm is calculated to be 51. Positive CO_2 adsorption is thus attributed to the highly populated open active framework. Furthermore, even after five cycles, FJI-H14 maintained 100% adsorption capability, showing that it is well suited for CO_2 capture.

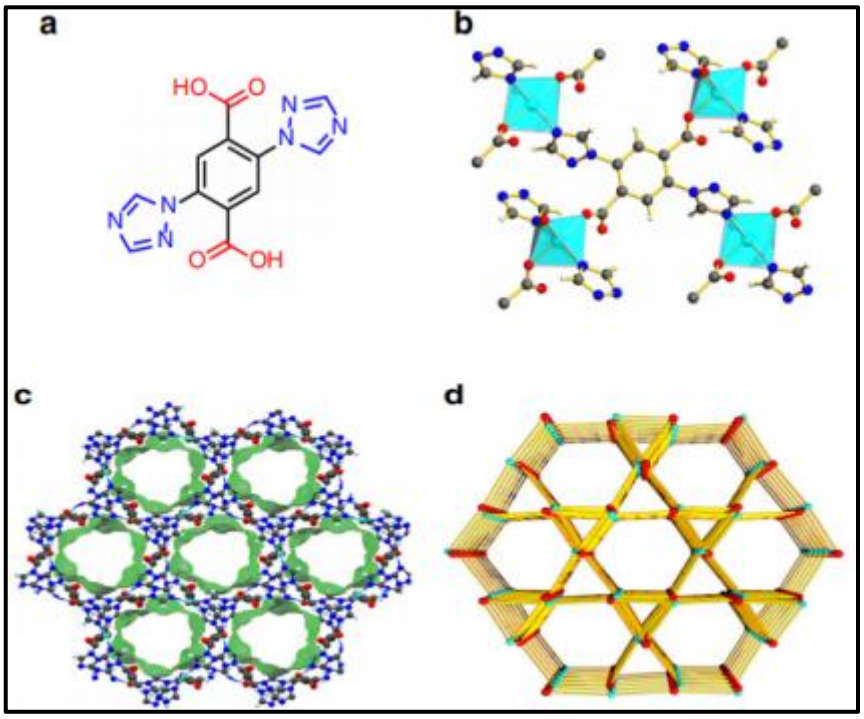

Fig: 2.7 Structural illustration of FJI-H14 a) The selected ligand H_2BTTA for the construction of FJI-H14 b) The coordination environment of the Cu(II) ions as four-connected nodes and BTTA also as a four-connected node c) The one-dimensional nanoporous channels along the crystallographic c direction d) The framework of USF topology (Cu atom, cyan; C atom, gray; O atom, red; N atom, blue; H atom, white)

Nika Vrtovec et al., 2020 synthesized HKUST-1 solvothermally and functionalized it with Ethylenediamine at Cu/ED molar ratios of 0.07, 0.14, and 0.3, respectively, and labeled the functionalized materials HKUST-1-5ED, 10ED, and 20ED. The addition of Ethylenediamine results in the creation of extra openings inside the framework with pore sizes of up to 1 μm. On further investigation pure HKUST-1 shows a CO_2 uptake value of 4.1mmol/g up to 1 bar, whereas HKUST-1-5D had a CO_2 uptake of 2.1mmol/g, and HKUST-1-20ED of 2.1mmol/g , this is because as the concentration of ED increases it not only occupy free metal sites, but also undergo partial multilayer adsorption, which blocks a portion of the amine sorption site resulting in a reduction in CO_2 absorption The selectivity of CO_2 over N_2 (0.15/0.85) was doubled for HKUST-1-ED and marginally enhanced for HKUST-1-10ED. However, the sample with the greatest ED (HKUST-1-20ED) shows a significant decrease because N_2 adsorption becomes more competitive due to multilayer ethylenediamine adsorption and eventual occlusion of the Lewis basic site.

Furthermore, the faster adsorption of modified material is attributed to hierarchical porosity, which becomes more prominent when ED increases, allowing for improved accessibility and faster CO_2 diffusion towards sorption sites.

Tari et al., 2016, used the Microwave method to synthesize an MCM-41/Cu(BDC) composite for selective CO_2 adsorption. They used a cyanotripropyltriethoxysilane linker with Cu(BDC) MOF to functionalize MCM-41. At 298 K and 4-40 pressure, the MOF demonstrated excellent CO_2 capacity and selectivity adsorption over CH_4. The quadrupole moments of CO_2 and the presence of negative and positive charges of COO- and Cu^{2+} ions in the framework were ascribed with these improvements. In comparison to the parent MOFs, the composite's BET surface area was improved (1084, 1063, and 624 m^2g^{-1} for composite, MCM-41, and Cu(BDC, respectively). Furthermore, following three cycles of cyclic CO_2 and CH_4 adsorption, the composite only lost 1% of its capacity, indicating that its structure is very stable.

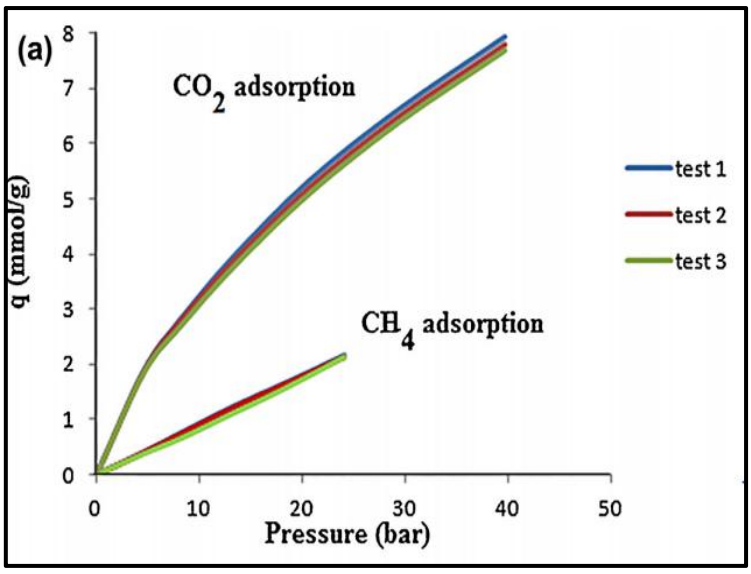

Fig: 2.8 Isotherm of recyclability of MCM-41/Cu(BDC) composite for CO_2 and CH_4 adsorption

Lifei Zou et al., 2013, employed mixed ligand strategy to solvothermally create the 3D porous framework $[(CH_3)_2NH_2][Zn_2(ABTC)(Tz)]3DMF$. A typical Zn-paddlewheel $[Zn_2(COO)_4]$ and a metal cluster of $[Zn_2(Tz)_2(COO)_4]$ are found in the corresponding framework. A Type 1 adsorption isotherm exhibited by this framework suggests the presence of microporous features. The Langmuir and BET surface area of this framework was reported to be 1315 and 976m^2g^{-1}. The CO_2 adsorption capacity of this framework at 1 atm is 92.1 and 46.4cm^3g^{-1} at 273 and 298K, respectively. This high CO_2 absorption capacity is owed to well-calculated pore size and a

synergistic interaction between CO_2 and the framework, as revealed by isosteric heat of adsorption (Qst). The selectivity of CO_2 over CH_4(0.5/0.5, 0.05/0.095) is 5.5 and 5.1 which is very much higher than that of some other well known MOFs like MIL-53(Al) - (2.3), ZIF-8 - (1.32) and Cu3$(BTC)_2$ - (2.28).

Hui-Fang Zhou et al., 2017 rationally synthesized and reported a self penetrating 3D porous framework constructed from H_4PDBDC with Zn_4O cluster, $[Zn_4O(PDBDC)1.5]\cdot 1.5DMF\cdot 2H_2O$, which possesses exceptional chemical stability. The BET and Langmuir surface area were evaluated to be 511 and 554m^2g^{-1}. Examining the CO_2 absorption performance at ambient temperature its adsorption capacity reached 157mgm-1(15.7wt%) at 273k and 115mgm-1 (11.5 wt%) at 298 K. With realistic operating temperature, (i.e) at about 313-333K the CO_2 uptake reached 95 mg g-1 (9.5 wt%) significantly higher than that of previous MOFs under similar conditions. The powder X-ray diffraction (PXRD) pattern clearly shows that the crystallinity and skeletal integrity of this framework can be well preserved in a variety of boiling solvents (methanol, acetone, acetonitrile, toluene, hexanes). The excellent CO_2 adsorption capacity of this framework is mainly attributed to its permanent porosity and excellent stability.

Zhaodong Niu et al., 2018, reported a novel lithium doped metal–organic framework (i.e., Li/UiO-66) synthesized by an economically-feasible method by impregnating it in an ethanol solution of lithium nitrate instead of expensive and toxic organolithium. XRD, XPS, FTIR, and other techniques were used to examine the textural and surface properties, and the results revealed that the doped lithium is coupled to the free carboxylate groups in the structure, forming lithium carboxylate groups. It's worth a mention that the doped lithium cations have no effect on the pure sample's thermal stability. Furthermore, the Li/UiO-66 has a significantly increased CO_2 adsorption capacity and CO_2/N_2 selectivity, which can be attributed to a strong synergistic impact between CO_2 molecules and the adsorbent, as well as extra active sites. The in situ DRIFTS data suggest that doped lithium cations can provide novel active metal sites for CO_2 adsorption(Li-O)

Joonho Park et al., 2012 synthesized MOF-74 and optimized M-MOF-74 analogues by metal substitution, with M= Mg, Ca, and first transition metal elements(Sc, Ti, V, Cr, Mn, Fe, Co, Ni, Cu, & Zn), in order to build a more efficient CO_2 capture media. The findings suggest that Ti- and V-MOF-74 have a higher CO_2 binding affinity than Mg-MOF-74, and that the source of this strong binding is a local electric field generated by a positive charge on the open metal site that stabilizes CO_2, as well as orbital interactions of the lone-pair of CO_2 with the empty d-levels of

metals, as in a coordination bond. Transition metals like Ti and V have a larger binding energy than Mg because they establish additional weak coordination with CO_2 by forward donation.

Wahiduzzaman et al., 2017 described the sonochemical production of MOF nanoparticles of 30–200 nm and electrospraying of those particles on electrospun nanofibers to process a MOF-attached nanofibrous membrane. From a mixed gas flow of 1% CO_2 and 99.9% N_2, this membrane showed substantial selectivity for CO_2 and capacity of adsorbing with 4000–5000 ppm difference. The CO_2 collecting performance of the electroplated membrane was significantly improved after it run for a total of 80 minutes. When compared to N_2, CO_2 molecules have a greater quadrupolar moment and a smaller kinetic diameter. As a result, CO_2 interacts strongly with the open metal sites of MOF, resulting in a greater binding energy. This also backs up HKUST-1's CO_2 selectivity and outstanding adsorption capability.

Osama Shekhah et al., 2014 developed an isostructural water stable metal-organic framework (SIFSIX-3-Cu) based on pyrazine/copper(II) two-dimensional periodic square grids pillared by silicon hexafluoride anions, which allows the pore system to be further contracted to 3.5 compared to 3.84 for the parent zinc(II) derivative. At very low pressure, the Cu counterpart had significantly steeper variable temperature adsorption isotherms than the Zn analogue, indicating that CO_2- SIFSIX-3-Cu interactions are stronger. The competitive adsorption kinetics of CO_2/N_2:10/90, CO_2/CH_4:50/50, and CO_2/H_2:30/70 gas combination adsorption were also investigated. The findings suggested that when CO_2 containing mixtures come into contact with SIFSIX-3-Cu, CO_2 adsorbs more strongly and quickly than N_2 and CH_4. Further, the Qst of CO_2 adsorption in the contracted structure is reported to be increased by 20%, from 45 to 54 kJ $mol^{-1.}$ This improved adsorption energetics, resulting in carbon dioxide uptake and selectivity at very low partial pressures, a performance previously unattainable with other kinds of porous materials is mainly attributed to the material design and control in pore size approach.

Jinjie Qian et al., 2017, reported on robust indium-based MOF(InOF-15) synthesized using quinoline - based dicarboxylic acid linker. This framework, which is embellished with Lewis basic sites (LBSs) derived from quinoline moieties and possible open metal sites (OMSs) derived from $[In_3O(CO_2)_6]$ SBUs, encourages researchers to dig deeper into the possibilities for carbon dioxide separation and storage. CO_2 uptake of this framework is reported to be 78.0 cm^3g^{-1} (3.48 mmol g^{-1}, 153.1 mg g^{-1}) at 273 K and 1.0 bar, which is substantially higher than CH_4 (24.2 cm^3g^{-1}, 1.08 mmol g^{-1}, 17.3 mg g^{-1}) and N_2 (4.0 cm^3g^{-1}, 0.18 mmol g^{-1}, 5.0 mg g^{-1}). The selectivity of CO_2 over CH_4 & N_2 were were investigated using Ideal adsorbed solution theory

(IAST), and the calculations show that the InOF-15 sample has a moderate selectivity factor of 98.2 in a 15:85 molar ratio of CO_2 and N_2 mixtures at 273 K and 1.0 bar and the projected CO_2/CH_4 selectivity value from equimolar gas-phase mixtures is 7.7, which is significantly greater than the zero coverage value (29.3). The modest Lewis basic Npyridyl•••C(=O)$_2$ distance of 3.99 supports the strong inclination of Indium(III) centres to attach to nearby CO_2 molecules with a distance of 3.09 in an In(III)•••O=C=O manner. Furthermore, a very weak cooperative supramolecular interaction between CO_2 oxygen atoms and H atoms from nearby phenyl C–H groups in an O=C=O•••H phenyl supports the combination of In(III)•••O=C=O and Npyridyl•••C(=O)$_2$ which attributes to effective selectivity of CO_2 by InOF-15 over other gasses.

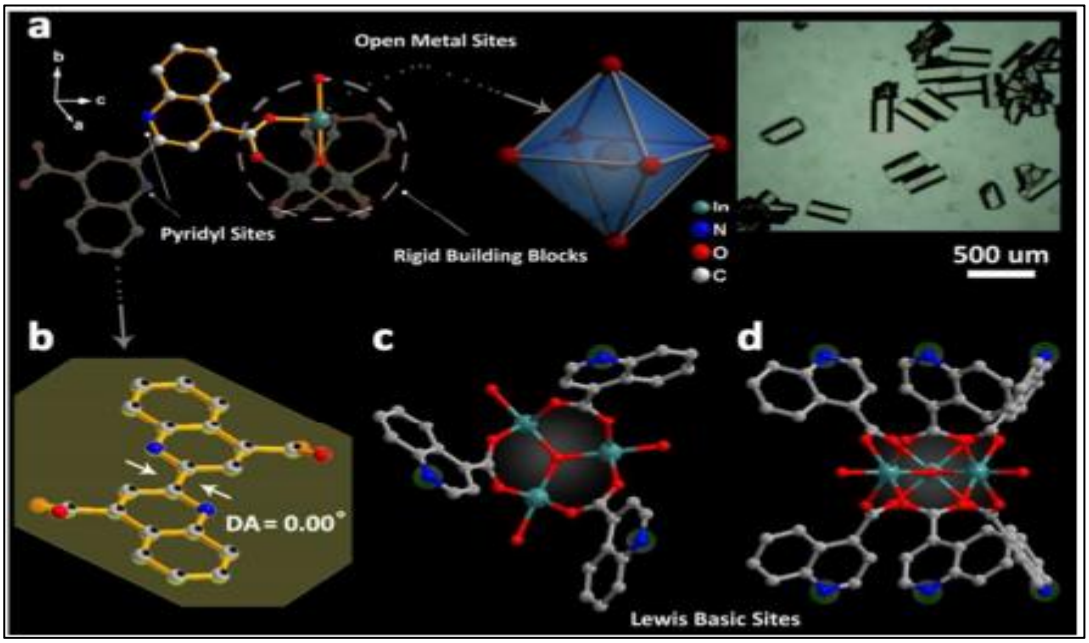

Fig: 2.9 (a) Highlighted asymmetric unit of InOF-15 and the coordination environment of BQDC2- ligand; octahedral In(III) cations with terminally coordinated MeOH molecules, the photograph of crystals is on the top right (b)The dihedral angle between two biquinoline planes within each BQDC2- ligand (c) 6-connected indium-based [$In_3O(CO_2)_6$] SBU

By integrating N,N'-dimethylethylenediamine(mmen) into $H_3[(Cu_4Cl)_3(BTTri)_8$ (CuBTTri; H_3BTTri =1,3,5-tri(1H-1,2,3-triazol-4-yl)benzene) **Thomas M. McDonald et al., 2011** created a water-stable, triazolate-bridged framework. Despite stoichiometric attachment of mmen to the framework's open metal sites, high porosity was maintained, yielding a BET surface area of 870 $m^2\ g^{-1}$. When compared to the unappended framework, the CO_2 adsorption performance of mmen-CuBTTri is vastly improved at all pressures between 0 and 1.1 bar. At 25°C and 1 pressure, mmen-CuBTTri adsorbs 4.2 mmol g^{-1} of CO_2 (15.4 wt%), which is a 15% increase in gravimetric capacity over the unmodified CuBTTri framework, and adsorbs roughly 4.7 times more CO_2 in

terms of volume than CuBTTri at 0.15 bar. CO_2 selectivity over N_2 at all pressures between 0 and 1.1 bar, is greater than CuBTTri. This is owing to the reduction in specific surface area caused by the addition of mmen. Thus the higher quantity of amines accessible to guest CO_2 molecules in mmen-CuBTTri accounts for the significantly higher CO_2 adsorption.

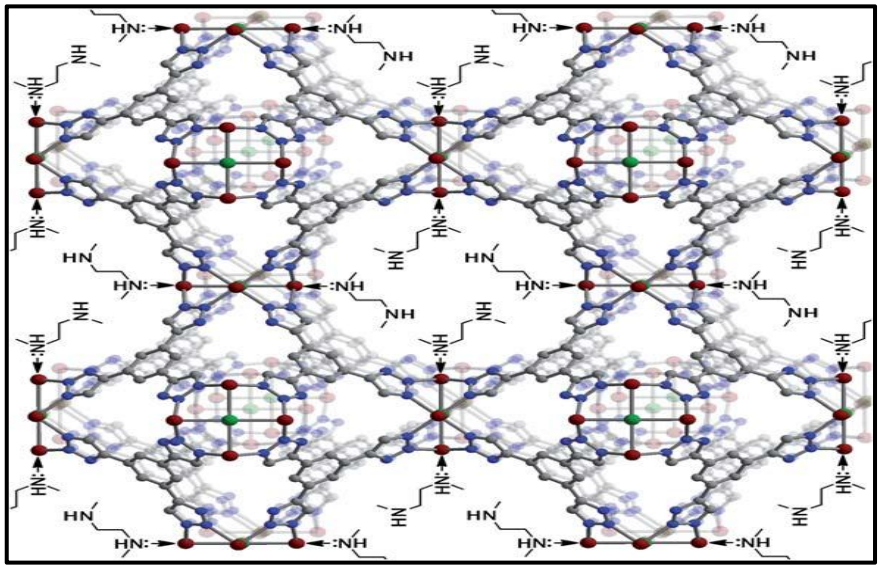

Fig: 2.10 A portion of the structure of the amine functionalized metal–organic framework mmen-CuBTTri, with red, green, blue and gray spheres representing Cu, Cl, N and C atoms

The effect of inter-crystalline spacing on CO_2 adsorption in Mg-MOF-74 was studied by **Siddharth Gautam et al., 2020.** They reported that the amount of CO_2 adsorbed in Mg-MOF-74 significantly enhanced as inter-crystalline space was introduced between the crystallites. This enhancement starts diminishing when increasing this space beyond 5 Å. This is because the CO_2 molecules require strong adsorption sites at lower pressures. The surface of the crystallite becomes exposed at an inter-crystalline space of 3Å, resulting in increased adsorption in S1 compared to S0. Because CO_2's kinetic diameter (3.3 nm) is larger than this inter-crystalline region, adsorption on the surface is challenging, and the amount of CO_2 adsorbed is limited by geometrical constraints. On the relaxation of geometrical restriction, by adding inter-crystalline space greater than the kinetic diameter of CO_2 is in S_2, the adsorption amount is greatly increased. It is concluded from their work that, CO_2 molecules adsorbed within the crystallite pores dominate the adsorption amount for smaller inter-crystalline spacings, whereas the adsorption is predominantly at the crystallite surface for larger inter-crystalline spacings and especially at high pressures.

Hamid Reza Mahdipoor et al., 2021, reported on the series of solvothermally synthesized MOF MIL-101(Fe), MIL-53(Fe), and Amino-MIL-101(Fe) employing BDC ligands & Fe-based precursors. The maximal CO_2 adsorption efficiency of MIL-101(Fe)–NH_2 at 25°C is about 13 mmol g^{-1} and the adsorption capacities of MIL-101(Fe) and MIL-53(Fe) are 9.3 and 8.6 mmol g^{-1} respectively. The greater CO_2 adsorption by MIL-101(Fe)-NH_2 over framework is mainly due to the increased interaction between the electric field of MOF and the quadrupole moment of CO_2 by the NH_2 functional group, as well as hydrogen bonding. Furthermore,the achieved heats of adsorption for MIL- 101(Fe), MIL-53(Fe) and MIL-101(Fe)–NH_2 were reported to be 36.6, 58.7, and 46.7 kJ mol^{-1}, this reveals that, in addition to physical adsorption of CO_2 by Amino-MIL-101(Fe), chemisorption of CO_2 by an NH_2 agent in the sorbent structure has a significant impact on the adsorption mechanism.

Effects of mixed BDC-NO_2 and BDC-NH_2 linkers on the adsorption and separation of CO_2 and CH_4 in Zr based metal organic frameworks (Zr-MOFs) was studied by **Z.H. Rada et al., 2018.** UiO-66 with single or binary -NO_2 and -NH_2 samples were synthesized under solvothermal conditions and activated by solvent exchange using methanol. UiO-66-NO_2-NH_2 10% and UiO-66-NH_2-NO_2 10% exhibited greater surface areas of 867 m^2g^{-1} and 1152 m^2g^{-1}, than single linker functionalized samples UiO-66-NO_2 and UiO-66-NH_2, which had surface areas of 771 m^2g^{-1} and 1025 m^2g^{-1}. Mixed UiO-66-NH_2-NO_2 10% exhibited higher CO_2 and CH_4 uptakes than single UiO-66-NH_2, but UiO-66-NH_2-NO_2 75% exhibited lower CO_2 and CH_4 adsorption values than UiO-66-NH_2. This is because high interconnection between the linkers of UiO-66-NH_2-NO_2 75% leads to decrease in their surface area whereas the surface area and porosity of UiO-66-NH_2-NO_2 10% are increased. This shows that adding a limited amount of BDC-NO_2 group can improve the structure's affinity for CO_2 and boost the polarity of the linker. This is attributed to dipole-quadrupole interaction of extremely polar -NO_2 groups with negative charge density on O atoms with the Lewis acidic C core of CO_2 molecules. It is concluded from this work that due to strong impact of electron withdrawing nature of the nitro group, addition of BDC–NO_2 to UiO-66-NH_2 improves the selectivity while addition of BDC-NH_2 to UiO-66-NO_2 can result in a lower selectivity.

In CO_2 capture, **David Britt et al., 2009** reported on the rival competing material Mg-MOF -74 with open metal sites. They conducted breakthrough studies to determine Mg-CO_2 MOF-74's adsorption capacity, and the resulting breakthrough curve shows that Mg-MOF-74 completely separates CO_2 from the CH_4 stream. This experiment reported that Mg-MOF-74 takes up 8.9 wt. % CO_2 before breakthrough, corresponding to 0.44 molecules of CO_2 per magnesium

ion which equates to a volumetric capacity of 81 g of CO_2 per liter of adsorbent. The Zn-MOF-74 structure is structurally identical to the Mg-MOF-74 structure, with the exception of the metal that absorbs just 0.35 percent of CO_2, a 96 percent reduction over Mg-MOF-74. Successive breakthrough experiments reveal that Mg-MOF-74 retains a capacity of 7.8 wt. % after this room temperature regeneration process, 87% of its intrinsic capacity. Further cycling does not lead to further reduction of capacity. This result implies that the metal ion is certainly the key factor in CO_2 binding. Following a series of breakthrough experiments, it is concluded that Mg-MOF-74 can maintain a capacity of 7.8% wt.%, or 87 percent of its intrinsic capacity.

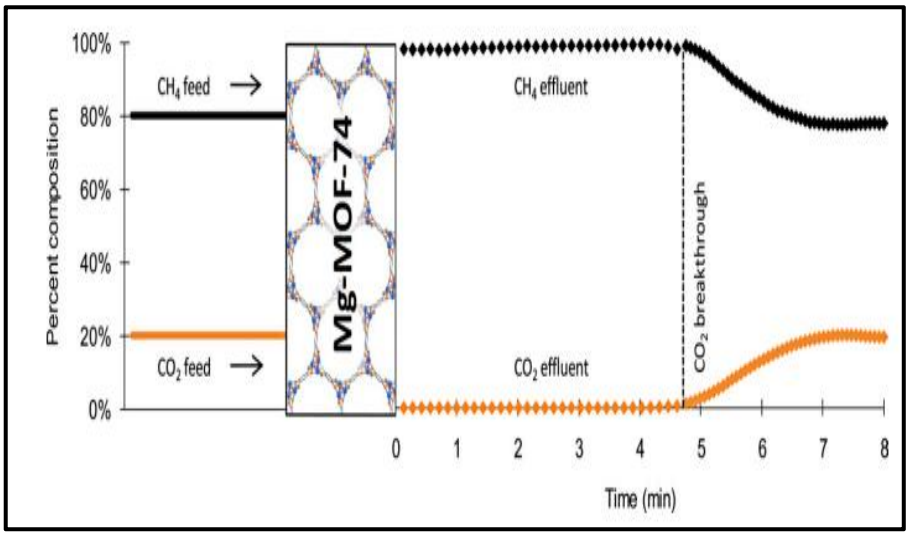

Fig:2.11 CO_2 Breakthrough Experiment

Yixing Li et al., 2019 used a solvothermal technique to make an effective Zn(Bmic)(AT) MOF by integrating the mixed ligands 5-aminotetrazole (HAT) and 1-benzimidazole-5-carboxylic acid (H_2Bmic). The type I adsorption isotherm of the produced Zn(Bmic)(AT) suggested the presence of persistent micropores. Zn(Bmic)-(AT) has a BET surface area of 444.3 m^2/g and a total pore volume of roughly 0.20 cm^3/g. At 273 and 298 K, the CO_2 adsorption capabilities of Zn(Bmic)(AT) were examined, demonstrating high CO_2 adsorption characteristics of 79 cm^3 /g at 273 K and 52 cm^3 /g at 298 K. Thus the plentiful NH2, non coordinating oxygen atoms, and many open metal sites (OMSs) in the crystal structure of Zn(Bmic)-(AT) make the accessible channels ideal for CO_2 adsorption. Zn(Bmic)(AT) is reported to have a Qst value of 28 kJ/mol, which is lower than MOF-5 (34 kJ/mol) and TEA@bio-MOF-1(Zn) (35 kJ/mol). Based on these characteristics, CO_2 adsorbed in Zn(Bmic)(AT) is easily released and regenerated.

Da-Ae Yang et al., 2011, prepared Mg-MOF-74 crystals in 1 h by sonochemical method after which triethylamine (TEA) was added as a deprotonating agent. The textural features of Mg-

MOF-74(S) (1640 m^2 g^{-1} BET surface area) were almost similar to those of a high-quality MOF sample synthesized in 24 hours using the solvothermal method (Mg-MOF-74(C), 1525 m^2 g^{-1}) but mesoporous were also generated, most likely as a result of TEA's competitive binding to Mg^{2+} ions. The adsorption isotherm for CO_2 of Mg-MOF-74(S) revealed a high adsorption capacity of 350 mg g^{-1} at 298 K. Breakthrough experiment also exhibits strong selectivity of CO_2 over N_2 at ambient circumstances. The adsorption capacity of Mg-MOF-74 did not decrease across ten adsorption–desorption cycles at 298 K, indicating its strong stability under humid conditions.

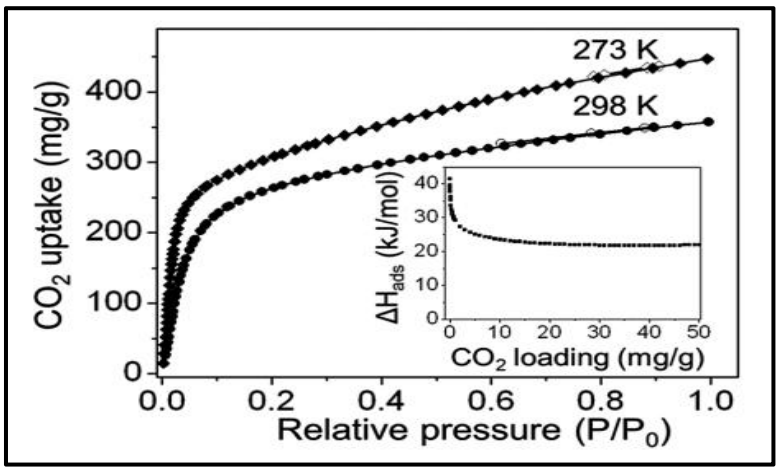

Fig: 2.12 CO_2 adsorption–desorption isotherms of Mg-MOF-74(S) at 273 and 298 K

Caitlin E. Bien et al., 2018 presented on the Zn benzotriazolate MOF[$Zn(ZnO_2CCH_3)_4$ $(bibta)_3$] which has been exposed to a mild $CH_3CO_2^-$ /HCO_3– ligand exchange method followed by thermal activation to yield biomimetic Zn–OH species. When exposed to 5% CO_2 in N_2 and pure CO_2 at 300 K, the MOF exhibited CO_2 uptakes of 9 and 14 wt%, respectively. On examining CO_2 uptake capacity from mixture of gasses(395 ppm CO_2, 21% O_2, N_2)exhibited 5.8% weight percent uptake. In CFA-1, the distance between neighboring SBUs' Zn centers (7.7) is short enough to allow inter-cluster hydrogen bonding between coordinated ligands, facilitating CO_2 uptake at partial pressures relevant for trace CO_2 capture from air.

The assembly of oxygen-friendly Ba(II) ions with two comparable linkers, 2-(imidazol-1yl) terephthalic acid and 2-(1H-1,2,4-triazol-1-yl)terephthalic acid, gave two novel metal–organic frameworks (MOFs) [$Ba(L1)(H_2O)_2$]n.nH_2O (MOF 1) and [B $(H_2L_2)(-H_2O)_2$]n.0.5nDMF.0.5nH_2O (MOF 2) which was synthesized by **Ying Zhao et al., 2020** MOF -1 is a three-dimensional (3D) stacking dense network, whereas MOF 2 presents a 3D nanotube porous framework with cylindrical tunnels developed by replacing the imidazole group in the ligand with a triazole group.

Due to which MOF 2 posses a larger density of active sites and Lewis acid sites in the porous surface and its selectivity of CO_2 over CH_4 was measured at 195, 273 and 298 K and found to be 146.7, 101.01, and 55.08 cm^3g^{-1}, respectively. Further only a small amount of CH_4 is captured by MOF 2a. The rationale for this is that the kinetic diameter of CO_2 (0.33 nm) is less than that of CH_4 (0.38 nm), which may help boost CO_2 uptake. The Ba(II) ions, as well as the abundant uncoordinated N atoms trapped in the porous surface of the channels, are primarily responsible for the high separation of CO_2, causing the highly polar host framework and the guest CO_2 molecules to be tightly interlocked while also enhancing the electrostatic interactions of the porous surface and CO_2 species.

The assembly of oxygen-friendly Ba(II) ions with two comparable linkers, 2-(imidazol-1yl) terephthalic acid and 2-(1H-1,2,4-triazol-1-yl)terephthalic acid, gave two novel metal–organic frameworks (MOFs) $[Ba(L1)(H_2O)_2]n.nH_2O$ (MOF 1) and $[B\ (H_2L_2)(-H_2O)_2]n.0.5nDMF.0.5nH_2O$ (MOF 2) which was synthesized by **Ying Zhao et al., 2020** MOF -1 is a three-dimensional (3D) stacking dense network, whereas MOF 2 presents a 3D nanotube porous framework with cylindrical tunnels developed by replacing the imidazole group in the ligand with a triazole group. Due to which MOF 2 posses a larger density of active sites and Lewis acid sites in the porous surface and its selectivity of CO_2 over CH_4 was measured at 195, 273 and 298 K and found to be 146.7, 101.01, and 55.08 cm^3g^{-1}, respectively. Further only a small amount of CH_4 is captured by MOF 2a. The rationale for this is that the kinetic diameter of CO_2 (0.33 nm) is less than that of CH_4 (0.38 nm), which may help boost CO_2 uptake. The Ba(II) ions, as well as the abundant uncoordinated N atoms trapped in the porous surface of the channels, are primarily responsible for the high separation of CO_2, causing the highly polar host framework and the guest CO_2 molecules to be tightly interlocked while also enhancing the electrostatic interactions of the porous surface and CO_2 species.

Rahul Maity et al., 2019 described two new water-stable amine functionalized MOFs, IISERP-MOF26 ($[NH_2\ (CH_3)_2]$) and IISERP-MOF27 ($[NH_2\ (CH_3)_2]$). IISERP-MOF27 ($[NH_2\ (CH_3)_2]$) and $[Cu_2O(Ad(BDC)](H_2O)_2$ (DMA) 1/2 $[Zn_4O(Ad)_3\ (BDC)_2\ ] \cdot(H_2O)_2$ (DMF)1/2. The free amine group from the adenine and the polarizing oxygen atoms from the terephthalate units decorate the above 1D channels. Furthermore, dimethyl ammonium (DMA^+) cations are present in the pore, creating an electrostatic environment within the channels. The surface areas of Brunauer-Emmett-Teller (BET) and Langmuir were calculated to be 210.6 and 481.1 m^2g^{-1}, respectively. With high CO_2 /N_2 and moderate CO_2 /CH_4 selectivity, activated Cu- and ZnMOFs physisorbed around 2.7 and 2.2 $mmolg^{-1}$ of CO_2, respectively. The predicted heat of adsorption

(HOA=21–23 kJmol@ 1) for CO_2 in both MOFs suggests excellent physical interactions, which is supported by their simple CO_2 on-off cycling. Both MOFs keep their crystallinity and porosity after soaking in water for 24 hours and after being exposed to steam for the same amount of time. These MOFs are potential sorbents for selective CO_2 capture applications because of their exceptional thermal and chemical stability, favorable CO_2 uptakes and selectivity.

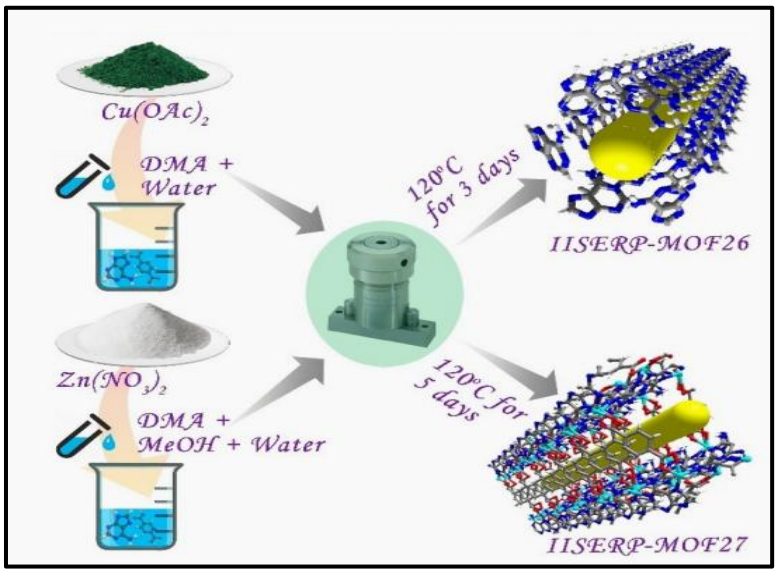

Fig: 2.13 Reaction Scheme for the synthesis of IISERP-MOF26 and IISERP-MOF27

Zhaolin Shi et al., 2020 described a method for adding amino groups to the triazolate linkers of MOFs to improve chemical stability in aqueous, acidic, and basic environments. CO_2 adsorption isotherms at 195 K revealed type I adsorption isotherms, confirming the frameworks' permanent porosity. Because of their distinct adsorptive sites at the channel center for CO_2 and at the corner for H_2O, these MOFs display not only CO_2/N_2 thermodynamic adsorption selectivity of up to 120 which is 8 times higher than that of pristine ZnF(TZ), but also CO_2/H_2O kinetic adsorption selectivity of up to 70. This research suggests that ZnF(daTZ) MOF can be used as designable solid adsorbents for CO_2 capture in high-humidity flue gasses with little energy input.

Kang Zhang et al., 2016 created 120 Zr-MOFs from 40 topological nets, utilizing Zr_6O_8 and tetrazolate as basic building blocks, and then evaluated their CO_2 capture performance.They compared the performance of carboxylate and tetrazolate-based Zr-MOFs, which have the same structure, Zr_6O_8 cluster, and organic building unit; the only difference is that the Zr_6O_8 cluster is coordinated with either tetrazolate or carboxylate. When compared to its carboxylate analog, each tetrazole MOF has a substantial increase in CO_2 absorption. This supports the idea that N-rich tetrazolate can help with CO_2 adsorption.

Changwei Chen et al., 2018 used hydrothermal (HT), condensation reflux (CE), and microwave assisted (MW) techniques to create a range of MOF-74 (Ni) materials with narrow micropore channels and abundant unsaturated metal sites. Isotherm and dynamic adsorption studies revealed that the MW technique is a quick and easy way to make MOF-74 (Ni) materials with a high CO_2 capture capacity of 5.22 mmol/g at 25 °C, which is nearly 6 times greater than commercial activated carbon (0.89 mmol/g). Under humid conditions (RH = 90%), dynamic adsorption studies revealed that the MW-140 material has the maximum CO_2 adsorption capability of 3.37 mmol/g. The synergistic impact of plentiful narrow micropore channels and rich five-coordinated Ni^{2+} open metal sites is attributed to excellent capture potential.

MOF-199 was designed and built using a solvothermal technique by **Rana Th. A. Alrubaye et al., 2019.** The BET specific surface areas and pore volumes reported were 5518 m^2g^{-1} and 0.609 cm^3g^{-1}, respectively. Over a pressure range of 0-5 bar, the experimental adsorption isotherms of CO_2 on MOF-199 were measured at (36, 40, 60, 70 ^oC). As the temperature rises, the adsorption capability of MOF-199 falls. The high adsorption capacity of 4.9 mmol/g was obtained in this work at 5 bar and 36 ^oC. That's because as the temperature rises, the CO_2 adsorbed on the MOF-199 surface becomes unstable due to enhanced molecular diffusion, which causes more CO_2 molecules to desorb.

Midhun Mohan et al., 2020 constructed three novel lanthanide metal organic frameworks - La(III), Ce(III), and Pr(III) labeled IRHs-(13) supported by cyamelurate linkers, which comprises a large number of heteroatoms (O and N atoms) increases the bonding force between the host and guest, favoring carbon dioxide (CO_2) adsorption over methane (CH_4). CO_2 is largely adsorbed on the walls made of organic linkers and around the metal sites, whereas CH_4 has no distinct adsorption site. At 298 K, single-component sorption isotherms for CO_2 and CH_4 for all activated IRHs indicate a significant rise in adsorption capacity reaching 2.6, 3.1, and 2.8 mol/kg for CO_2 whereas CH_4 uptake is minimal. The ideal adsorbed solution theory (IAST) at 25 °C and 1 bar predicted that the CO_2/CH_4 binary mixture would have excellent selectivity of 2.7 and 0.07 mol/kg and the predicted selectivity for CO_2/CH_4 (1:1) was 27, which is among the best values for MOF materials.

Incorporating multiwalled carbon nanotubes into MOF-199, **Samira Salehi et al., 2017** created CNT@MOF-199, which has a higher micropore volume, increased gas storage capacity, and improved stability than MOF-199. On subjecting to isotherm measurements (CO_2 and CH_4) at 298, 323, and 348 K it was revealed that the amount of CO_2 adsorbed was much more than the

amount of CH_4. This is because it has a significant quadrupole moment, which is why it interacts strongly with the adsorbent, whereas CH_4 has neither a dipole nor a quadrupole moment. By introducing amine groups, the adsorption capacity and selectivity of CNT@MOF-199 for CO_2 over CH_4 can be increased. Impregnation with varied loadings of PZ (10, 20, and 30 wt percent) was used to carry out adsorbent functionalization. When the percentage ratio of PZ was increased from 10 to 30 wt percent, the adsorption capacity for CO_2 on all adsorbates increased noticeably. This is indicative of the fact that the amine sites on this adsorbent have a high affinity for CO_2 molecules.

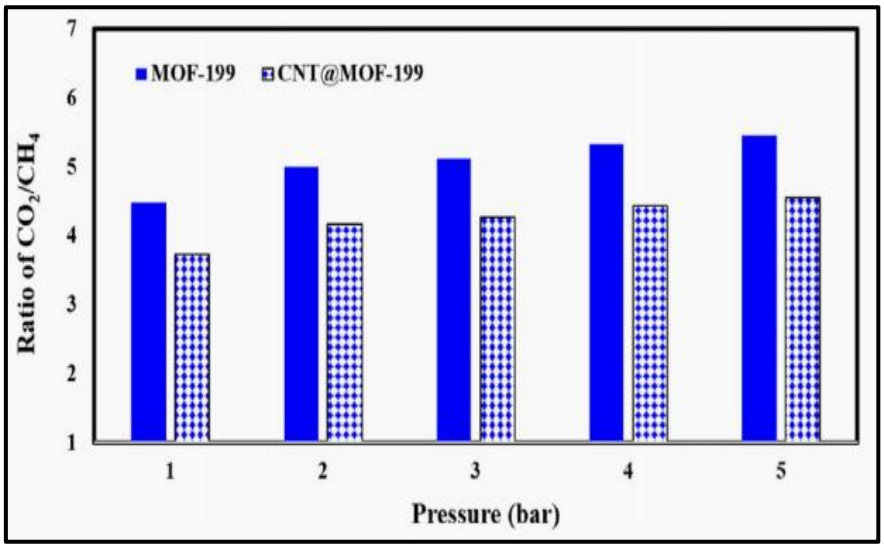

Fig:2.14 Adsorption selectivities of CO_2/CH_4 on MOF-199 and CNT@MOF-199 at 298 K and diffffferent pressures

The mixed-ligand Cd(II)-framework $[Cd1.5(L)_2(bpy)(NO_3)].2DMF.2H_2O$ (CSMCRI-5) was reported by **Manpreet Singh et al., 2020**; HL = 4-(4- carboxyphenyl)-1,2,4-triazole, bpy = 4,4′-bipyridine). It had a BET surface area of 168 m^2 /g . At 273 and 298 K, it exhibited maximum CO_2 uptakes of 35.7 cm^3 /g (1.59 mmol/g) and 24.7 cm^3 /g (1.10 mmol/g), respectively. At 273 K, the sorption behaviors toward additional gasses (N_2 and CH_4) were investigated, revealing that CH_4 absorption was 7.32 cm^3 /g (0.32 mmol/g) while N_2 adsorption was minimal. The better interaction between uncoordinated triazolyl nitrogen atoms oriented along the porous channels and polar CO_2 molecules is ascribed to this. Even after five uptake release cycles, the MOF's resilience toward multicyclic CO_2 collection is outstanding.

Xiuling Zhang et al., 2020 solvothermally assembled two-fold interpenetrated pillared double-walled-layer Co(II)-based framework by employing mixed-ligand 4,4',4"-nitrilotribenzoic

acid & 1,4-bis(pyrid-4-yl)benzene with Brunauer-Emmett-Teller (BET) of 490m^2g^{-1}. The corresponding mof reveals a CO_2 uptake amount of 65.9 cm^3g^{-1} at 273 K and 39.8 cm^3g^{-1} at 298 K. CO_2/CH_4 selectivity is 5.5 at 273 K and 7.0 at 298 K, and CO_2/N_2 selectivity is 18.0 at 273 K and 66.7 at 298 K, according to an ideal adsorbed solution theory (IAST) calculation. The strong contact between adsorbed CO_2 molecules and the framework, which is induced by unsaturated Co^{3+} centers and narrow pores through framework interpenetration attributed to this superior CO_2 separation results.

NH_2–MIL–101, an amine functionalized vanadium-based metal–organic framework (MOF) material was solvothermally synthesized by **Qionghao Xu et al., 2020**. MIL–101(V) and NH_2–MIL–101(V) had BET surface areas of 2623 m^2 /g and 2340 m^2 /g, respectively. At 25 °C and 100 kPa, the synthesized NH_2–MIL–101(V) had a CO_2 uptake capacity of 1.9 mmol/g, which was higher than the adsorption capacity (1.4 mmol/g) of MIL–101(V) under the same conditions. In NH_2–MIL–101(V), the selectivity of CO_2 over N_2 was as high as 10:1. Because CO_2 has a substantially greater quadrupole moment than N_2, it was more strongly absorbed in NH_2–MIL–101(V).

Yunus Güclu et al., 2021 solvothermally synthesized a variety of novel CO_2-philic oxalamide-functionalized MOFs,(Zn-OATA),(Cd-OATA), and (Co-OATA) (H_4OATA = N,N′-bis(3,5-dicarboxyphenyl)oxalamide). These novel MOFs have CO_2-philic oxalamide groups on their channels and open metal sites. Cu-OATA has a substantial CO_2 adsorption capacity of 25.35 wt% (138.85 cm^3 /g) at 273 K and 9.84 wt% (50.08 cm^3 /g) at 298 K under 1 bar, with an isosteric heat of adsorption (Qst) of around 25 kJ/mol. Cu-OATA absorbed 25.35 wt% CO_2 at 273 K and 9.84 wt% at 298 K, 1 bar. Cu-OATA's isosteric heat of adsorption at 0% coverage was calculated experimentally to be 58 kJ/mol, which is one of the best values among the known MOF type adsorbents. Furthermore, at 0.1 pressure and 298 K, Cu-OATA had a very high selectivity of 5.2 for CO_2/CH_4 separation and 44.6 for CO_2/N_2 separation. The doubly interpenetrated framework of Cd-OATA exhibited a CO_2 adsorption of 11.90 wt % at 273 K and 2.26 wt % at 298 K, 1 bar. This work reveals that the presence of CO_2-philic and flexible oxalamide groups in MOFs is insufficient to promote CO_2 adsorption and separation at room temperature. Apart from the functionalization of MOFs with CO_2-philic groups, the kind of metal ions and topological aspects of frameworks are also critical for improving CO_2 sorption qualities.

Jiewei Liu et al., 2020 reported the in situ synthesis of Au nanoparticles in the coordination interspaces of Ir-PCN-222, resulting in a porphyrin metal-organic framework

composite Au@Ir-PCN-222. The adsorption behaviors of Ir-PCN-222 and Au@Ir-PCN-222 towards CO_2 at different temperatures (e.g. 298 and 308 K) are investigated, and it is discovered that both Ir-PCN-222 and Au@Ir-PCN-222 have a high CO_2 adsorption capability at 1 bar, but Au@Ir-PCN-222 has a higher adsorption performance. This is due to the accumulation of Au NPs to the interior cavities of Ir-PCN-222, which has a stronger affinity with CO_2 molecules than Ir-PCN-222.

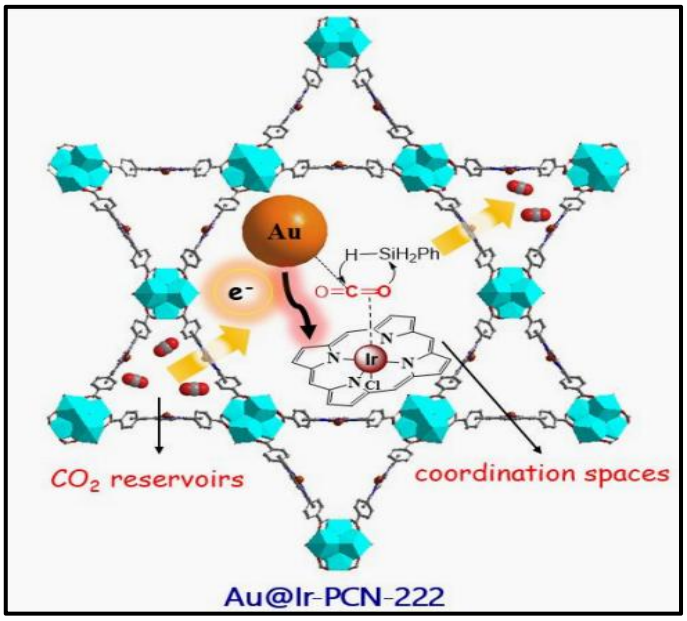

Fig:2.15 CO_2 adsorption, diffusion and activation in the inner cavities of Au@Ir-PCN-222

Yong-Zhi Li et al., 2021 used a bipyridyl-substituted isophthalic acid ligand to create a novel metal organic framework (MOF), [Ni(dpip)]2.5DMFH_2O, which has two types of tubular channels decorated by various carboxylate O atoms and aryl rings in organic groups. The selectivity values for CO_2/CH_4 combinations are in the range of 7.59.1 at 298 K and 100 kPa, which is greater than those of other MOFs. Furthermore, under ambient conditions (298 K, 1 atm), breakthrough tests revealed excellent separation performance for C_2H_4/CH_4, C_2H_2/CH_4, and CO_2/CH_4 mixtures, with separation factors of 7.1, 7.8, and 2.9, respectively, as well as efficient separation for C_2H_2/CO_2 mixtures, with a separation factor of 2.6.

Fangyuan Gai et al., 2021 created MOF (ZIF-8)-derived N-doped porous carbons (NPCs) by co-carbonizing and activating ZIF-8 with pomelo peel, during which the pomelo peel may effectively prevent nitrogen loss from the ZIF-8 backbone by pre-melting and polymerization while also providing the optimum porosity and BET surface area to create high-performance

CO2 adsorbent. The sample NPC-800-4 generated at 800°C had both ultrahigh surface area (1967 m^2 g^{-1}) and high N content after tweaking the ZIF-8 loading capacity and activation temperature (B13.15 wt percent). Due to its comparatively high amount of pyrrolic-N (N5 B 61.2 percent) and pyridinic-N (N6 B 16.5 percent), as well as the correct pore size distribution(0.64 nm), CO_2 capacity of NPC-800-4 attained 5.51 mmol g^{-1} at 25 ˚C and 9.01 mmol g^{-1} at 0 ˚C under 1 bar. NPC-800-CO_2 4's adsorption energy (Qst) also indicated a high desorption activation temperature and energy, implying a substantial CO2 binding capacity. Furthermore, in 8 successive adsorption–desorption cycles, NPC-800-4 showed practically consistent CO_2 absorption, showing that the sample has excellent stability and recyclability.

Jiao Liu et al., 2020 developed a new monometallic metal–organic framework (MOF), $[Pb_2(L)_2(H_2O)].H_2O$ (MOF-1) using N, O-mixed 2-(imidazol-1-yl)terephthalic acid (H_2L) ligand. Because of the varied coordination affinity of oxygen and nitrogen atoms with various metal ions of MOF-1 by using it as the precursor a first novel porous d–p heterometallic MOF (HMOF), namely $[PbZn(L)_2].DMA.H_2On$ (2), was synthesized using Zn(II) ions. MOF 1 is a condensed packing motif, whereas HMOF 2 is a porous three dimensional (3D) framework with unsaturated Pb(II) and Zn(II) active sites, uncoordinated carboxylate oxygen atoms, and two kinds of porous channels due to the introduction of Zn(II) ions into the framework of MOF 1, endowing HMOF 2 with excellent sorption and selectivity for CO_2 over CH_4. BET and Langmuir surface areas are 221 and 611 m^2 g^{-1}. It has a higher sorption capacity of 39.3 cm^3 g^{-1} (7.8%) at 273 K and 25.5 cm^3 g^{-1} (5.0 wt%) at 298 K, which is better than monometallic Zn(II) or Pb(II)-based MOFs with similar void volume at 298 K. As a result, the CO_2/CH_4 selectivity ranges from 4.5 to 16.3 at 298 K, which is better than many other MOFs with polar pores or open metal sites that have been reported.

Arman Soleimanpour et al., 2021 used the solution mixing approach to generate a new composite based on activated carbon and MIL-53(Al) at various MOF weight fractions. In the isothermal batch and continuous apparatus, the CO_2 adsorption capability of composite was investigated. Activated carbon and composite frameworks containing 10% and 30% MOF had CO_2 adsorption capacities of 1.46, 1.608, and 1.792 mmol gr1, respectively. In comparison to activated carbon, synergic mixing of MIL-53(Al) with activated carbon in composite 10% increased CO_2 loading capacity by 10.1 percent while decreasing N_2 loading capacity by roughly 11.78 percent. This work revealed that increased MOF content in the synthesized composite improves CO_2 selectivity.

Gouri Chakraborty et al., 2021 utilizing a dual - ligand method comprised of tetrakis(4-pyridyloxymethylene)methane and dibenzothiophene-5,5′-dioxide-3,7-dicarboxylic acid synthesized polar sulfone-appended copper(II) metal−organic framework (MOF; 1). The Brunauer−Emmett−Teller surface area was reported to be 385 m^2 g^{-1}. Lewis acidic open-metal sites, as well as polar sulfone groups oriented on the pore walls, were also detected. Under flue gas combustion circumstances, MOF 1 has a significant absorption of CO_2 over N_2 and CH_4, with a strong selectivity for CO_2/N_2 (15:85). The presence of both Lewis acidic Cu(II) centers as well as polar sulfone groups and free O atoms can be attributed to these high CO_2 uptake values. It is also reported to have exceptional recyclability for repeated CO_2 sorption investigations.

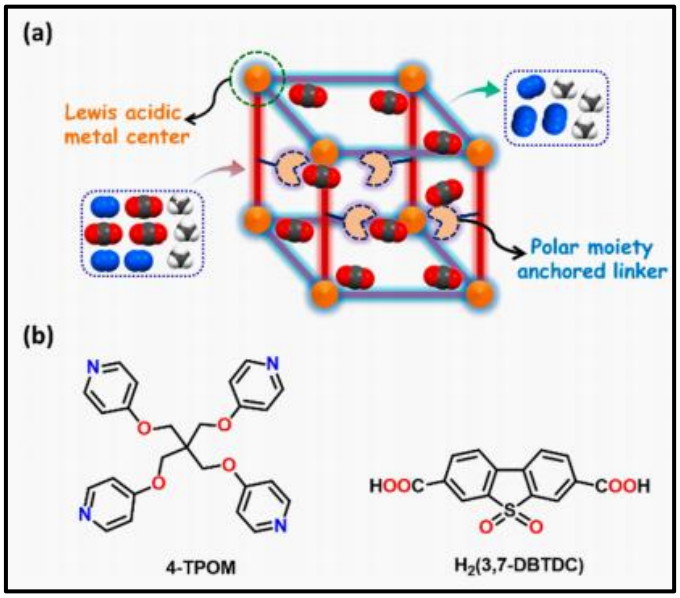

Fig:2.16 (a) Schematic Representation of an MOF with Features Required for Selective CO_2 Capture and (b) Chemical Structures of 4-TPOM and H_2(3,7-DBTDC)

Using grand canonical Monte Carlo simulations, **Genjian Xu et al., 2019** explored CO_2 capture and separation from CO_2/CH_4, CO_2/CO, and CO_2/H_2 mixtures in selected metal–organic frameworks (MOF-177, MOF-180, and MOF-200) and their C60-impregnated derivatives. When CO_2 separation from CO_2/CH_4, CO_2/CO, and CO_2/H_2 mixtures is simulated, it is discovered that C60 impregnation greatly enhances separation performance, with the most notable improvement occurring at CO_2/H_2 separation at pressures ranging from 0.2 to 2.0 bars and 298 K. C60@MOF-177 is also said to outperform C60@MOF-180 and C60@MOF-200 in CO_2/CH_4, CO_2/CO, and CO_2/H_2 separations. Greater CO_2 adsorption heat and more adsorption sites due to increased surface area are responsible for this improvement

Xiaokang Wang et al., 2020 reported on a novel Ba-MOF (UPC-70)[$H_2N(CH_3)2$]0.5[Ba1.5(L)(DMA)] 1.5DMA 1.5H_2O (UPC-70, H_3L = 2-(4-carboxy-2 methylphenyl)-1,3- dioxoisoindoline-5,6-dicarboxylic acid, DMA = N,N-dimethylacetamide), generated on the basis of the partial hydrolysate. After removing the solvents, the as-synthesized 3D network with 1D open channels of various diameters (24 and 10) comprises a large number of open metal sites, which favors CO_2 adsorption. UPC-70 exhibited distinct capacities for CO_2 (0.53 mmol/g), CH_4 (0.07 mmol/g), and N_2 (0.03 mmol/g) at 1 atm and 298 K. The adsorbed quantities of CO_2, CH_4, and N_2 at 273 K are 0.68, 0.18, and 0.04 mmol/g, respectively. CO_2 adsorption quantities are clearly higher than those of CH_4 and N_2 at both temperatures and 1 atm, which can be attributed to the combined effect of small pore size, the presence of methyl functional groups, and $[NH_2(CH_3)_2]^+$ on the microporous surface.

Sandeep Singh Dhankhar et al., 2018 created a porous, three-dimensional Co(II) metal–organic framework with a stiff, tetratopic H_4TCPB ligand. Based on the CO_2 adsorption isotherm performed at 273 K, the predicted BET and Langmuir surface area of MOF1 was found to be (87.6 $m^2\ g^{-1}$ & 199.1 $m^2\ g^{-1}$). It was calculated that the isosteric heat of adsorption (Qst) for CO_2 is 35.4 kJ mol^{-1}. MOF1 adsorption tests with other gasses (H_2, Ar, and N_2) revealed insignificant absorption with 0.27, 0.15, and 0.24 mmol g^{-1} of N_2, H_2, and Ar, respectively, and the estimated selectivity values for CO_2/H_2, CO_2/Ar, and CO_2/N_2 were 52, 36, and 33. The higher interaction of carbon dioxide with the unsaturated Co(II) metal sites lined in MOF1's 1D channels, owing to its high polarizability and substantial quadrupole moment (1.4×10^{-39} Cm^2) over other gasses, might be attributed to MOF1's selective CO_2 adsorption capability (N_2, Ar and H_2).

Hai-Hua Wang et al., 2015 created a 3D cationic metal–organic framework (MOF) [Mn_2(Hcbptz)$_2$ (Cl)(H_2O)]ClDMF0.5CH_3CN with an unique (3,4)-connected 3,4T1 topology and 1D cavities. At 298 K N_2, CO_2, and CH_4 sorptions revealed little adsorption for N_2 (2.2 $cm^3(STP)g^{-1}$) and low CH_4 uptake (15.3 $cm^3(STP)g^{-1}$), but an exceptionally high CO_2 loading of 70.1 $cm^3(STP)g^{-1}$, this high CO_2 capture is attributed to the cationic framework, exposed metal centers, accessible N sites, and Cl^- basic anions which induce strong affinity towards CO_2. It also exhibits strong CO_2/N_2 selectivity, reaching 177.4 at 298 K and 1 atm for an equimolar CO_2/N_2 combination. At 298 K, it is likely to show strong CO_2/CH_4 selectivities of 10.3 and 8.8 for binary mixtures containing 50 and 5% CO_2. The high selectivity is due to the pores distinctive properties, which include exposed metal sites, N-rich aryl units, cationic framework, and Cl^- anions, as well as many CO_2 -philic sites. Because of its huge quadrupole moment and strong polarizability, they make the framework highly polar and subject it to particular interactions with CO_2.

Sanjit Gaikwad et al., 2021 improved the CO_2 adsorption capability of MOF-177 by utilizing three distinct amines: polyethyleneimine (PEI), tetraethylenepentamine (TEPA), and diethylenetriamine(DETA). The adsorption kinetics were used to assess the CO_2 adsorption capability of the amine-modified MOF-177 samples. The TEPA-modified MOF-177 powders showed a considerable improvement (4.8 times) in CO_2 adsorption capacity at 298 K compared to the parent MOF-177, even at 20% loading, while the PEI and DETA-modified samples showed only marginal improvements. CO_2 adsorption capacity is enhanced with increasing temperature, reaching 4.6 mmol/g at 328 K, which is greater than previously reported amine modified adsorbents (1.6–3.8 mmol/g at 318–348 K). MOF-177 powders containing 20% TEPA were successfully converted into pellets, while capacity was slightly reduced. Adsorption - desorption cycles at 298 and 373 K were used to assess the regenerability of MOF-177-TEPA-20 percent pellet, which revealed consistent CO_2 capture capability.

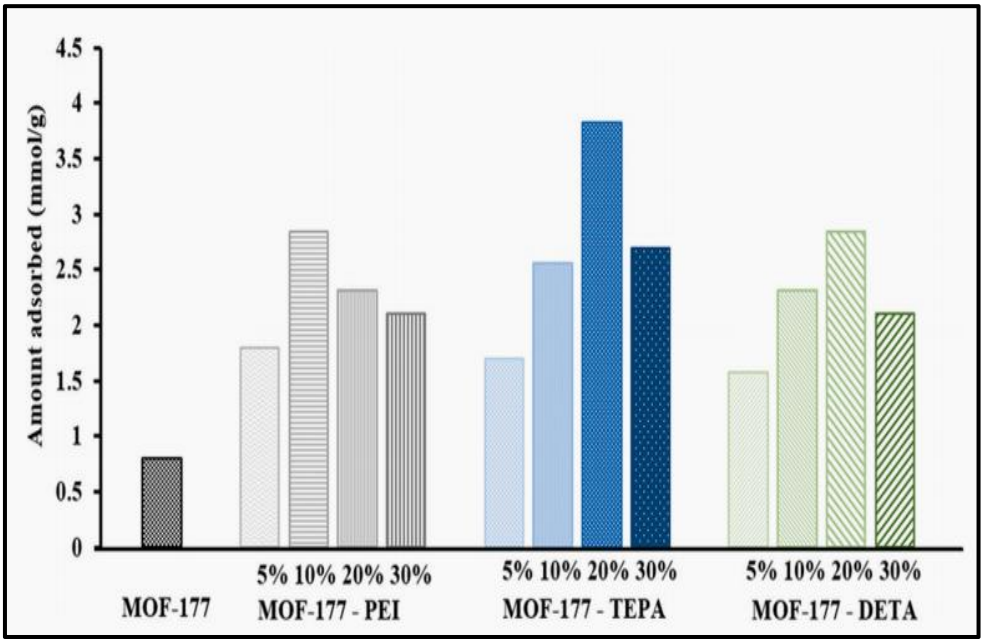

Fig: 2.17 CO_2 adsorption capacities of MOF-177, MOF-177-PEI, MOF-177-TEPA, and MOF-177-DETA powder samples at 298 K and 1 bar

From a nanosized linear diisophthalate ligand with linking acylamide groups and Cu(II)-paddlewheel clusters, **Baishu Zheng et al., 2018** developed and manufactured a highly porous acylamide functionalized MOF (HNUST-7), which has a (4, 4)-connected NbO-type 3D open framework with two different types of metal-organic cages, according to structural study. It is reported to have a high BET surface area of 2804 m^2g^{-1} after activation. HNUST-7 has significant CO_2 uptake capabilities of 26.1 and 19.4 mmol g^{-1} at 273 and 298 K, respectively, under 30 bar.

Furthermore, HNUST-7 has a very selective adsorption ability for CO_2 over CH_4 and N_2, with exceptional selectivity of 6.92 and 22.39 for the CO_2/CH_4 and CO_2/N_2 gas mixtures, at 273 K, indicating that HNUST-7 has significant potential for CO_2/CH_4 and CO_2/N_2 separations.

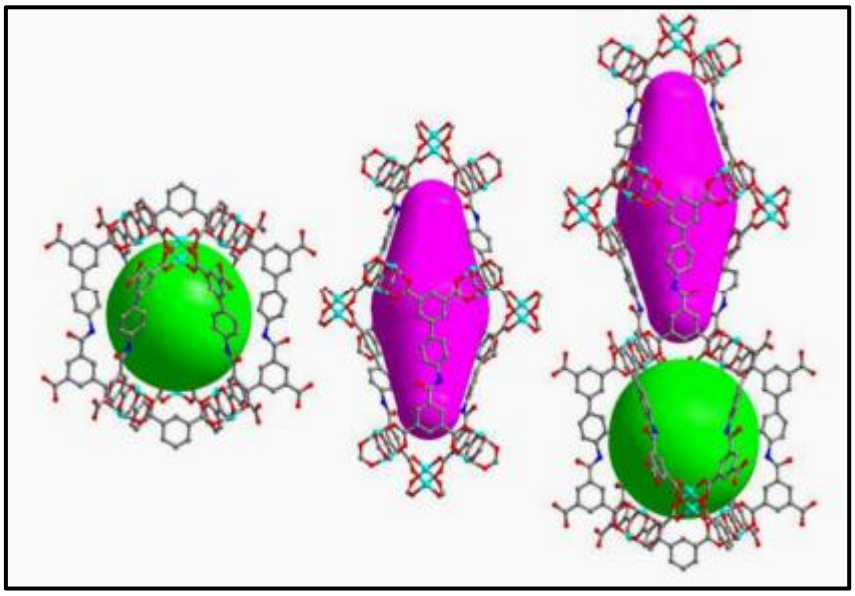

Fig: 2.18 Schematic representation of (4, 4)-connected MOF-505 type Network structure of HNUST-7, which contains two types of cages (the spherical and shuttle shaped cage)

Wenjuan Zhuang et al., 2011 investigated the solvothermal interaction of a flexible octatopic carboxylate ligand, tetrakis[(3,5-dicarboxyphenyl)- oxamethyl]methane with Cu(II) to produce a new MOF, $Cu_4(H_2O)_4$(TDM)xS - PCN-26xS. PCN-26 combines two types of cages, octahedral and cuboctahedral, to form a three-dimensional polyhedron-stacked framework with open channels in three orthogonal directions. It has a total pore volume of 0.84 cm^3/g, a Langmuir surface area of 2545 m/g, a Brunauer Emmett Teller (BET) surface area of 1854 m^2/g. Furthermore, a t 273 K, PCN-26 has a CO_2/N_2 selectivity of 49:1 and a CO_2/CH_4 selectivity of 8.4:1. This strong porous 3D MOF can also adsorbs 2.57 wt% H_2 (77 K and 760 Torr) and 109.1 cm^3/g CO_2 (800 Torr and 298 K). Based on these findings, it is concluded that the gas-adsorption selectivity of PCN-26 is greater than the majority of the reported values for MOF materials.

Junxiong Liao et al., 2020 created a microporous (3,24)-connected rht-type acylamide functionalized MOF(HNUST-9) using dicopper(II)-paddlewheel clusters and a novel C2-symmetric acylamide linking hexacarboxylate. Furthermore, the framework is densely packed with strong CO_2 binding sites, such as open copper(II) sites and acylamide groups. The framework has a moderate porosity, with a BET surface area of 2429 $m^2\ g^{-1}$ but it has an

extremely high excess CO_2 uptake capacity (21.8 mmol g- 1 at 25 bar and 273 K), as well as efficient CO_2 separation ability from CO_2/CH_4 and CO_2/N_2 binary gas mixtures under dynamic conditions at 1 bar and 298 K, respectively. These findings unequivocally show that the open copper(II) metal sites and the acylamide groups in HNUST-9 can both function as strong CO_2-philic sites and play an important role.

Ijlal Aamer et al., 2021 worked on pillared layer MOFs, which are pre-synthetic functionalized MOFs. DABCO (1,4-diazabicyclo[2.2.2] octane) is added to the MOFs Zn-BDC and Co-BDC as a pillar to construct 3D structured MOFs Zn-BDC-DABCO and Co-BDC-DABCO, and their performance in CO_2 capture applications was examined. When the pressure was increased to a maximum of 25 bar, the adsorption capacity of Zn-BDC-DABCO and Co-BDC-DABCO was 6.3 mmol g^{-1} and 4.4 mmol g^{-1} CO_2 respectively at room temperature, which is a significant increase when compared to the 0.95 mmol g^{-1} and 0.67 mmol g^{-1} of the Zn-BDC and Co-BDC, respectively. From these results it is confirmed that adding DABCO as a pillar to MOFs improves CO_2 adsorption. This is due to two basic parameters: (i) the pillar converts our 2D structure to a 3D structure, resulting in increased surface area and, as a result, increased adsorption capacity; and ii) because DABCO is an amino functionalized group, it increases the material's CO_2 affinity, resulting in increased adsorption capacity.

Jiajia Sun et al., 2019, created a new mixed-matrix material for CO_2 separation by incorporating a novel metal organic framework MOF-801 into a polyether-block-amide (PEBA) polymer. When compared to a pure PEBA membrane, the homogeneous integration of microporous MOF-801 with preferred CO_2 adsorption offered rapid and selective transport channels for CO_2 over N_2, resulting in an increase in both CO_2 permeance and CO_2/N_2 mixed-gas selectivity. Under mixed-gas permeation tests, the optimized MOF-801/PEBA mixed-matrix composite membrane (MOF loading of 7.5 wt%) demonstrated high and stable separation performance, with CO_2 permeance of 22.4 GPU and CO_2/N_2 selectivity of 66, indicating tremendous promise for practical CO_2 separation.

Shanshan Shang et al., 2020 synthesized CuBTC@GO using a mixed solvent strategy. When compared to conventionally synthesized CuBTC, the newly synthesized CuBTC had a much higher surface area and total pore volume. As a result, the as-synthesized CuBTC had a CO_2 adsorption capacity of 8.02 mmol/g at 273 K, 1 bar, which was 17–90% higher than the reported CO_2 capacity of CuBTC. The fabrication of CuBTC@GO composites increased CO_2 adsorption capacity primarily due to increased porosity and dispersion force. The binary breakthrough

experiments revealed improved CO_2/N_2 selectivity for CuBTC@1% GO compared to CuBTC, which is useful for practical gas separations. The cyclic adsorption experiments for regenerability evaluation revealed that the CO2 adsorption reversibility for CuBTC@1% GO composite could remain above 90% after five adsorption-desorption cycles, whereas CuBTC dropped to less than 74% after five adsorption-desorption cycles. Thus from this it has been concluded that the CuBTC@GO composite would be a promising CO_2 capture adsorbent due to its high CO_2 adsorption capacity and outstanding regeneration performance.

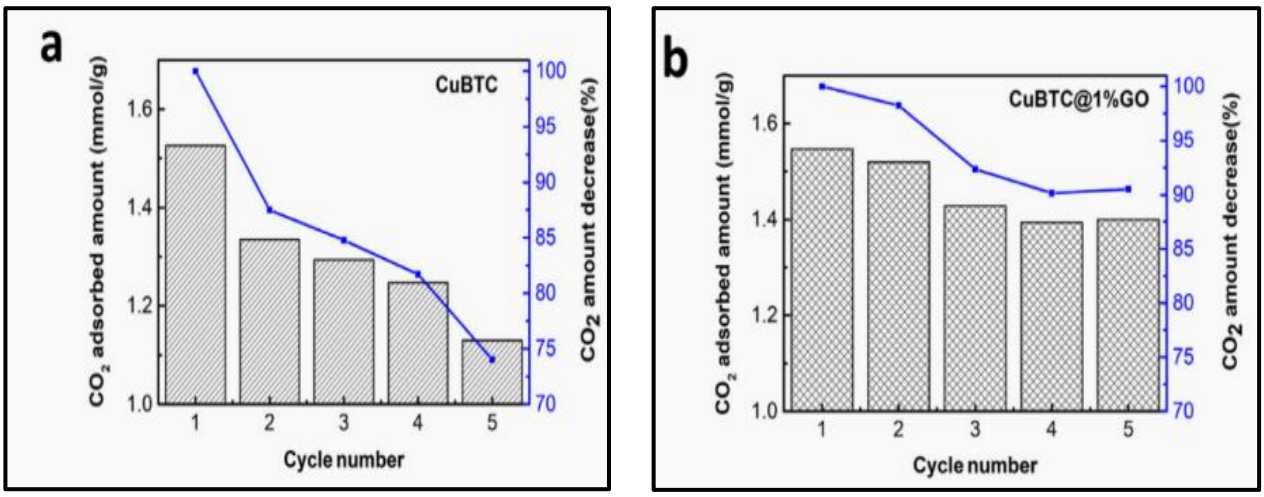

Fig: 2.19 CO_2 adsorption capacity for CuBTC and CuBTC@1%GO composite at 298 K and 1 atm over multiple cycles of adsorption-desorption process.

Mani Ganesh et al., 2014 created a novel Zr-fum metal organic framework by reacting zirconium chloride and fumaric acid under solvothermal conditions without the use of a formic acid modulator and evaluated it for CO_2 adsorption. The material could withstand temperatures of up to 300°C. At 25°C and 1 bar of pressure, the amount of physisorbed CO_2 by Zr-fum MOF was 8 wt% (1.818 mmol/g). As a result, it is concluded that the synthesized Zr-fum MOF could be employed as a sorbent for CO_2 capture and storage after combustion.

Wufeng Wu et al., 2019 describe a versatile polydopamine(PDA) grafting post modification technique for improving CO_2 separation performance of MOF membranes. A simple and delicate method is used to implant PDA on the UiO-66 membrane. The CO_2/N_2 and CO_2/CH_4 selectivities of the modified PDA/UiO-66 membrane are 51.6 and 28.9, respectively, which are 2-3 times greater than the previous MOF membranes with similar permeance. Meanwhile, because PDA alteration has no effect on UiO-66 intrinsic pores or membrane thickness, the CO_2 permeance is up to 3.7×10^{-7} mol m^{-2} s^{-1} Pa^{-1} compared to membranes with similar selectivity.

Furthermore, the PDA/UiO-66 membrane shows outstanding long-term stability for CO_2 capture under moist conditions in 36 hours of measurement.

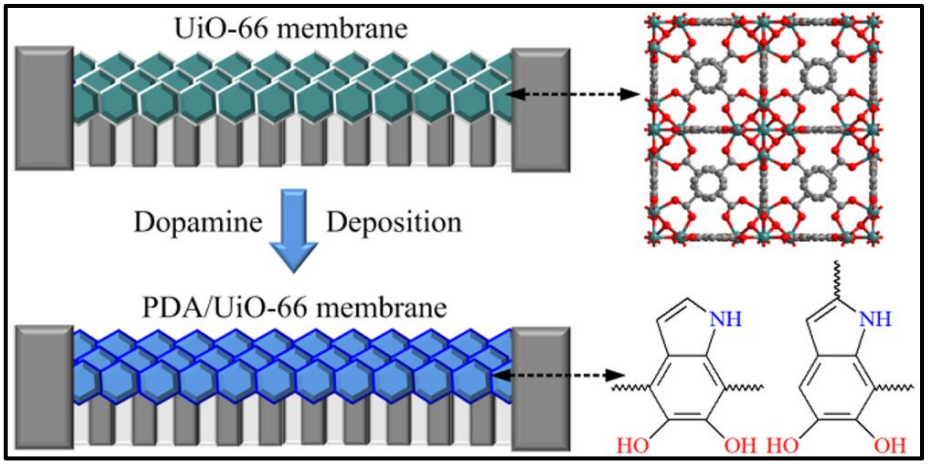

Fig: 2.20 Postmodification of the UiO-66 membrane by PDA

Through the use of alkali-philic tetrazole-based assemblies as binding sites, **Na Li et al., 2019** developed a new approach for immobilizing alkali metal ions (K^+) in MOFs. This approach was used to create NKU-521a, which has particular K^+ binding sites that act as CO_2 traps and successfully facilitate CO_2 sorption and separation. K^+ cations are efficiently anchored in a trinuclear Co^{2+}-tetrazole coordination motif of NKU-521a(NKU = Nankai University). Water removal exposes the embedded K^+ sites to the pores of NKU-521, and the isosteric heat (Qst) for CO_2 is increased to 41 kJ mol^{-1}. The K^+ cations act as gas traps, increasing CO_2-framework affinity by 24 percent as assessed by the Qst. The initial selectivities for CO_2:CH_4 and CO_2:N_2 at 298 K are higher than most previously reported MOFs under the same circumstances. NKU-521a has CO_2/CH_4 selectivities of 45 (10/90) and 36 (50/50) at 273 K and 24 (10/90) and 22 (50/50) at 298 K, which are greater than numerous well-known MOFs at 273 K and a 50/50 gas mix, including HKUST-1, MIL-53(Al), UTSA-16, and SIFXIS-2-Cu-i. CO_2/N_2 (15:85) selectivities are 170 at 273 K and 51 at 298 K, which is greater than most reported MOFs under similar conditions.

Zhaoqiang Zhang et al., 2021, presented a novel anion-functionalized ZU-16-Co(TIFSIX-3-Co, TIFSIX=hexafluorotitanate (TiF6 2−), 3=pyrazine)with one-dimensional pore chann els adorned with numerous F atoms for effective CO_2 extraction at 400–10,000 ppm. ZU-16-Co with a fine-tuned pore size of 3.62Å demonstrates the maximum CO_2 uptake at 0.01 bar (10,000 ppm) and 1 bar (2.63 and 2.87 mmol g−1, respectively). The fine-tuned pore dimensions with strong F···C=O host-guest interactions and comparatively large pore volumes resulting from

the longer coordinated Ti–F– Co distance (3.9Å) give ZU-16-Co its high CO_2 capture potential. Dynamic breakthrough experiments for CO_2/N_2 (1/99 and 15/85) and CO_2/CH_4 (50/50) combinations confirmed the outstanding carbon trapping performance. The fine-tuned pore structure with periodic arrays of exposed functionalities results in adsorption and separation performances that show ultramicroporous ZU-16-Co can be a promising adsorbent for low-concentration carbon capture.

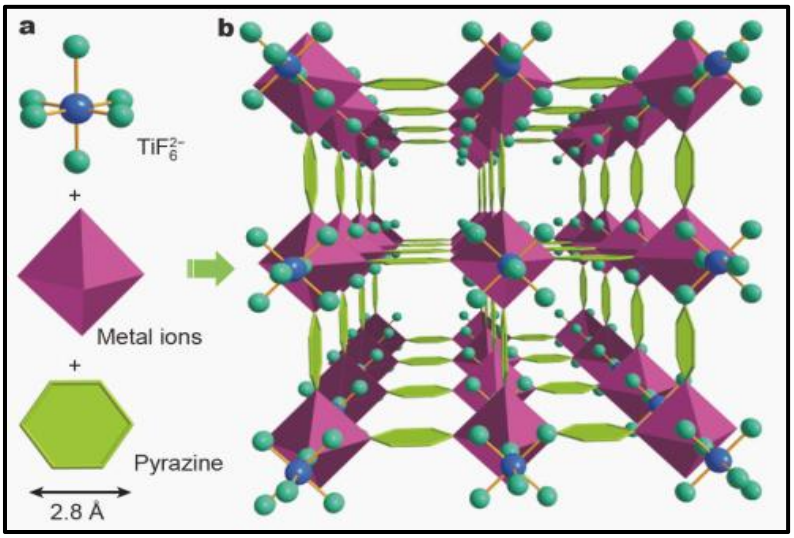

Fig:2.21 Schematic representation of the (a) construction (b)the pore structure of ZU-16 (TIFSIX-3) materials with pyrazine linker

The effect of MOF-5 and MOF-5 modified with multi-wall carbon nanotubes (MWCNTs) and expandable graphite (EG) on CO_2 adsorption performance was examined by **Sami Ullah et al., 2014**. According to the results of the CO_2 adsorption investigation, modified MOF-5 has better CO_2 adsorption than pure MOF-5. The increase in CO_2 absorption capabilities of MOF materials was attributed to the use of multi-walled carbon nanotubes and EG to reduce pore size and increase micropore volume in MOF-5. The synthesized MOF-5@MWCNTs have a larger BET surface area than MOF-5. At 298 K and 1 bar, the CO_2 sorption capacities of MOF-5 and MOF-5@MWCNTs increased from 0.00008 to 0.00048 mol g-1. Modified MOF-5@MWCNTs had the maximum CO_2 adsorption, followed by modified MOF-5@ EG, and finally MOF-5.

Weibin Liang et al., 2019 developed a fluorinated MOF with the precise pore system to enable efficient CO_2 extraction from flue gas at 298 K using an interpenetration technique. At 10% CO_2 and 298 K, the MOF, dptz-CuTiF6, had greater volumetric and gravimetric CO_2 uptakes than the standard aqueous amine method, with much less energy input for regeneration(38 kJ mol-

[1] versus 105 kJ mol^{-1}). Under inert gas purging, dptz-CuTiF6 obtains full CO_2 desorption at 298 K in cyclic breakthrough experiments. The exceptional CO_2 adsorption capacity, moderate CO_2 heat of adsorption, and high CO_2-N_2 selectivity are due to the optimal packing of CO_2 molecules within the MOF, as well as favorable thermodynamics and kinetics from cooperative host-guest interactions, according to single-crystal X-ray diffraction studies.

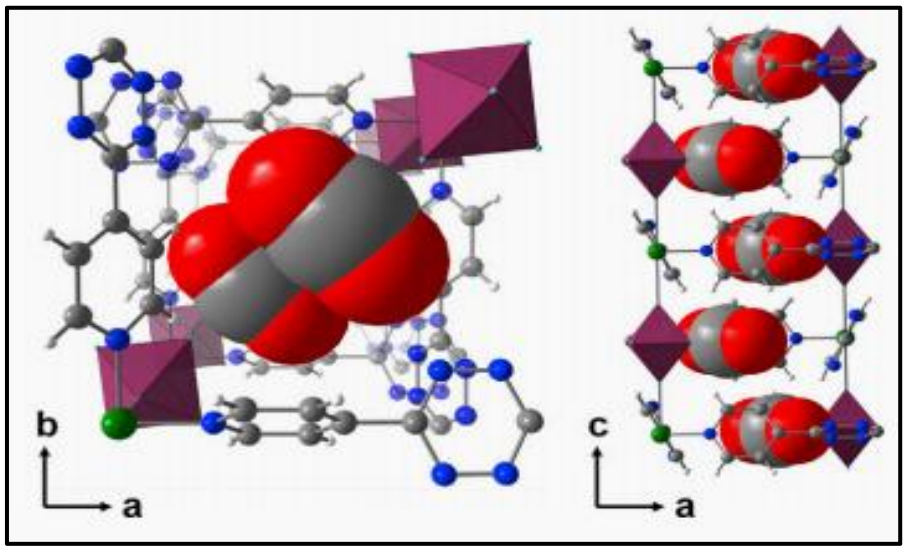

Fig: 2.22 Direct visualization of CO_2 molecules inside the crystal structure of dptz-CuTiF6

The effect of MOF-5 and MOF-5 modified with multi-wall carbon nanotubes (MWCNTs) and expandable graphite (EG) on CO_2 adsorption performance was examined by **Sami Ullah et al., 2014**. According to the results of the CO_2 adsorption investigation, modified MOF-5 has better CO_2 adsorption than pure MOF-5. The increase in CO_2 absorption capabilities of MOF materials was attributed to the use of multi-walled carbon nanotubes and EG to reduce pore size and increase micropore volume in MOF-5. The synthesized MOF-5@MWCNTs have a larger BET surface area than MOF-5. At 298 K and 1 bar, the CO_2 sorption capacities of MOF-5 and MOF-5@MWCNTs increased from 0.00008 to 0.00048 mol g-1. Modified MOF-5@MWCNTs had the maximum CO_2 adsorption, followed by modified MOF-5@ EG, and finally MOF-5.

Ijlal Aamer et al., 2021 worked on pillared layer MOFs, which are pre-synthetic functionalized MOFs. DABCO (1,4-diazabicyclo[2.2.2] octane) is added to the MOFs Zn-BDC and Co-BDC as a pillar to construct 3D structured MOFs Zn-BDC-DABCO and Co-BDC-DABCO, and their performance in CO_2 capture applications was examined. When the pressure was increased to a maximum of 25 bar, the adsorption capacity of Zn-BDC-DABCO and Co-

BDC-DABCO was 6.3 mmol g^{-1} and 4.4 mmol g^{-1} CO_2 respectively at room temperature, which is a significant increase when compared to the 0.95 mmol g^{-1} and 0.67 mmol g^{-1} of the Zn-BDC and Co-BDC, respectively. From these results it is confirmed that adding DABCO as a pillar to MOFs improves CO_2 adsorption. This is due to two basic parameters: (i) the pillar converts our 2D structure to a 3D structure, resulting in increased surface area and, as a result, increased adsorption capacity; and ii) because DABCO is an amino functionalized group, it increases the material's CO_2 affinity, resulting in increased adsorption capacity.

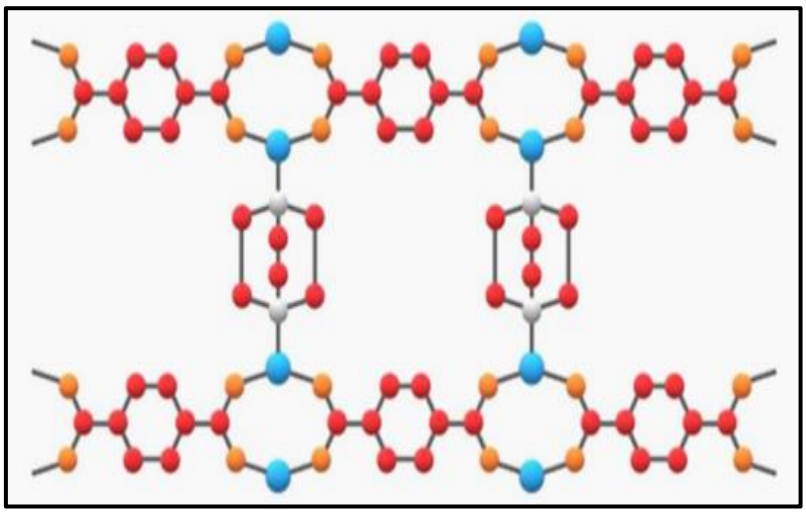

Fig:2.23 Structure of M-BDC-DABCO (C, red; O, orange; N, grey; Metal, blue)

Cu-BDC MOF was produced by **Aisha Asghar et al., 2019** using a hexamethylene tetramine additive. The resultant MOF crystallized into a solid with rod-like crystallites. Cu-BDC⊃HMTA is thermally more stable than Cu-BDC MOF, according to thermographic measurements. Furthermore, carbon dioxide adsorption experiments for these materials show that the amine-modified framework has significantly greater carbon dioxide uptake (5.25 wt percent for Cu-BDC and 21.2 wt percent for Cu-BDC⊃HMTA, respectively, at 273 K and 1 bar). The insertion of nitrogen atoms results in increased CO_2 gas adsorption, which is attributed to favorable interactions between CO_2 molecules and the nitrogen-modified pores. Cu-BDC⊃HMTA, the modified MOF, has improved cyclic stability and can be reused for three cycles. Using HMTA as a cheap addition, this study provides a cost-effective technique for incorporating amine groups in MOF structures for increased CO_2 collection applications.

Phillip J. Milner et al., 2017 developed a new diamine-functionalized metalorganic framework consisting of 2,2-dimethyl-1,3-diaminopropane (dmpn) attached to the Mg^{2+} sites

lining the channels of Mg_2(dobpdc) (dobpdc4 = 4,4′-dioxidobiphenyl-3,3′-dicarboxylate) for the removal of CO_2. It showed efficient CO_2 adsorption from coal flue gas at 40 °C and near full CO_2 desorption at 100 °C, allowing for a high CO_2 working capacity (2.422 mmol/g, 9.1 wt%) with a moderate 60 °C temperature swing. In contrast to many adsorbents, thermogravimetric analyses and breakthrough experiments show that dmpnMg2(dobpdc) absorbs CO_2 effectively in the presence of water and can withstand 1000 humid adsorption/desorption cycles with negligible degradation. This material adsorbs CO_2 via the formation of both ammonium carbamates and carbamic acid pairs, which are crystallographically verified for the first time in a porous material, according to solid-state ^{13}C NMR spectra and single-crystal X-ray diffraction structures. Taken together, these characteristics make dmpnMg_2(dobpdc) one of the most promising carbon capture adsorbents.

The amine groups have a great affinity to adsorb CO_2 molecules. Ethylenediamine (en) is the most common functional group which is used in PSM(Post Synthetic Modification). A good example of en grafted MOF is en-MOF-74 with amine loading of 16.7 wt. %. This modified MOF exhibited an exceptional CO_2 uptake (13.7 wt. %) at 298 K and 0.15 bar. The value of the isosteric heat was also very high (49 to 51 kJ mol-1) that exhibited chemisorption between CO_2 molecules and amine groups resulting in formation of carbamic acid. This MOF just lost 3 % of the CO_2 uptake capacity after 5 cycles of adsorption-desorption notwithstanding chemisorption of CO_2 and amine groups. Besides, en-MOF-74 exhibited high water stability in different amounts of moisture. Hence, en modified MOF possessed a great potential for CO_2 adsorption, **Lee et al., 2014**

3. MATERIALS AND METHODS

3.1 MATERIALS USED

In this study, Metal nitrates, chlorides and organic acid were used to fabricate MOF. The chosen metal nitrates, chlorides, organic acids and solvents were listed below.

The analytical grade metal nitrates, chlorides and solvents were purchased and used without any further purification.

1. Chromium(III) nitrate [$Cr(NO_3)_3$]
2. Manganese(II) chloride tetrahydrate [$MnCl_2.4H_2O$]
3. Iron(III) Chloride [$FeCl_3$]
4. Cobalt(II) nitrate hexahydrate [$Co(NO_3)_2.6H_2O$]
5. Magnesium nitrate hexahydrate [$Mg(NO_3)_2.6H_2O$]
6. Strontium chloride hexahydrate [$SrCl_2.6H_2O$]

Organic Ligand:

7. Benzenedicarboxylic acid [Terephthalic acid]

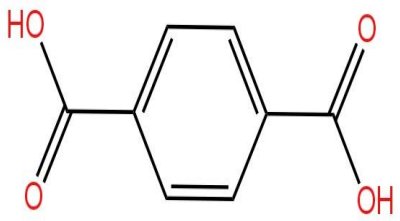

Structure of BDC (King Draw)

Solvents:

8. Dimethyl Formamide(DMF)

N,N-dimethylformamide (dmf) was chosen as a solvent for MOF synthesis because of its high boiling point and ability to dissolve carboxylic acids and metal salts.

9. NaOH- used to maintain pH
10. Ethanol- used for washing the final product

3.2 Synthesis of MOF

The MOFs were synthesized by following the procedure reported by **Nurettin Sahiner et al., 2017** with slight modification. The following MOFs were synthesized by taking metals and linker in 1:2 ratio

3.2.1 Preparation of Cr-BDC MOF

1.2g of Chromium(III) nitrate and 1.7g of Benzenedicarboxylic Acid(BDC) were taken in two separate beakers. The BDC was dissolved in 20ml of DMF and the metal nitrate was dissolved in 10ml of DMF. Then the metal ion solution was added into the BDC solution and stirred well. The Aqueous solution of 5N NaOH(6ml) was added drop by drop to the above mixture so that the pH was maintained at 8. Thus the BDC and metal ion solution mixtures were stirred using a magnetic stirrer at 500 rpm mixing rate for 12hrs at room temperature. The product obtained was filtered with the help of a vacuum pump. The precipitate was washed with 30ml of ethanol three times. Thus the Cr-BDC MOF was obtained by drying the product in the oven at 80°C for 5hrs.

Fig: 3.1 Cr-BDC MOF

3.2.2 Preparation of Mn-BDC MOF

0.9g of $MnCl_2.4H_2O$ and 1.7g of Benzenedicarboxylic Acid(BDC) were taken in two separate beakers. The BDC was dissolved in 20ml of DMF and the metal chloride was dissolved in 10ml of DMF. Then the metal ion solution was added into the BDC solution and stirred well. The aqueous solution of 5N NaOH(4ml) was added drop by drop to the above mixture so that the

pH was maintained at 8. Thus the BDC and metal ion solution mixtures were stirred using a magnetic stirrer at 500 rpm mixing rate for 12hrs at room temperature. The product obtained was filtered with the help of a vacuum pump. The precipitate was washed with 30ml of ethanol three times. Thus the Cr-BDC MOF was obtained by drying the product in the oven at 80°C for 5hrs.

Fig: 3.2 Mn-BDC MOF

3.2.3 Preparation of Fe-BDC MOF

0.9g of $FeCl_3$ and 1.7g of Benzenedicarboxylic Acid(BDC) were taken in two separate beakers. The BDC was dissolved in 20ml of DMF and the metal chloride was dissolved in 10ml of DMF. Then the metal ion solution was added into the BDC solution and stirred well. The aqueous solution of 5N NaOH(4ml) was added drop by drop to the above mixture so that the pH was maintained at 8. Thus the BDC and metal ion solution mixtures were stirred using a magnetic stirrer at 500 rpm mixing rate for 12hrs at room temperature. The product obtained was filtered with the help of a vacuum pump. The precipitate was washed with 30ml of ethanol three times. Thus the Cr-BDC MOF was obtained by drying the product in the oven at 80°C for 5hrs.

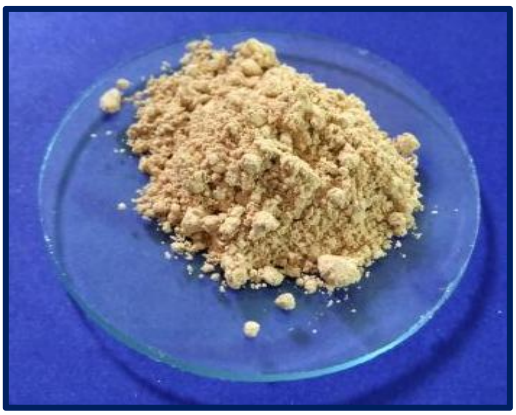

Fig: 3.3 Fe-BDC MOF

3.2.4 Preparation of Co-BDC MOF

1.5g of $Co(NO_3)_2 .6H_2O$ and 1.7g of Benzenedicarboxylic Acid(BDC) was taken in two separate beakers. The BDC was dissolved in 20ml of DMF and the metal nitrate was dissolved in 10ml of DMF. Then the metal ion solution was added into the BDC solution and stirred well. The aqueous solution of 5N NaOH(5ml) was added drop by drop to the above mixture so that the pH was maintained at 8. Thus the BDC and metal ion solution mixtures were stirred using a magnetic stirrer at 500 rpm mixing rate for 12hrs at room temperature. The product obtained was filtered with the help of a vacuum pump. The precipitate was washed with 30ml of ethanol three times. Thus the Co-BDC MOF was obtained by drying the product in the oven at 80°C for 5hrs.

Fig: 3.4 Co-BDC MOF

3.2.5 Preparation of Mg-BDC MOF

1.3g of $Mg(NO_3)_2.6H_2O$ and 1.7g of Benzenedicarboxylic Acid(BDC) was taken in two separate beakers. The BDC was dissolved in 20ml of DMF and the metal nitrate was dissolved in 10ml of DMF. Then the metal ion solution was added into the BDC solution and stirred well. The aqueous solution of 5N NaOH(7ml) was added drop by drop to the above mixture so that the pH was maintained at 8. Thus the BDC and metal ion solution mixtures were stirred using a magnetic stirrer at 500 rpm mixing rate for 12hrs at room temperature. The product obtained was filtered with the help of a vacuum pump. The precipitate was washed with 30ml of ethanol three times. Thus the Mg- BDC MOF was obtained by drying the product in the oven at 80°C for 5hrs.

Fig: 3.5 Mg-BDC MOF

3.2.6 Preparation of Sr-BDC MOF

1.4g of $SrCl_2$. $6H_2O$ and 1.7g of Benzenedicarboxylic Acid(BDC) was taken in two separate beakers. The BDC was dissolved in 20ml of DMF and the metal chloride was dissolved in 10ml of DMF. Then the metal ion solution was added into the BDC solution and stirred well. The aqueous solution of 5N NaOH(6ml) was added drop by drop to the above mixture so that the pH was maintained at 8. Thus the BDC and metal ion solution mixtures were stirred using a magnetic stirrer at 500 rpm mixing rate for 12hrs at room temperature. The product obtained was filtered with the help of a vacuum pump. The precipitate was washed with 30ml of ethanol three times. Thus the Cr-BDC MOF was obtained by drying the product in the oven at 80°C for 5hrs.

Fig: 3.6 Sr-BDC MOF

3.4 Characterization

The Metal Organic Framework synthesized by the above procedure are subjected to various characterization methods such as Fourier Transform Infrared spectroscopy, Powder X-ray diffraction (P-XRD), Thermogravimetric analysis (TGA), Scanning Electron Microscopy(SEM). Characterization using those techniques provided information about functional groups, bond formation between ligand and metal ion, morphology and thermal stability of the MOF.

3.4.1 Fourier Transform Infrared Spectroscopy

FT-IR is an effective analytical technique to ascertain the presence of functional groups in the synthesized compounds. Infrared spectroscopy of the synthesized MOF was obtained using a **Shimadzu IR spectrometer** in which the MOF powder was directly placed in a zinc selenide sample cavity and scanned over the spectral region of **400 to 4000 cm^{-1}**.

3.4.2 Powder X-ray diffraction

Powder XRD is an effective tool for investigating crystalline properties. An X-ray diffractometer's geometry is such that the sample rotates at an angle in the path of the collimated X-ray beam, while the X-ray detector is mounted on an arm that rotates at an angle of 2θ to collect the diffracted X-rays. When an X-ray hits the crystal's face, it diffracts in a pattern that is unique to the crystal's structure. The diffraction pattern is obtained from a powder of the material rather than an individual crystal in powder X-ray diffraction**(Carreon, M. A et al., 2020).** Here, the P-XRD pattern of Co-BDCMOF were collected on **XPERT - PRO** over an angle of 5 to 60° in 2θ

3.4.3 Thermogravimetric Analysis

TGA is a useful tool for determining the thermal stability of MOFs and it has been widely used to quantify MOF composition. TGA analysis relies on a high degree precision in three measurements - weight, temperature and temperature change. Here, the thermal stability of Co-BDC was investigated by **TG/DTA - EXSTAR/6300 (ThermoGravimetric Analyser)**. The thermograms were taken in continuous Nitrogen flow with sample held in alumina pan and weight loss against temperature plots were prepared for each sample.

3.4.4 Field Emission Scanning Electron Microscopy

SEM is a useful tool for determining MOF properties such as particle size, morphology, and atomic composition. A focused beam of high-energy electrons is used in SEM to generate a variety of signals at the sample's surface. In a SEM, accelerated electrons carry a lot of kinetic energy, which is dissipated as a variety of signals caused by electron-sample interactions. Secondary electrons are the most useful for displaying morphology (as a 2D image) and topography on samples**(Carreon, M. A et al., 2020)**. Here, the SEM images were collected using **Jeol JSM 6390 Scanning Electron Microscope.**

3.4.5 CO_2 adsorption analysis

The CO_2 adsorption analysis was carried out by conventional method to study the CO_2 adsorption performance of Co-BDC MOF. Carbon dioxide is produced by reaction of acids with carbonates. Here, we have used Calcium carbonate and concentrated Hydrochloric acid to produce carbon dioxide gas.

About 10g of $CaCO_3$ was taken in a boiling tube and 15ml of conc. HCl was added to it. The resulting carbon dioxide gas is made to pass through another boiling tube containing 0.10g of the sample(Co-BDC).

Fig: 3.7 CO_2 adsorption test setup

The sample has been kept in Carbon dioxide atmosphere for 5hrs. During this process, a colour change was noted from **Dirty white to Pale dirty white and finally Distemper green** which indicates that CO_2 gas is being adsorbed by the MOF.

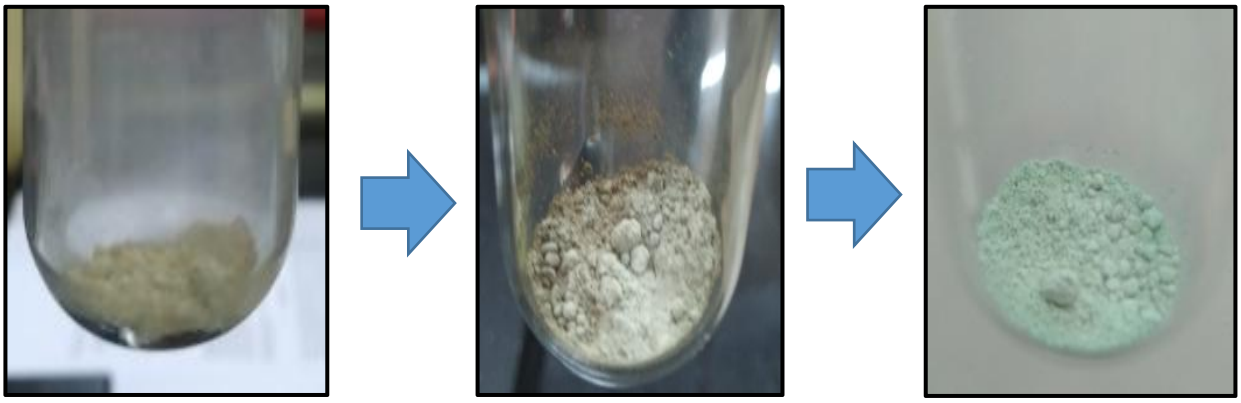

(a) **(b)** **(c)**

Fig: 3.8 Colour Change in Co- BDC MOF during CO_2 adsorption

The adsorption of CO_2 into the Co-BDC MOF is further confirmed by doing characterization technique like Fourier- Transform Infrared Spectroscopy, Thermogravimetric analysis and Weight gain method.

4. RESULTS AND DISCUSSIONS

4.1 FOURIER TRANSFORM INFRARED SPECTRA

FT-IR spectrum reveals the functional groups of MOF. The sharp peak with high intensity from 1400 cm^{-1} to 1600 cm^{-1} indicates the asymmetric and symmetric stretching modes of coordinated carboxylic acid. The mid intense band at 700 to 800cm^{-1} were attributed to C-H bending modes of the aromatic ring. The characteristic coordination bonds of Metal-oxygen was observed at the lowest wavenumber from 400-600cm^{-1}. The broad peak in the spectral region of 3600-3800 cm^{-1} was due to acidic OH of carboxylic acid **(Reda S. Salama et al., 2018), (Duyen Thi Cam Nguyen et al., 2019)**

Table: 4.1 Functional Group analysis of synthesized MOFs by FT-IR Spectroscopy

Functional Groups	**O-H**	**γ_{as} (C-O)**	**γ_s C-O**	**C-H**	**M-O**
Synthesized MOFs	Wavenumber(Cm^{-1})				
Cr-BDC	3700	1558.48	1411.89	740.67	462.92
Mn-BDC	3718.76	1558.48	1411.89	740.67	432.05
Fe-BDC	3446.79	1558.48	1411.89	740.67	520
Co-BDC	3633.89	1558.48	1411.89	740.67	493.78
Mg-BDC	3650	1558.48	1411.89	740.67	455.20
Sr-BDC	3564.45	1566.20	1411.89	740.67	516.92

The presence of bonding between organic linker and metal species is confirmed by the above FT-IR spectrum values, suggesting the development of MOF framework.

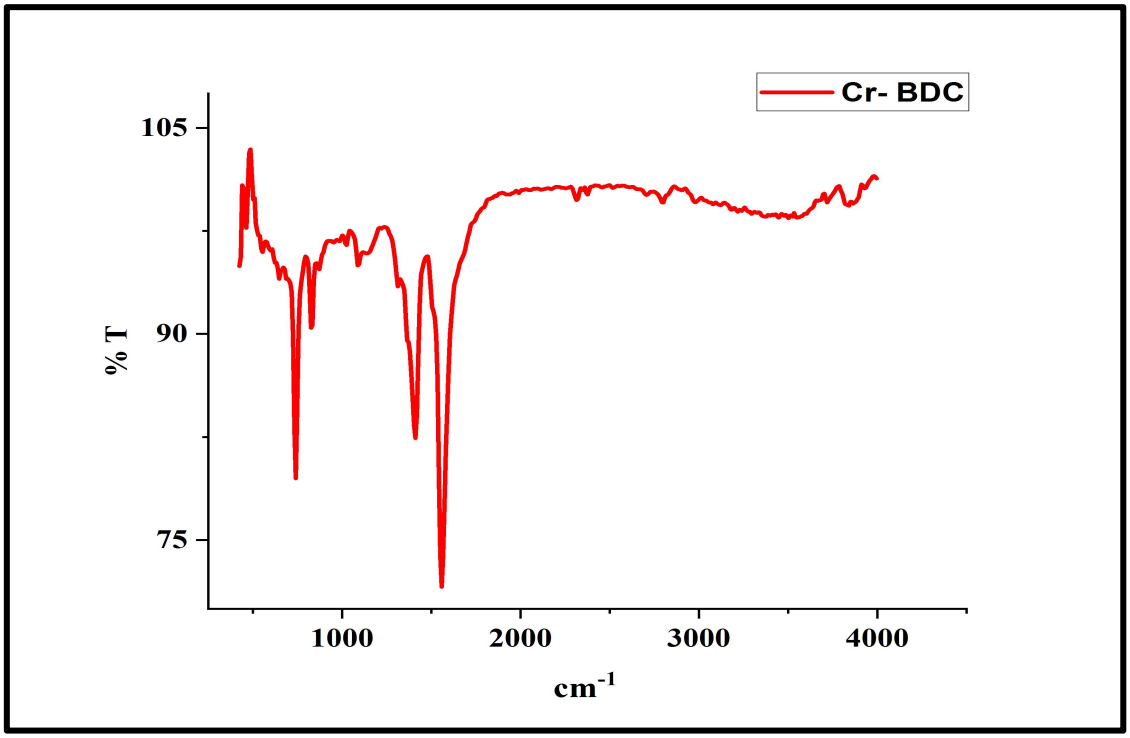

Fig: 4.1 FT-IR Spectra of Cr- BDC MOF

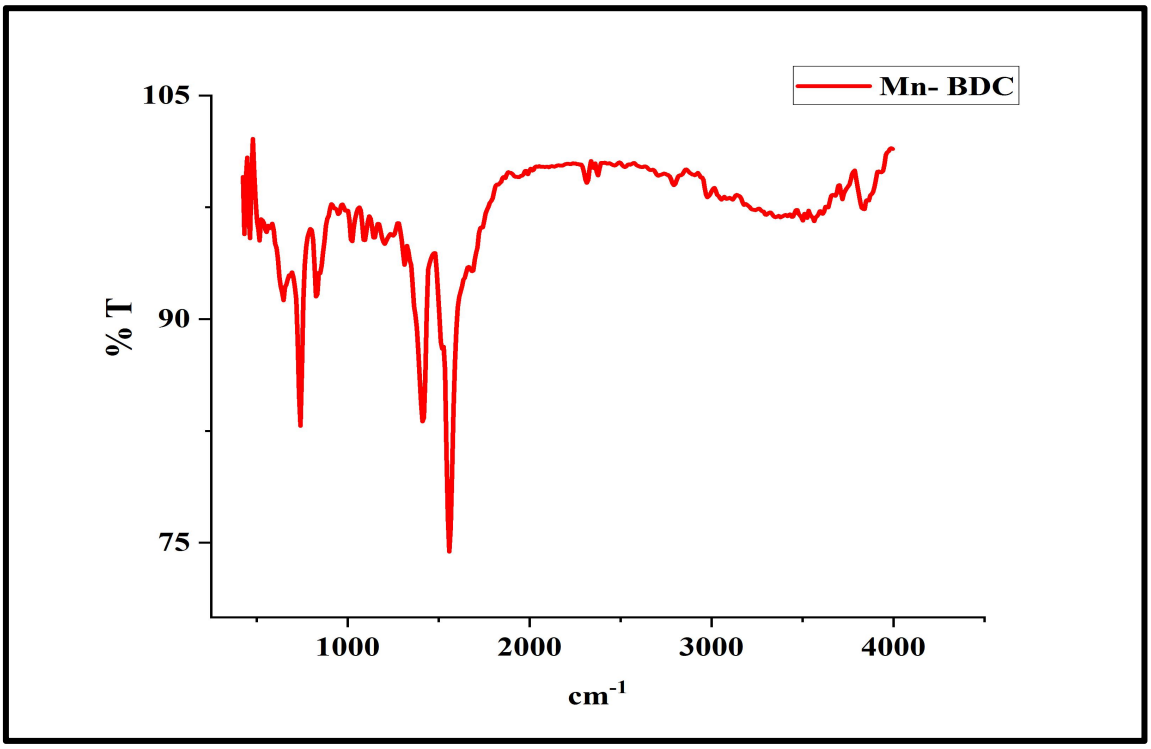

Fig: 4.2 FT-IR Spectra of Mn- BDC MOF

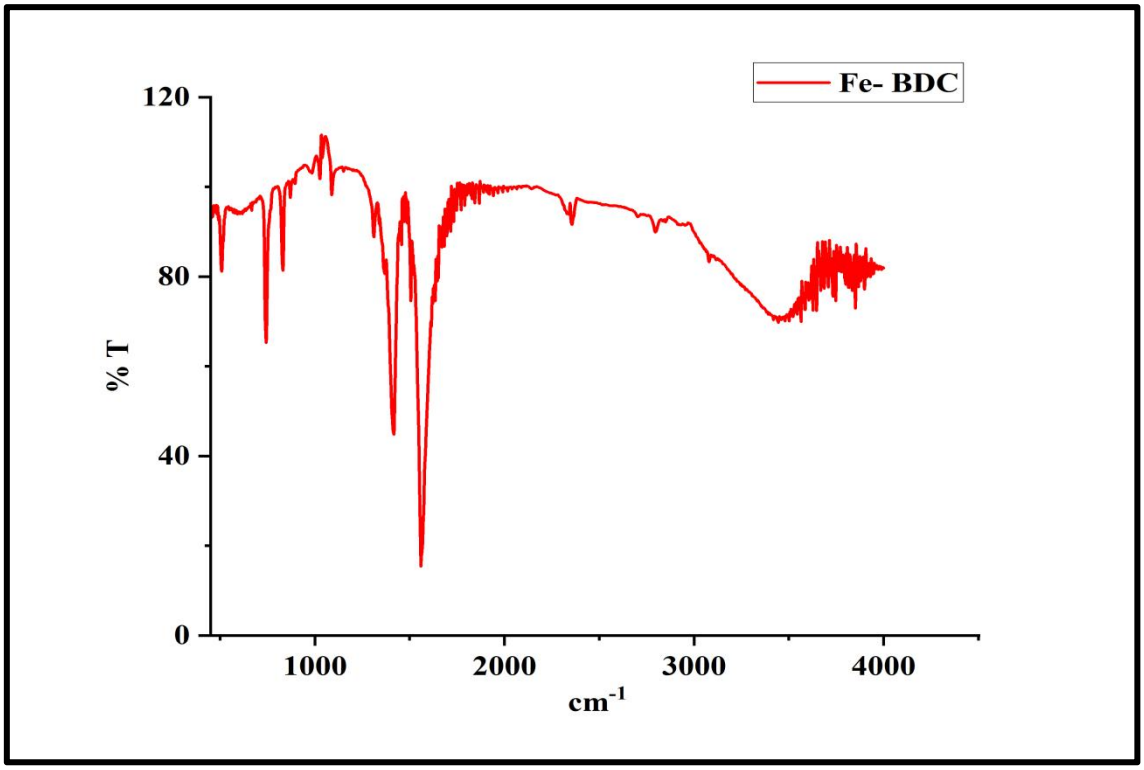

Fig: 4.3 FT-IR Spectra of Fe- BDC MOF

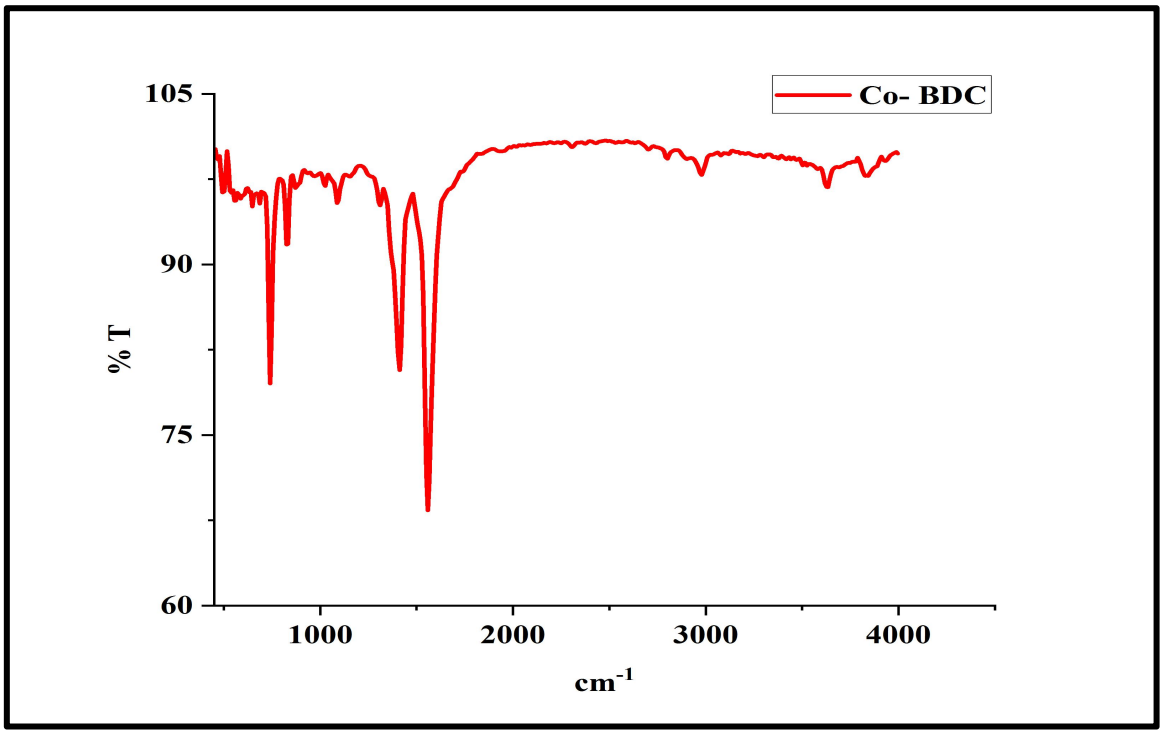

Fig: 4.4 FT-IR Spectra of Co- BDC MOF

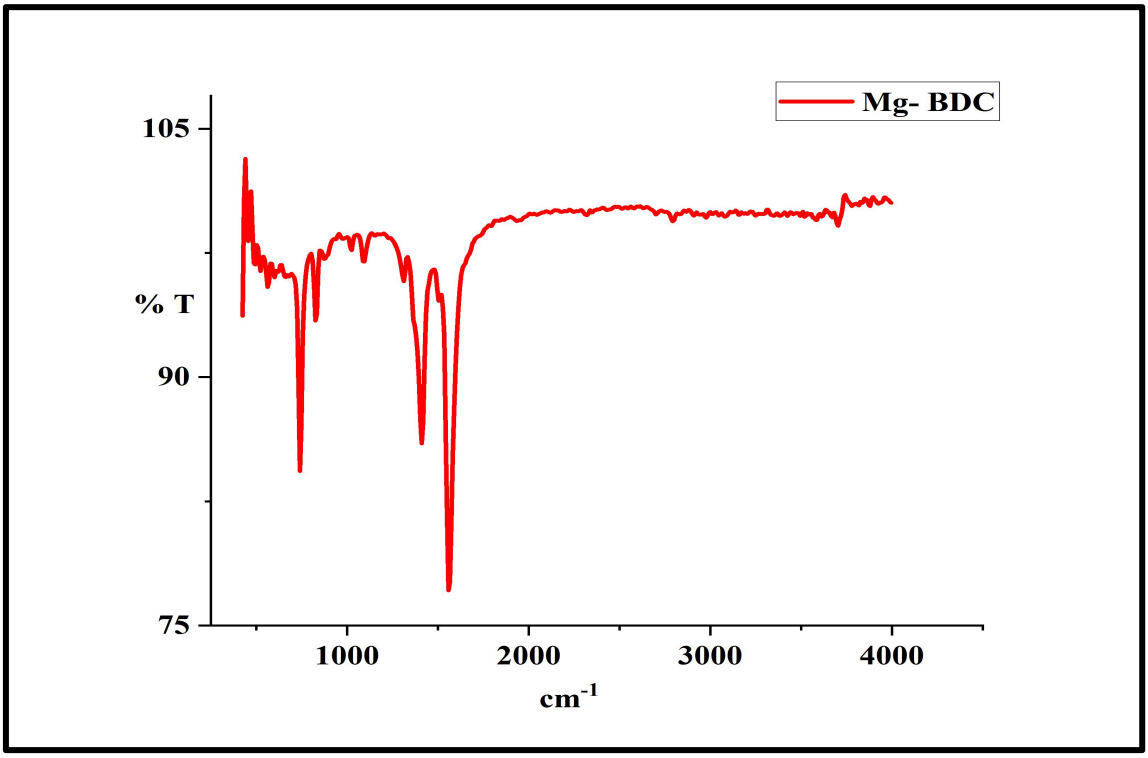

Fig: 4.5 FT-IR Spectra of Mg- BDC MOF

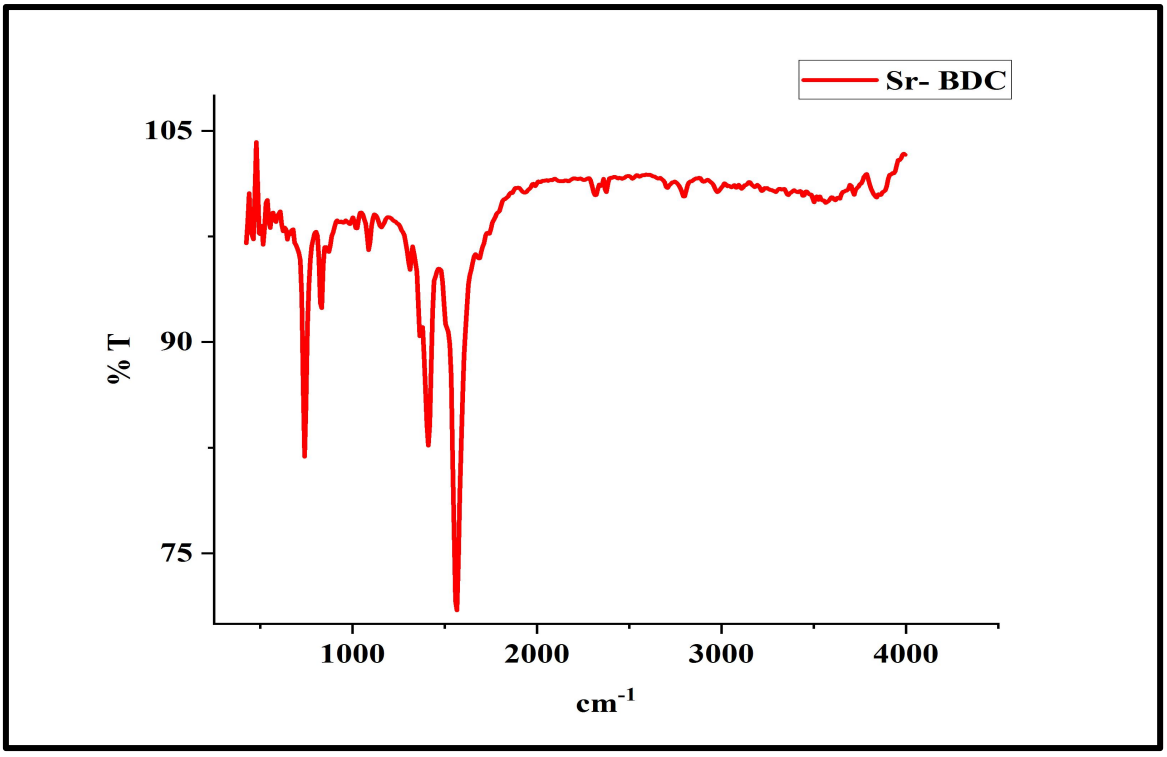

Fig: 4.6 FT-IR Spectra of Sr- BDC MOF

4.2 POWDER X-RAY DIFRACTION

P-XRD is widely used to determine the structural parmetears and crystallinity of the MOFs. The sharpness of the peak in the XRD pattern shows the sample's crystalline nature. The X-ray diffraction pattern of Co- BDC MOF is shown in Fig: 4.7. The relative crystallinity was calculated by using the diffraction peaks at 2Ɵ values at 17.20, 19.19, 30.78, 32.56, 38.08, 51.53, 58.02 and 61.76°. This infers about the coordination of metal with ligand to form complex **(Omkaramurthy B M et al., 2020).**

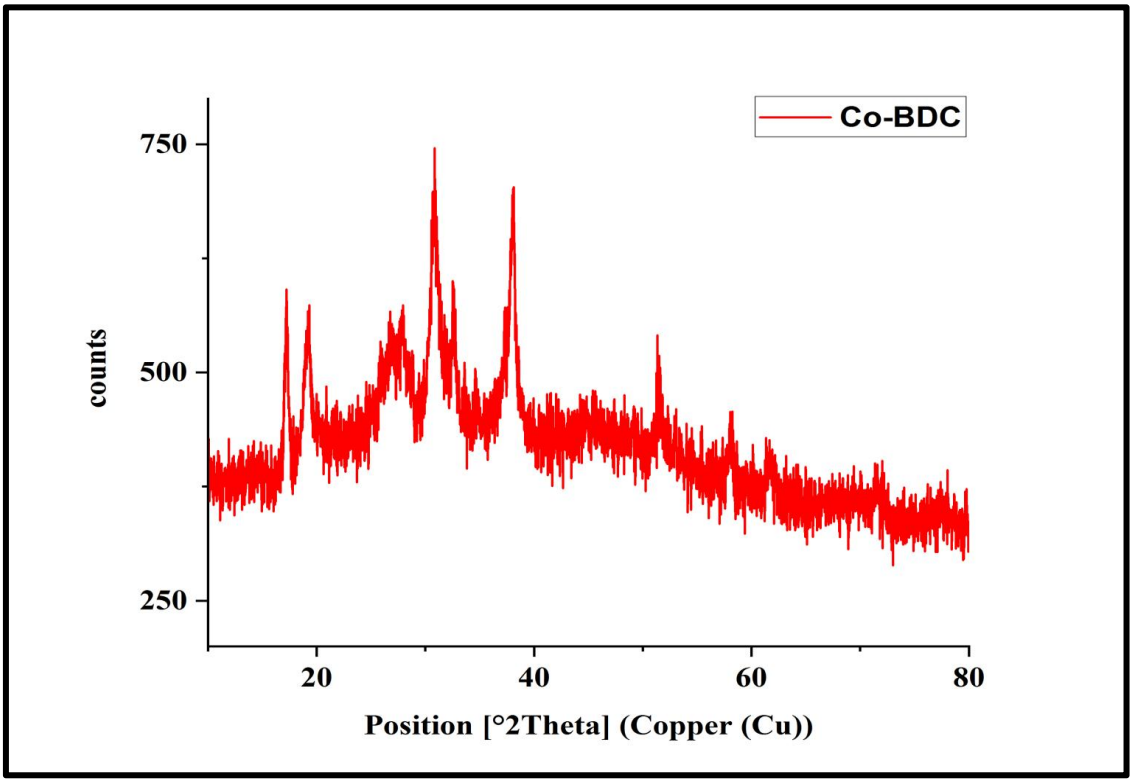

Fig: 4.7 P-XRD pattern of Co- BDC MOF

Measurement Conditions:

Goniometer=PW3050/60 (Theta/Theta); Minimum step size 2Theta:0.001; Minimum step size Omega:0.001

Sample stage=PW3/xx Bracket

Diffractometer system=XPERT-PRO

Measurement program=Fast - 10-80, Owner=User-1, Creation date=3/11/2012 2:08:19 PM

Thin films

Measurement Date / Time 3/18/2022 11:13:16 AM

Operator Administrator
Raw Data Origin XRD measurement (*.XRDML)
Scan Axis Gonio
Start Position [°2Th.] 10.0084
End Position [°2Th.] 79.9804
Step Size [°2Th.] 0.0170
Scan Step Time [s] 5.7150
Scan Type Continuous
PSD Mode Scanning
PSD Length [°2Th.] 2.12
Offset [°2Th.] 0.0000
Divergence Slit Type Fixed
Divergence Slit Size [°] 0.4354
Specimen Length [mm] 10.00
Measurement Temperature [°C] 25.00
Anode Material Cu
K-Alpha1 [Å] 1.54060
K-Alpha2 [Å] 1.54443
K-Beta [Å] 1.39225
K-A2 / K-A1 Ratio 0.50000
Generator Settings 30 mA, 45 kV
Diffractometer Type 0000000011088974
Diffractometer Number 0
Goniometer Radius [mm] 240.00
Dist. Focus-Diverg. Slit [mm] 100.00
Incident Beam Monochromator No
Spinning No

Thus the fig: 4.7 infers both sharp and broad peaks which indicates that the sample is Semi- crystalline in nature. The crystallite size of Co- BDC MOF is calculated using the **Scherrer's equation** as follows**(Jorge Bedia et al., 2019)**

$$\mathbf{D = \mathit{K} . \lambda / \beta . \cos\theta}$$

D = Crystallite size

K = a size factor (values among 0.84–0.98 depending on the equipment)

λ = X- ray wavelength

β = the full width at half maximum height of the peak (FWHM)

θ = the Bragg angle

Table: 4.2 Crystal Size Calculation

Position (2Ɵ)	FWHM (2Ɵ)	d-spacing(Å)	Crystalline size (nm)
17.2029	0.2676	5.15469	31.35
19.1933	0.5353	4.62438	15.71
30.7850	0.4684	2.90449	18.37
32.5670	0.2676	2.74952	32.29
38.0849	0.4015	2.36289	21.65
51.5344	0.4015	1.77343	22.73
58.0289	0.4015	1.58946	23.41
61.7694	0.8029	1.50189	12.03

The default value of wavelength of X- ray diffraction is set set as 0.15418(Cu K-alpha) which is mostly used in the instruments. The crystalline size of Co- BDC MOF was caculated by using XRD Crystallite Size caculator (Scherrer Equation)- InstaNANO. https://instanano.com/characterization/calculator/xrd/crystallite-size/ (accessed May 23rd, 2022)

4.3 THERMOGRAVIMETRIC ANALYSIS

4.3.1 THERMOGRAVIMETRIC ANALYSIS OF Co-BDC MOF

Weight loss of MOF begins at 150°C indicating the framework of Co-BDC MOF is stable below 150°C. The weight loss of Co-BDC MOF is from 150-210°C, which was ascribed to the loss of coordinated DMF molecules. A second weight loss between 360-420°C indicates the decomposition of dicarboxylate linker and another weight loss between 540-630°C is ascribed to the totally decomposition of the MOF structure, while the residual materials are converted into metal oxide **(Ijlal Aamer et al., 2021), (Aisha Asghar et al., 2019)**

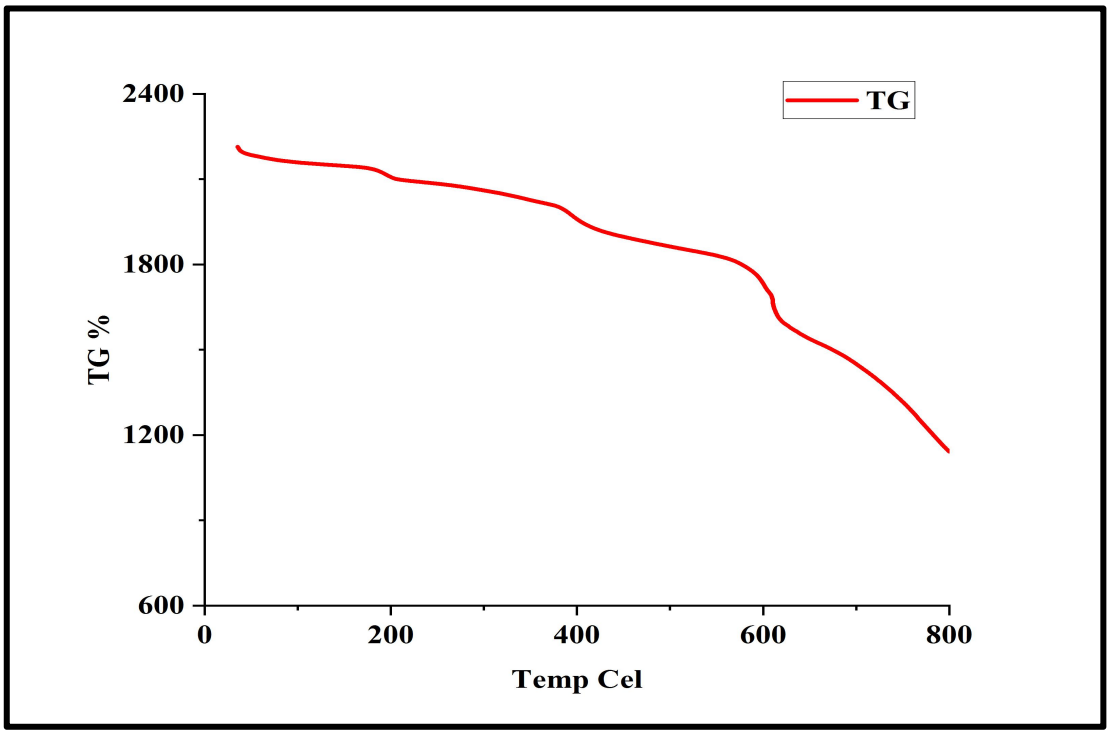

Fig: 4.8 Thermogravimetric analysis of Co- BDC MOF

4.4 SCANNING ELECTRON MICROSCOPE

Scanning electron microscopy is a technique that enables the study of the microstructure of MOF. FE-SEM micrographs of Co- BDC MOF is presented in Fig: 4.9(a, b, c, shows the distribution of particles in Co- BDC MOF with wide range of dimension. It can be identified from Fig: 4.9 (d & e) that the distribution of particles in Cobalt BDC MOF is irregular shaped flakes arranged as flower- like clusters **(Ezekiel Dixon Dikio et al., 2013)**

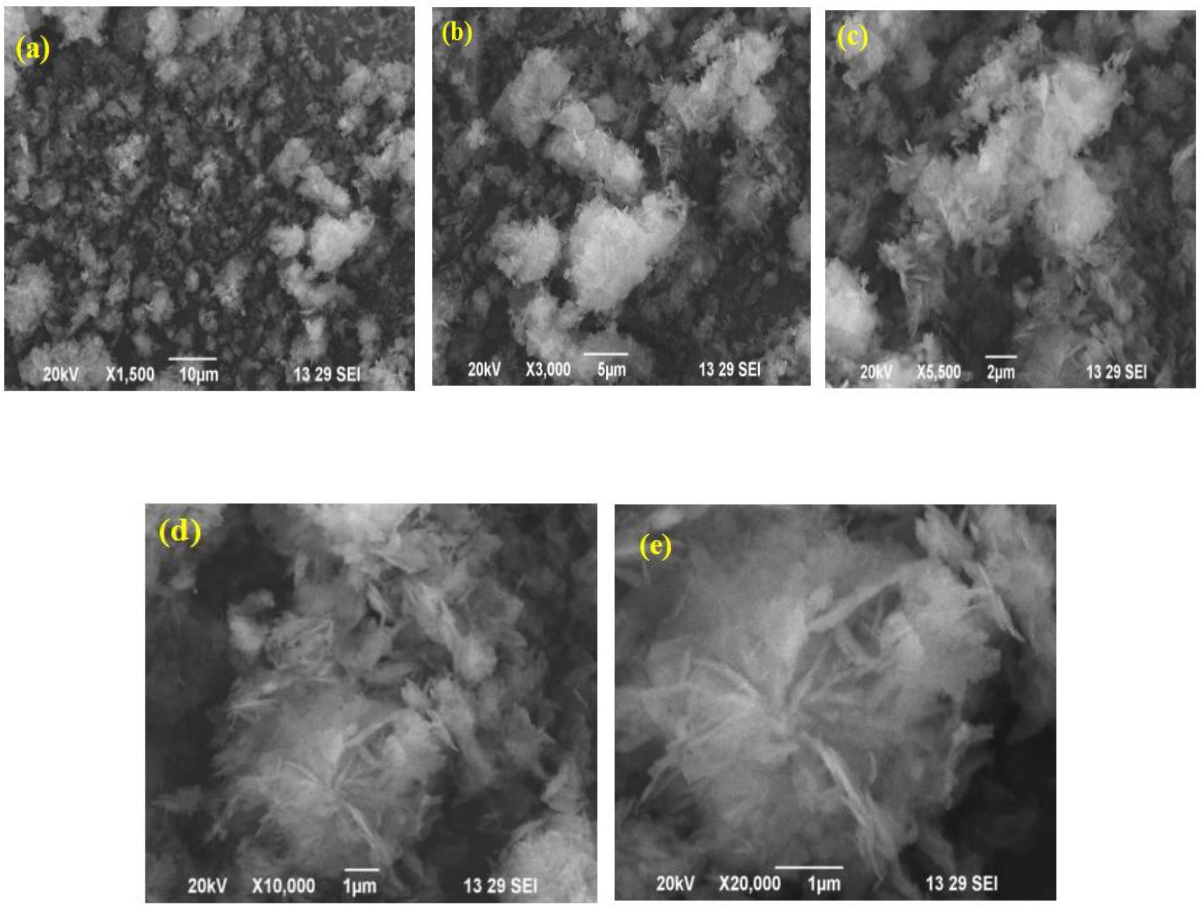

Fig: 4.9 FE-SEM micrographs of Co- BDC MOF with different magnifications

4.5 CARBON DIOXIDE ADSORPTION STUDY

CO_2 adsorption into Co- BDC MOF was confirmed by noting the colour change from **Dirty white to Pale dirty white and finally Distemper green** on exposing it to CO_2 atmosphere for 5hrs.

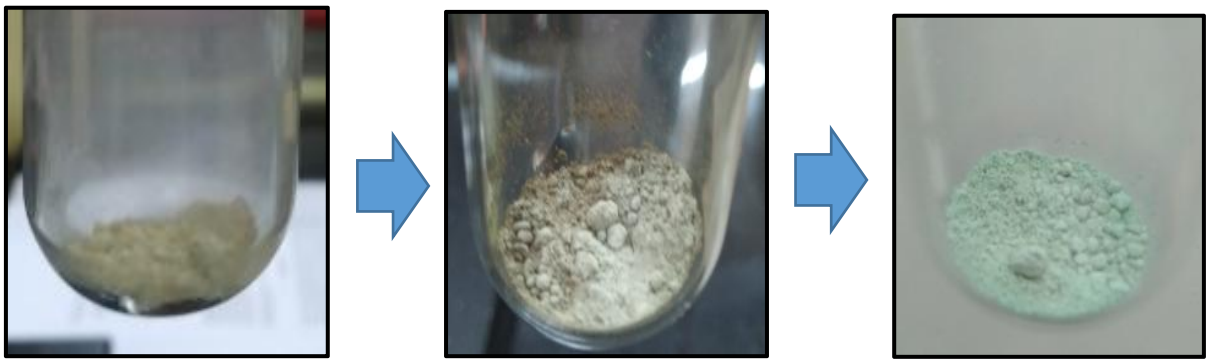

(a) **(b)** **(c)**

Fig:4.10 Colour Change in Co- BDC MOF during CO_2 adsorption

CO_2 adsorption into Co- BDC MOF is further confirmed by FT-IR, TGA and Weight gain method.

4.5.1 FOURIER TRANSFORM INFRARED SPECTRA

The comparison of FT-IR spectrum of Co- BDC MOF before and after CO_2 treatment confirms the adsorption of CO_2 into Co- BDC MOF by CO_2 peak.

The FT-IR spectrum of raw Co- BDC MOF displayed two characteristic band at 1558.48cm^{-1} and 1411.89cm^{-1} which corresponds to asymmetric and symmetric stretching mode of coordinated carboxylic acid. The band at 740.67cm^{-1} was attributed to C-H bending modes of aromatic ring. The characteristic coordination bond between metal-oxygen was observed at 493.78cm^{-1}. The broad band in the spectral region of 3633.89cm^{-1} was due to acidic OH of carboxylic acid **(Duyen Thi Cam Nguyen et al., 2019)**

The FT-IR spectrum of Co- BDC MOF after CO_2 adsorption displayed two characteristic band at 1674.21cm^{-1} and 1566.20cm^{-1}, related to asymmetric and symmetric stretching mode of carboxylic acid. The band at 732.95cm^{-1} was associated with C-H bending modes of aromatic ring, The characteristic band at 455.20cm^{-1} was due to metal-oxygen bond.

The spectral band at 3700cm^{-1} was due to acidic OH of carboxylic acid **(Duyen Thi Cam Nguyen et al., 2019)**

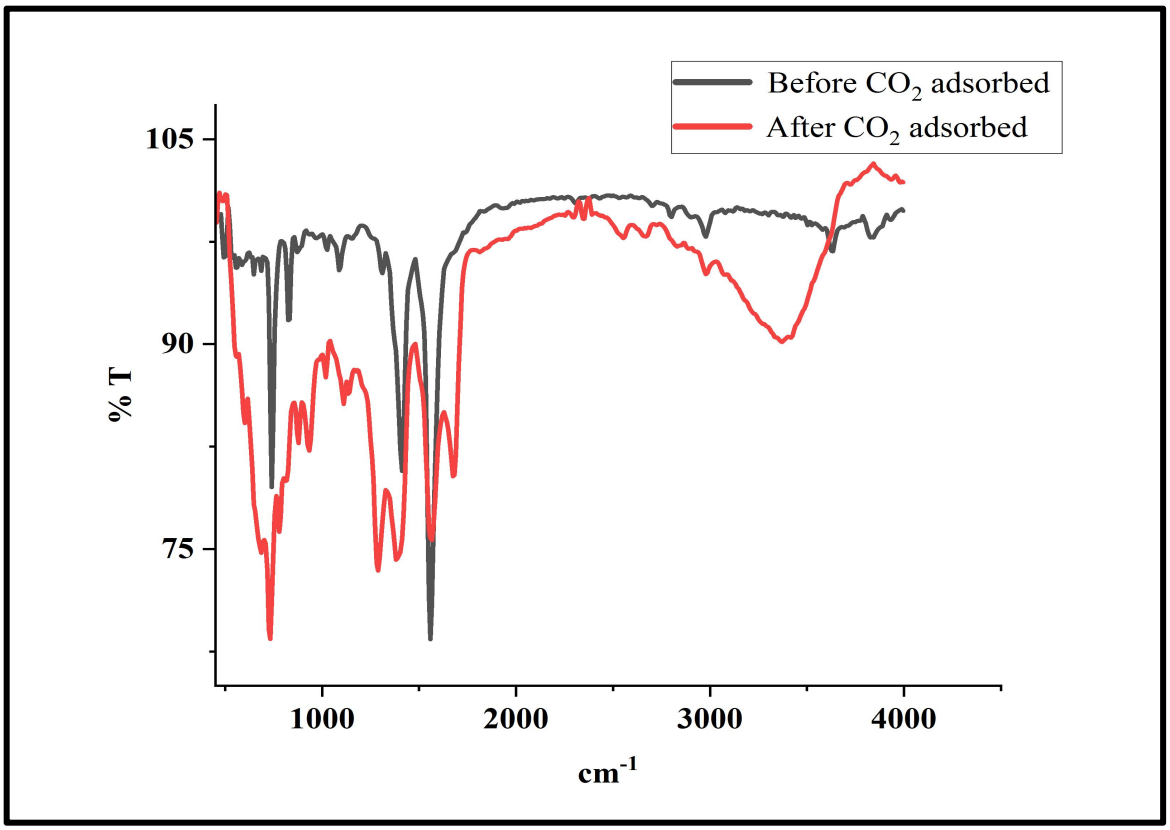

Fig: 4.11 FT-IR Spectrum of Co- BDC MOF before and after CO_2 adsorption

All of the characteristic peaks of raw Co- BDC MOF were retained in the FT-IR spectra of CO_2 adsorbed Co- BDC MOF. The asymmetric stretching mode of adsorbed CO_2, that was not seen in raw Co- BDC MOF FT-IR, was responsible for the formation of a new vibration band at 2353.16cm^{-1}. The occurrence of this peak was due to CO_2 interacting with the unsaturated metal centre through its oxygen atom **(Nour Nijem et al., 2012)**

4.5.2 THERMOGRAVIMETRIC ANALYSIS OF CO_2 ADSORBED Co-BDC MOF

Thermal decomposition process for Co- BDC sample after exposing to CO_2 atmosphere for 5hours was examined using TGA technique.

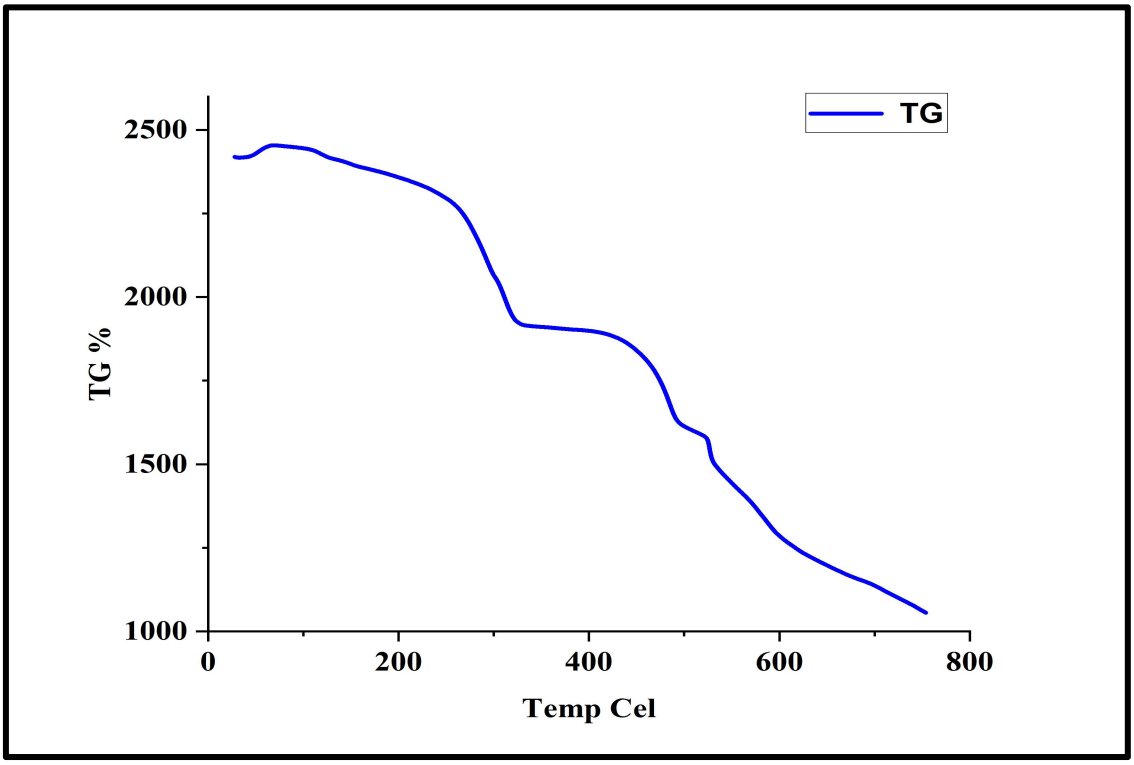

Fig: 4.12 Thermogravimetric analysis of CO_2- adsorbed Co- BDC MOF

The first weight loss between 50°C - 140°C is caused by the elimination of physically adsorbed DMF solvent. The second weight loss between 170°C - 310°C corresponds to the chemisorbed CO_2. The third thermal decomposition between 390°C - 480°C is due to the loss of dicarboxylate linker. Another weight loss between 500°C - 540°C is due to the complete metal-oxide formation, and at that temperature there will be complete regeneration of CO_2 **(Gutierrez-Bonilla Elvira et al., 2016)**

4.5.3 WEIGHT GAIN METHOD

Weight difference was noted before and after exposing the Co- BDC MOF for 5hrs. The difference between initial and final mass of MOF sample determine the CO_2 adsorption capacity of the MOF.

Weight of the empty Boiling tube = 32.9222g
Weight of the sample = 0.1003g
Weight of Boiling tube with sample= 33.0213g
Weight of Boiling tube with sample after exposing to CO_2 gas for 5hrs= 33.0730g
Difference between initial and final mass= 33.0730 - 33.0213

= 0.0517g

Therefore, the amount of CO_2 present in the sample is 0.0517g, thus this weight difference also confirms the presence of CO_2 in the Co- BDC MOF.

5. SUMMARY AND CONCLUSION

Metal organic frameworks are a new class of porous crystalline material that has attracted enormous scientific reserch. This is attributed to their outstanding properties, such as high porosity and surface area, which make them ideal for a wide range of applications, involving gas separation and storage, controlled drug release, waste water treatment, and so on.

The current work on **"Synthesis of Benzenedicarboxylic acid based metal organic framework and its application in carbon dioxide adsorption"** is summarized as follows.

This thesis work is focused on the feasible syntheis of six types of Metal organic frameworks named Cr- BDC, Mn- BDC, Fe- BDC, Co- BD, Mg-BDC, Sr- BDC MOFs. Fourier Transform Infrared Spectroscopy technique was used to validate the development of the metal organic framework. The synthesized Co- BDC MOF was further chacterized using various techniques like Powder X-ray diffraction, Thermogravimetric analysis, Scanning Electron Microscopy and it was also tested for CO_2 adsorption. CO_2 adsorption in Co- BDC MOF was performed on a laboratory scale using conventional methods, and the results were verified using the colour change of the sample, FT-IR, TGA, and the Weight Gain method.

- The synthesized MOFs were highly water stable and insoluble in all commonly used solvents which confirms the formation of MOF.

- Presence of various functional groups like O-H, γ_{as} (C-O), γ_s C-O, C-H has been confirmed by FT-IR analysis. Further, the peaks around 400-550cm^{-1} indicates the formation of Metal-oxo bond between metal and the ligand. This results also confirms the formation of MOF.

- The semi- crystalline nature of Co- BDC MOF was confirmed by P-XRD results. The crystalline size of the MOF particle is calculated using Scherrer equation.

- During CO_2 adsorption process, characteristic colour change was noted from Dirty white to Pale Dirty white and finally Distemper green color which indicates the CO_2 adsorption into the framework.

- FT-IR results after CO_2 adsorption showed a characteristic peak at 2353.16cm^{-1}. The occurence of this peak is due to the interaction of CO_2 with unsaturated metal centre, which confirms its adsorption into the framework.

- TGA result showed weight loss between 170 - 310°C which indicates the weight loss of chemisorbed CO_2.

- A weight difference of 0.01517g was observed in the Co- BDC MOF before and after CO_2 adsorption, indicating that CO_2 has been absorbed into the framework.

FUTURE WORK

- The preliminary studies detailed in this work, such as producing CO_2 gas in laboratory by conventional method and the investigation of CO_2 adsorption in MOF by FT-IR, TGA and Weight gain method, it is recommended that further research can be conducted to include adsorption tests under real flue gas composition and doing adsorption test at elevated temperature and pressure.

- To accurately quantify the amount of CO_2 adsorbed by MOFs, CO_2 adsorption isotherm measurements are required.

- Furthermore, extensive research should be conducted to fully understand the mechanism of CO_2 adsorption.

6. BIBLIOGRAPHY

1. Ghanbari, T., Abnisa, F., & Daud, W. M. A. W. (2020). A review on production of metal organic frameworks (MOF) for CO2 adsorption. *Science of The Total Environment*, *707*, 135090.

2. Sadatshojaie, A., & Rahimpour, M. R. (2020). CO2 emission and air pollution (volatile organic compounds, etc.)–related problems causing climate change. In *Current trends and future developments on (bio-) membranes* (pp. 1-30). Elsevier.

3. Salehi, S., & Anbia, M. (2017). High CO2 adsorption capacity and CO2/CH4 selectivity by nanocomposites of MOF-199. *Energy & Fuels*, *31*(5), 5376-5384.

4. Kidanemariam, A., Lee, J., & Park, J. (2019). Recent innovation of metal-organic frameworks for carbon dioxide photocatalytic reduction. *Polymers*, *11*(12), 2090.

5. Chen, C., Feng, X., Zhu, Q., Dong, R., Yang, R., Cheng, Y., & He, C. (2019). Microwave-assisted rapid synthesis of well-shaped MOF-74 (Ni) for CO2 efficient capture. *Inorganic Chemistry*, *58*(4), 2717-2728.

6. Roth, E. A. (2013). *Nanoclay-Based Solid-Amine Adsorbents for Carbon Dioxide Capture*. West Virginia University.

7. Thambimuthu, K., Soltanieh, M., Abanades, J. C. (2018). Capture of CO_2 IPCC Special Report on Carbon dioxide Capture and Storage, 106-178, https://www.ipcc.ch/site/assets/uploads/2018/03/srccs_chapter3-1.pdf

8. Lee, S. Y., & Park, S. J. (2015). A review on solid adsorbents for carbon dioxide capture. *Journal of Industrial and Engineering Chemistry*, *23*, 1-11.

9. Pettinari, C., & Tombesi, A. (2020). Metal–organic frameworks for carbon dioxide capture. *MRS Energy & Sustainability*, *7*.

10. Chaemchuen, S., Kabir, N. A., Zhou, K., & Verpoort, F. (2013). Metal–organic frameworks for upgrading biogas via CO2 adsorption to biogas green energy. *Chemical Society Reviews*, *42*(24), 9304-9332.

11. Chen, C., Lee, Y. R., & Ahn, W. S. (2016). CO2 adsorption over metal-organic frameworks: A mini review. *Journal of nanoscience and nanotechnology*, *16*(5), 4291-4301.

12. Liu, Y., Wang, Z. U., & Zhou, H. C. (2012). Recent advances in carbon dioxide capture with metal‐organic frameworks. *Greenhouse Gases: Science and Technology*, *2*(4), 239-259.

13. Vaidya B. P, Sasane V. V. (2016). Application of Zeolite for Post Combustion Carbon Capture. *International Journal of Engineering Research & Technology (IJERT)*. **5**, 690-695

14. Sabouni, R., Kazemian, H., & Rohani, S. (2014). Carbon dioxide capturing technologies: a review focusing on metal organic framework materials (MOFs). *Environmental Science and Pollution Research*, *21*(8), 5427-5449.

15. Abd, A. A., Naji, S. Z., Hashim, A. S., & Othman, M. R. (2020). Carbon dioxide removal through physical adsorption using carbonaceous and non-carbonaceous adsorbents: a review. *Journal of Environmental Chemical Engineering*, *8*(5), 104142.

16. Baumann, A. E., Burns, D. A., Liu, B., & Thoi, V. S. (2019). Metal-organic framework functionalization and design strategies for advanced electrochemical energy storage devices. *Communications Chemistry*, *2*(1), 1-14.

17. Chen, L., Zhang, X., Cheng, X., Xie, Z., Kuang, Q., & Zheng, L. (2020). The function of metal–organic frameworks in the application of MOF-based composites. *Nanoscale Advances*, *2*(7), 2628-2647.

18. Lee, Y. R., Kim, J., & Ahn, W. S. (2013). Synthesis of metal-organic frameworks: A mini review. *Korean Journal of Chemical Engineering*, *30*(9), 1667-1680.

19. Cubillas, P., Etherington, K., Anderson, M. W., & Attfield, M. P. (2014). Crystal growth of MOF-5 using secondary building units studied by in situ atomic force microscopy. *CrystEngComm*, *16*(42), 9834-9841.

20. Tibbetts, I., & Kostakis, G. E. (2020). Recent bio-advances in metal-organic frameworks. *Molecules*, *25*(6), 1291.

21. Ha, J., Lee, J. H., & Moon, H. R. (2020). Alterations to secondary building units of metal–organic frameworks for the development of new functions. *Inorganic Chemistry Frontiers*, *7*(1), 12-27.

22. Kalmutzki, M. J., Hanikel, N., & Yaghi, O. M. (2018). Secondary building units as the turning point in the development of the reticular chemistry of MOFs. *Science advances*, *4*(10), eaat9180.

23. Soni, S., Bajpai, P. K., & Arora, C. (2020). A review on metal-organic framework: Synthesis, properties and ap-plication. *Characterization and Application of Nanomaterials*, *3*(2), 87-106.

24. Jiao, L., Seow, J. Y. R., Skinner, W. S., Wang, Z. U., & Jiang, H. L. (2019). Metal–organic frameworks: Structures and functional applications. *Materials Today*, *27*, 43-68.

25. Sakamaki, Y., Tsuji, M., Heidrick, Z., Watson, O., Durchman, J., Salmon, C., ... & Beyzavi, H. (2020). Preparation and Applications of Metal–Organic Frameworks (MOFs): A Laboratory Activity and Demonstration for High School and/or Undergraduate Students. *Journal of chemical education*, *97*(4), 1109-1116.

26. Sharmin, E., & Zafar, F. (2016). Introductory chapter: metal organic frameworks (MOFs). In *Metal-organic frameworks*. IntechOpen.

27. Sun, Y., & Zhou, H. C. (2015). Recent progress in the synthesis of metal–organic frameworks. *Science and technology of advanced materials*.

28. Ding, M., Flaig, R. W., Jiang, H. L., & Yaghi, O. M. (2019). Carbon capture and conversion using metal–organic frameworks and MOF-based materials. *Chemical Society Reviews*, *48*(10), 2783-2828.

29. Sumida, K., Rogow, D. L., Mason, J. A., McDonald, T. M., Bloch, E. D., Herm, Z. R., ... & Long, J. R. (2012). Carbon dioxide capture in metal–organic frameworks. *Chemical reviews*, *112*(2), 724-781.

30. Rehman, A., Farrukh, S., Hussain, A., & Pervaiz, E. (2020). Synthesis and effect of metal–organic frame works on CO2 adsorption capacity at various pressures: a contemplating review. *Energy & Environment*, *31*(3), 367-388.

31. Zhao, X., Bu, X., Zhai, Q. G., Tran, H., & Feng, P. (2015). Pore space partition by symmetry-matching regulated ligand insertion and dramatic tuning on carbon dioxide uptake. *Journal of the American Chemical Society*, *137*(4), 1396-1399.

32. Qazvini, O. T., Babarao, R., & Telfer, S. G. (2021). Selective capture of carbon dioxide from hydrocarbons using a metal-organic framework. *Nature communications*, *12*(1), 1-8.

33. Peng, M. M., Kim, D. K., Aziz, A., Back, K. R., Jeon, U. J., & Jang, H. T. (2012). CO 2 Adsorption of Metal Organic Framework Material Cu-BTC via Different Preparation Routes. In *Computer Applications for Modeling, Simulation, and Automobile* (pp. 244-251). Springer, Berlin, Heidelberg.

34. Li, T., Chen, D. L., Sullivan, J. E., Kozlowski, M. T., Johnson, J. K., & Rosi, N. L. (2013). Systematic modulation and enhancement of CO 2: N 2 selectivity and water stability in an isoreticular series of bio-MOF-11 analogues. *Chemical Science*, *4*(4), 1746-1755.

35. Chen, D. M., Xu, N., Qiu, X. H., & Cheng, P. (2015). Functionalization of metal–organic framework via mixed-ligand strategy for selective CO2 sorption at ambient conditions. *Crystal Growth & Design*, *15*(2), 961-965.

36. Gao, W. Y., Tsai, C. Y., Wojtas, L., Thiounn, T., Lin, C. C., & Ma, S. (2016). Interpenetrating metal–metalloporphyrin framework for selective CO2 uptake and chemical transformation of CO2. *Inorganic chemistry*, *55*(15), 7291-7294.

37. Safarifard, V., Rodríguez-Hermida, S., Guillerm, V., Imaz, I., Bigdeli, M., Azhdari Tehrani, A., ... & Maspoch, D. (2016). Influence of the amide groups in the CO2/N2 selectivity of a series of isoreticular, interpenetrated metal–organic frameworks. *Crystal Growth & Design*, *16*(10), 6016-6023.

38. Benoit, V., Chanut, N., Pillai, R. S., Benzaqui, M., Beurroies, I., Devautour-Vinot, S., ... & Llewellyn, P. L. (2018). A promising metal–organic framework (MOF), MIL-96 (Al), for CO 2 separation under humid conditions. *Journal of Materials Chemistry A*, *6*(5), 2081-2090.

39. Pal, T. K., De, D., Senthilkumar, S., Neogi, S., & Bharadwaj, P. K. (2016). A partially fluorinated, water-stable Cu (II)–MOF derived via transmetalation: significant gas adsorption with high CO2 selectivity and catalysis of Biginelli reactions. *Inorganic Chemistry*, *55*(16), 7835-7842.

40. Chen, C., Feng, X., Zhu, Q., Dong, R., Yang, R., Cheng, Y., & He, C. (2019). Microwave-assisted rapid synthesis of well-shaped MOF-74 (Ni) for CO2 efficient capture. *Inorganic Chemistry*, *58*(4), 2717-2728.

41. Vrtovec, N., Mazaj, M., Buscarino, G., Terracina, A., Agnello, S., Arčon, I., ... & Zabukovec Logar, N. (2020). Structural and CO2 Capture Properties of Ethylenediamine-Modified HKUST-1 Metal–Organic Framework. *Crystal growth & design*, *20*(8), 5455-5465.

42. Liang, L., Liu, C., Jiang, F., Chen, Q., Zhang, L., Xue, H., ... & Hong, M. (2017). Carbon dioxide capture and conversion by an acid-base resistant metal-organic framework. *Nature communications*, *8*(1), 1-10.

43. Tari, N. E., Tadjarodi, A., Tamnanloo, J., & Fatemi, S. (2016). Synthesis and property modification of MCM-41 composited with Cu (BDC) MOF for improvement of CO2 adsorption Selectivity. *Journal of CO2 Utilization*, *14*, 126-134.

44. Zou, L., Yuan, J., Yuan, Y., Gu, J., Li, G., Zhang, L., & Liu, Y. (2019). A Zn (ii) metal–organic framework constructed by a mixed-ligand strategy for CO 2 capture and gas separation. *CrystEngComm*, *21*(21), 3289-3294.

45. Zhou, H. F., Liu, B., Hou, L., Zhang, W. Y., & Wang, Y. Y. (2018). Rational construction of a stable Zn 4 O-based MOF for highly efficient CO 2 capture and conversion. *Chemical Communications*, *54*(5), 456-459.

46. Niu, Z., Guan, Q., Shi, Y., Chen, Y., Chen, Q., Kong, Z., ... & Miao, R. (2018). A lithium-modified zirconium-based metal organic framework (UiO-66) for efficient CO 2 adsorption. *New Journal of Chemistry*, *42*(24), 19764-19770.

47. Park, J., Kim, H., Han, S. S., & Jung, Y. (2012). Tuning metal–organic frameworks with open-metal sites and its origin for enhancing CO2 affinity by metal substitution. *The journal of physical chemistry letters*, *3*(7), 826-829.

48. Wahiduzzaman, A. K., Stone, J., Harp, S., & Khan Mujibur, K. (2017). Synthesis and electrospraying of nanoscale MOF (Metal Organic Framework) for high performance CO2 adsorption membrane nanoscale. *Research Letters*, *12*.

49. Qian, J., Li, Q., Liang, L., Li, T. T., Hu, Y., & Huang, S. (2017). A microporous MOF with open metal sites and Lewis basic sites for selective CO 2 capture. *Dalton Transactions*, *46*(41), 14102-14106.

50. Shekhah, O., Belmabkhout, Y., Chen, Z., Guillerm, V., Cairns, A., Adil, K., & Eddaoudi, M. (2014). Made-to-order metal-organic frameworks for trace carbon dioxide removal and air capture. *Nature communications*, *5*(1), 1-7.

51. Gautam, S., & Cole, D. (2020). CO2 Adsorption in Metal-Organic Framework Mg-MOF-74: Effects of Inter-Crystalline Space. *Nanomaterials*, *10*(11), 2274.

52. McDonald, T. M., D'Alessandro, D. M., Krishna, R., & Long, J. R. (2011). Enhanced carbon dioxide capture upon incorporation of N, N′-dimethylethylenediamine in the metal–organic framework CuBTTri. *Chemical Science*, *2*(10), 2022-2028.

53. Mahdipoor, H. R., Halladj, R., Babakhani, E. G., Amjad-Iranagh, S., & Ahari, J. S. (2021). Synthesis, characterization, and CO 2 adsorption properties of metal organic framework Fe-BDC. *RSC Advances*, *11*(9), 5192-5203.

54. Rada, Z. H., Abid, H. R., Sun, H., Shang, J., Li, J., He, Y., ... & Wang, S. (2018). Effects of-NO2 and-NH2 functional groups in mixed-linker Zr-based MOFs on gas adsorption of CO2 and CH4. *Progress in Natural Science: Materials International*, *28*(2), 160-167.

55. Britt, D., Furukawa, H., Wang, B., Glover, T. G., & Yaghi, O. M. (2009). Highly efficient separation of carbon dioxide by a metal-organic framework replete with open metal sites. *Proceedings of the National Academy of Sciences*, *106*(49), 20637-20640.

56. Yang, D. A., Cho, H. Y., Kim, J., Yang, S. T., & Ahn, W. S. (2012). CO 2 capture and conversion using Mg-MOF-74 prepared by a sonochemical method. *Energy & Environmental Science*, *5*(4), 6465-6473.

57. Liang, W., Bhatt, P. M., Shkurenko, A., Adil, K., Mouchaham, G., Aggarwal, H., ... & Eddaoudi, M. (2019). A tailor-made interpenetrated MOF with exceptional carbon-capture performance from flue gas. *Chem*, *5*(4), 950-963.

58. Li, Y., Zhang, X., Lan, J., Xu, P., & Sun, J. (2019). Porous Zn (Bmic)(AT) MOF with abundant amino groups and open metal sites for efficient capture and transformation of CO2. *Inorganic Chemistry*, *58*(20), 13917-13926.

59. Bien, C. E., Chen, K. K., Chien, S. C., Reiner, B. R., Lin, L. C., Wade, C. R., & Ho, W. W. (2018). Bioinspired metal–organic framework for trace CO2 capture. *Journal of the American Chemical Society*, *140*(40), 12662-12666.

60. Maity, R., Singh, H. D., Yadav, A. K., Chakraborty, D., & Vaidhyanathan, R. (2019). Water‐stable Adenine‐based MOFs with Polar Pores for Selective CO2 Capture. *Chemistry–An Asian Journal*, *14*(20), 3736-3741.

61. Shi, Z., Tao, Y., Wu, J., Zhang, C., He, H., Long, L., ... & Zhang, Y. B. (2020). Robust metal–triazolate frameworks for CO2 capture from flue gas. *Journal of the American Chemical Society*, *142*(6), 2750-2754.

62. Zhao, Y., Liu, J., Han, M. L., Yang, G. P., Ma, L. F., & Wang, Y. Y. (2021). Two comparable Ba-MOFs with similar linkers for enhanced CO2 capture and separation by introducing N-rich groups. *Rare Metals*, *40*(2), 499-504.

63. Zhang, K., Qiao, Z., & Jiang, J. (2017). Molecular design of zirconium tetrazolate metal–organic frameworks for CO2 capture. *Crystal Growth & Design*, *17*(2), 543-549.

64. Alrubaye, R. T. A., & Kareem, H. M. (2019, June). Carbon Dioxide Adsorption on MOF-199 Metal-Organic Framework at High Pressure. In *IOP Conference Series: Materials Science and Engineering* (Vol. 557, No. 1, p. 012060). IOP Publishing.

65. Salehi, S., & Anbia, M. (2017). High CO2 adsorption capacity and CO2/CH4 selectivity by nanocomposites of MOF-199. *Energy & Fuels*, *31*(5), 5376-5384.

66. Mohan, M., Essalhi, M., Durette, D., Rana, L. K., Ayevide, F. K., Maris, T., & Duong, A. (2020). A Rational Design of Microporous Nitrogen-Rich Lanthanide Metal–Organic Frameworks for CO2/CH4 Separation. *ACS Applied Materials & Interfaces*, *12*(45), 50619-50627.

67. Singh, M., Senthilkumar, S., Rajput, S., & Neogi, S. (2020). Pore-functionalized and hydrolytically robust Cd (II)-metal–organic framework for highly selective, multicyclic CO2 adsorption and fast-responsive luminescent monitoring of Fe (III) and Cr (VI) ions with notable sensitivity and reusability. *Inorganic Chemistry*, *59*(5), 3012-3025.

68. Zhang, X., Zhang, R. H., Hu, H., Geng, L., Zhang, Y. Z., Gao, J., ... & Sheng, J. (2020). Combining unsaturated metal sites and narrow pores within a Co (ii)-based MOF towards CO 2 separation and transformation. *Dalton Transactions*, *49*(7), 2058-2062.

69. Liu, J., Fan, Y. Z., Zhang, K., Zhang, L., & Su, C. Y. (2020). Engineering porphyrin metal–organic framework composites as multifunctional platforms for CO2 adsorption and activation. *Journal of the American Chemical Society*, *142*(34), 14548-14556.

70. Xu, Q., Fang, L., Fu, Y., Xiao, Q., Zhang, F., & Zhu, W. (2020). Synthesis, characterization, and CO2 adsorption properties of metal–organic framework NH2–MIL–101 (V). *Materials Letters*, *264*, 127402.

71. Li, Y. Z., Wang, G. D., Ma, L. N., Hou, L., Wang, Y. Y., & Zhu, Z. (2021). Multiple functions of gas separation and vapor adsorption in a new MOF with open tubular channels. *ACS Applied Materials & Interfaces*, *13*(3), 4102-4109.

72. Güçlü, Y., Erer, H., Demiral, H., Altintas, C., Keskin, S., Tumanov, N., ... & Semerci, F. (2021). Oxalamide-Functionalized Metal Organic Frameworks for CO_2 Adsorption.

73. Chakraborty, G., Das, P., & Mandal, S. K. (2021). Efficient and Highly Selective CO2 Capture, Separation, and Chemical Conversion under Ambient Conditions by a Polar-Group-Appended Copper (II) Metal–Organic Framework. *Inorganic Chemistry*, *60*(7), 5071-5080.

74. Gai, F., Zhu, D., Wu, Y., Zhao, X., Liang, C., Liu, Z., ... & Wang, T. (2021). Tailored N-doped porous carbons via a MOF assembly process for high-performance CO 2 uptake. *Materials Advances*, *2*(2), 692-699.

75. Soleimanpour, A., Farsi, M., Keshavarz, P., & Zeinali, S. (2021). Modification of activated carbon by MIL-53 (Al) MOF to develop a composite framework adsorbent for CO2 capturing. *Environmental Science and Pollution Research*, *28*(28), 37929-37939.

76. Liu, J., Yang, G. P., Jin, J., Wu, D., Ma, L. F., & Wang, Y. Y. (2020). A first new porous d–p HMOF material with multiple active sites for excellent CO 2 capture and catalysis. *Chemical Communications*, *56*(16), 2395-2398.

77. Xu, G., Meng, Z., Guo, X., Zhu, H., Deng, K., Xiao, C., & Liu, Y. (2019). Molecular simulations on CO2 adsorption and adsorptive separation in fullerene impregnated MOF-177, MOF-180 and MOF-200. *Computational Materials Science*, *168*, 58-64.

78. Wang, X., Wang, Y., Lu, K., Jiang, W., & Dai, F. (2021). A 3D Ba-MOF for selective adsorption of CO2/CH4 and CO2/N2. *Chinese Chemical Letters*, *32*(3), 1169-1172.

79. Dhankhar, S. S., & Nagaraja, C. M. (2019). Construction of a 3D porous Co (ii) metal–organic framework (MOF) with Lewis acidic metal sites exhibiting selective CO 2 capture and conversion under mild conditions. *New Journal of Chemistry*, *43*(5), 2163-2170.

80. Gaikwad, S., Kim, Y., Gaikwad, R., & Han, S. (2021). Enhanced CO2 capture capacity of amine-functionalized MOF-177 metal organic framework. *Journal of Environmental Chemical Engineering*, *9*(4), 105523.

81. Zheng, B., Huang, L., Cao, X., Shen, S., Cao, H., Hang, C., ... & Wang, Z. (2018). A highly porous acylamide decorated MOF-505 analogue exhibiting high and selective CO 2 gas uptake capability. *CrystEngComm*, *20*(13), 1874-1881.

82. Wang, H. H., Shi, W. J., Hou, L., Li, G. P., Zhu, Z., & Wang, Y. Y. (2015). A Cationic MOF with High Uptake and Selectivity for CO2 due to Multiple CO2‐Philic Sites. *Chemistry–A European Journal*, *21*(46), 16525-16531.

83. Zhuang, W., Yuan, D., Liu, D., Zhong, C., Li, J. R., & Zhou, H. C. (2012). Robust metal–organic framework with an octatopic ligand for gas adsorption and separation: combined characterization by experiments and molecular simulation. *Chemistry of Materials*, *24*(1), 18-25.

84. Shang, S., Tao, Z., Yang, C., Hanif, A., Li, L., Tsang, D. C., ... & Shang, J. (2020). Facile synthesis of CuBTC and its graphene oxide composites as efficient adsorbents for CO2 capture. *Chemical Engineering Journal*, *393*, 124666.

85. Liao, J., Zeng, W., Zheng, B., Cao, X., Wang, Z., Wang, G., & Yang, Q. (2020). Highly efficient CO 2 capture and conversion of a microporous acylamide functionalized rht-type metal–organic framework. *Inorganic Chemistry Frontiers*, *7*(9), 1939-1948.

86. Sun, J., Li, Q., Chen, G., Duan, J., Liu, G., & Jin, W. (2019). MOF-801 incorporated PEBA mixed-matrix composite membranes for CO2 capture. *Separation and Purification Technology*, *217*, 229-239.

87. Ganesh, M., Hemalatha, P., Peng, M. M., Cha, W. S., & Jang, H. T. (2014). Zr-fumarate MOF a novel CO2-adsorbing material: Synthesis and characterization. *Aerosol and Air Quality Research*, *14*(6), 1605-1612.

88. Wu, W., Li, Z., Chen, Y., and Li. W. (2019). Polydopamine-Modifified Metal−Organic Framework Membrane with Enhanced Selectivity for Carbon Capture. *Environ. Sci. Technol*, 53, 3764−3772

89. Zhang, Z., Ding, Q., Cui, J., Cui, X., & Xing, H. (2021). High and selective capture of low-concentration CO2 with an anion-functionalized ultramicroporous metal-organic framework. *Science China Materials*, *64*(3), 691-697.

90. Liang, W., Bhatt, P. M., Shkurenko, A., Adil, K., Mouchaham, G., Aggarwal, H., ... & Eddaoudi, M. (2019). A tailor-made interpenetrated MOF with exceptional carbon-capture performance from flue gas. *Chem*, *5*(4), 950-963.

91. Aamer, I., Iqbal, N., Noor, T., & Asghar, A. (2021). Synthesis, characterization and CO2 adsorption studies of DABCO based pillared Zn-BDC and Co-BDC metal organic frameworks. *Materials Research Express*, *8*(7), 075506.

92. Ullah, S., Bustam, M. A., Shariff, A. M., Elkhalifah, A. E., Murshid, G., & Riaz, N. (2014, October). Synthesis and CO2 adsorption study of modified MOF-5 with multi-wall carbon nanotubes and expandable graphite. In *AIP Conference Proceedings* (Vol. 1621, No. 1, pp. 34-39). American Institute of Physics.

93. Asghar, A., Iqbal, N., Noor, T., Ali, M., & Easun, T. L. (2019). Efficient one-pot synthesis of a hexamethylenetetramine-doped Cu-BDC metal-organic framework with enhanced CO2 adsorption. *Nanomaterials*, *9*(8), 1063.

94. Li, N., Chang, Z., Huang, H., Feng, R., He, W. W., Zhong, M., ... & Bu, X. H. (2019). Specific K+ binding sites as CO2 traps in a porous MOF for enhanced CO2 selective sorption. *Small*, *15*(22), 1900426.

95. Milner, P. J., Siegelman, R. L., Forse, A. C., Gonzalez, M. I., Runčevski, T., Martell, J. D., ... & Long, J. R. (2017). A diaminopropane-appended metal–organic framework enabling efficient CO2 capture from coal flue gas via a mixed adsorption mechanism. *Journal of the American Chemical Society*, *139*(38), 13541-13553.

96. Lee, W. R., Hwang, S. Y., Ryu, D. W., Lim, K. S., Han, S. S., Moon, D., ... & Hong, C. S. (2014). Diamine-functionalized metal–organic framework: exceptionally high CO 2 capacities from ambient air and flue gas, ultrafast CO 2 uptake rate, and adsorption mechanism. *Energy & Environmental Science*, *7*(2), 744-751.

97. Sahiner, N., Demirci, S., & Yildiz, M. (2017). Synthesis and Characterization of Terephthalic Acid Based Cr3+, Sb3+, In3+ and V3+ Metal-Organic Frameworks. *Journal of Inorganic and Organometallic Polymers and Materials*, *27*(5), 1333-1341.

98. Carreon, M. A., & Venna, S. R. (2020). Metal Organic Frameworks History and Structural Features. *World Scientific Publishing Europe Ltd.: Singapore*, 1-29.

99. Salama, R. S., El-Hakam, S. A., Samra, S. E., El-Dafrawy, S. M., & Ahmed, A. I. (2018). Adsorption, equilibrium and kinetic studies on the removal of methyl orange dye from aqueous solution by using of copper metal organic framework (Cu-BDC). *Int. J. Mod. Chem*, *10*, 195-207.

100. Nguyen, D. T. C., Le, H. T. N., Do, T. S., Pham, V. T., Dai Tran, L., Ho, V. T. T., ... & Doan, V. T. (2019). Metal-organic framework MIL-53 (Fe) as an adsorbent for ibuprofen drug removal from aqueous solutions: response surface modeling and optimization. *Journal of Chemistry*, *2019*.

101. Omkaramurthy, B. M., Krishnamurthy, G., & Foro, S. (2020). Synthesis and characterization of mesoporous crystalline copper metal–organic frameworks for electrochemical energy storage application. *SN Applied Sciences*, *2*(3), 1-14.

102. Bedia, J., Muelas-Ramos, V., Peñas-Garzón, M., Gómez-Avilés, A., Rodríguez, J. J., & Belver, C. (2019). A review on the synthesis and characterization of metal organic frameworks for photocatalytic water purification. *Catalysts*, *9*(1), 52.

103. Nijem, N., Canepa, P., Kong, L., Wu, H., Li, J., Thonhauser, T., & Chabal, Y. J. (2012). Spectroscopic characterization of van der Waals interactions in a metal organic framework with unsaturated metal centers: MOF-74–Mg. *Journal of Physics: Condensed Matter*, *24*(42), 424203.

104. Dikio, E. D., & Farah, A. M. (2013). Synthesis, characterization and comparative study of copper and zinc metal organic frameworks. *Chemical Science Transactions*, *2*(4), 1386-1394.

105. Elvira, G. B., Francisco, G. C., Víctor, S. M., & Alberto, M. L. R. (2017). MgO-based adsorbents for CO2 adsorption: Influence of structural and textural properties on the CO2 adsorption performance. *Journal of Environmental Sciences*, *57*, 418-428.